332.8
P567

SPSE

Photographic SCIENCE AND ENGINEERING

LIBRARY
RECEIVED
JAN 23 1959
U. S. DEPT. OF AGRICULTURE

Louis-Philippe Clerc (a citation) • *Walter Clark* 185

Internal Gelatin in Photographic Silver Halide Grains
A. E. Ballard, C. W. Zuehlke, and R. S. Miller 186

On the Minimum Energy Detectable by Photographic Materials • *R. Clark Jones*
Part II. Results for Four Current Kodak Films 191
Part III. Energy Incident on a Microscopic Area of the Film 198

Analysis of the Variability Among Density-Log Exposure Curves of Black-and-White Negative Films by the Method of Principal Components
J. L. Simonds 205

The Use of Principal-Component Description of *D*-log *E* Curves in a Study of the ASA-DIN Speed Relationships • *J. L. Simonds* 210

Degradation of Phenidone in Developer Solutions During Storage
G. C. *Alletag* 213

Some Simplified Shutter, Flash Synchronization, and Motion-Picture Camera Tests • *Samuel L. Love* 219

System Analysis and Performance of a Feedback Scanning Printer
L. L. Blackmer and J. C. Marchant 225

Quantitative Estimation of Photographic Kink Susceptibility • *Beat Meerkämper* 231

Book Reviews and Abstracts 234

Technicalia Photographica • *Frank Smith* 236

Annual Index 246

DECEMBER • 1958

Volume 2 • Number 4

Editorial Policy

Photographic Science and Engineering is dedicated to the advancement of the knowledge and application of photography and other directly related sciences. Its pages are open to all who wish to report on new studies dealing with the theory of photosensitive systems, the design of photographic instruments and apparatus useful in the treatment of photographic materials, photographic optics and illuminants, the use of photography for scientific or engineering measurement or recording, and photographic instrumentation and data recording. Only original papers should be submitted except on special invitation.

Manuscripts should be typed double-spaced on white bond paper with $1^1/_4$-inch margins all around. Literature references should be exact, and should include titles of papers and journals, names of authors, numbers of volumes and pages, and year of publication. Book references should include title of volume, names of authors, publisher, number of edition, year of publication, and chapter and pages cited.

Graphs, charts, and other line illustrations should conform to good usage such as given in the American Standards Association Document Y-15, "A Guide for Preparing Technical Illustrations for Publication and Projection." Continuous-tone photographs should be made on 8- by 10-inch glossy paper and should show pertinent image detail sufficiently clearly to permit reduction to fit a 3-inch column in this journal. All illustrations should be numbered in soft blue pencil on the back to correspond with captions typed on a separate page. Tables should also be submitted on separate pages appropriately identified. An abstract should accompany each manuscript.

All papers submitted for publication will be reviewed by members of the Editorial Review Board and if not accepted will be returned to the author. Published papers become the property of the Society and are protected by appropriate copyrights. Authors receive five copies of issues in which their contributions appear. Additional copies and reprints may be obtained. The Society does not assume responsibility for material in transit, nor guarantee publication of unsolicited material.

Photographic
SCIENCE AND ENGINEERING

official publication of the
Society of Photographic Scientists and Engineers

DECEMBER 1958
Volume 2, Number 4

EDITORIAL STAFF

T. H. James, *Editor*
Jennie H. Allen, *Managing Editor*
Frank Smith, *Feature Editor*
Robert H. Zappert, *Feature Editor*
Willard W. Van Allen, *Associate Editor*
Jean St. Thomas, *Foreign Editor*

EDITORIAL REVIEW BOARD

T. H. James, *Chairman*
R. S. Barrows
R. Davis
H. E. Edgerton
R. Clark Jones
K. G. Leistner
J. A. Maurer
H. F. Nitka
Thomas D. Smith
J. H. Waddell
William West

Photographic Science and Engineering is published four times a year by the Society of Photographic Scientists and Engineers. The publication office is at 20th and Northampton Streets, Easton, Pa. Address correspondence to the Society at Box 1609, Main Post Office, Washington, D.C. Subscription to non-members of the Society, $8.00 per year, members $4.00; single copies, $2.00 each. The Society is not responsible for the accuracy of statements made by authors and does not necessarily subscribe to their views. Second-class mail privileges authorized at Easton, Pa.

© Copyright 1958 by the Society of Photographic Scientists and Engineers, Inc. Permission to reprint any part of the contents, except in reviews and abstracts, must be obtained in writing from the Editorial Vice President.

PHOTOGRAPHIC SCIENCE AND ENGINEERING
Volume 2, Number 4, December 1958

Photograph by André Gerbon

Louis-Philippe Clerc

Louis-Philippe Clerc, photographic scientist, teacher, and writer, has dominated the whole field of photography in France for well over fifty years, and his renown has extended far beyond the borders of his native land. He has worked intensively and unceasingly for the advancement of photography everywhere, and his contributions have been particularly outstanding in the fields of graphic arts, color photography, aerial photography, photographic chemistry, and the applications of photography to science and technology.

At the present time, Monsieur Clerc is probably best known by the wide scope and sagacity of his writing in most fields of photography, the great array of books that have come from his pen — there are more than twenty of them, many of which have been translated into several languages — and the outstanding monthly publication *Science et Industries photographiques*, which has been a particular devotion of his since 1921. This publication has been edited by Monsieur Clerc entirely alone, without any collaborator, a fact which testifies to the tremendous energy, organizing ability, and knowledge of the field which are characteristic of the man. Practically every day of his life since he was a youth has been devoted to teaching, writing, organizing scientific information, translating articles and books, and editing, and all of this has been done in an atmosphere of warmth, friendliness, and good living which has made for him a great number of friends of long standing all over the world.

He has had a long and distinguished career as a teacher of chemistry and photography, having started to teach analytical chemistry at the University of Paris in 1898. He founded in Paris, and directed for many years, a technical school of photography and cinématography, and taught photographic photometry at the Institute of Optics in Paris. Since 1900, he has played a very active part in organizing the International Congresses of Photography, which are concerned essentially with scientific and technical work; he has served for many years as the Permanent Chairman for the French Committee; and he edited the *Proceedings* of the Fifth, Sixth, and Ninth International Congresses of Photography.

Monsieur Clerc has made outstanding contributions to graphic arts in practice and theory. He was a pioneer in aerial photography and was decorated for his services in aerial photography during the war of 1914–1918. In 1949 the French Government decorated him as Chevalier of the Legion of Honour in recognition of the quality of his university work and his services to science, and for his work in the practical application of science to industry, particularly in the fields of photography and cinématography, by his publications. He has received a great number of honors from many countries, and the Society of Photographic Scientists and Engineers is very proud to have added to them, on October 9, 1958, at the Annual Conference, Rochester, N.Y., the highest honor that it can bestow, Honorary Membership in the Society, ". . . in recognition of his lifelong eminent service in the advancement of photography through dedicated research and inspired teaching and writing." — *Walter Clark*

Based on a citation by Dr. Walter Clark at the Annual Banquet held on 9 October 1958, during the Annual Conference, Rochester, N.Y.

PHOTOGRAPHIC SCIENCE AND ENGINEERING
Volume 2, Number 4, December 1958

Internal Gelatin in Photographic Silver Halide Grains

A. E. Ballard, C. W. Zuehlke, and R. S. Miller, *Research Laboratories, Eastman Kodak Company, Rochester, N.Y.*

Three analytical methods are described for the determination of "internal gelatin" in photographic silver halide grains. By the use of these methods, it is shown that photographic silver halide grains contain from 20 to 50 ppm of internal gelatin. There appears to be no real difference between the various halide types with respect to internal gelatin content.

There has long been speculation concerning the existence of "internal gelatin," that is, gelatin within the silver halide grains of a photographic emulsion. In 1921, Trivelli and Sheppard[1] stated: "Hence we must regard sensitive photographic emulsions not only as a suspension of silver halide crystals in gelatin, but also as a probably much more complex suspension of gelatin in crystalline silver halide." Even earlier, in 1911, Reinders[2] described experiments which purported to prove the existence of gelatin molecules within the silver halide crystal, but the evidence he presented to support this contention was not conclusive. In connection with this work, Reinders made the interesting observation that silver chloride crystals grown in solutions of erythrosin and Rose Bengal were uniformly tinted by the dye. This observation makes more plausible the supposition that large organic molecules may be incorporated into a growing silver halide crystal.

The first serious attempt to detect and measure internal gelatin by analytical methods was published recently by Davis.[3,4] As the result of his work, Davis reached the conclusion that photographic silver halide grains do not contain significant amounts of internal gelatin.

Internal gelatin, if it is present, might have an important bearing on the photographic sensitivity of the silver halide grains. Because the results reported by Davis are at variance with observations made by one of us a number of years ago, it seemed appropriate to check the Davis work. This paper covers our findings on the Davis procedure, and will describe several alternate methods for the determination of internal gelatin in silver halide grains.

The Davis Procedure

The Davis method is based on the following sequence of operations: (a) The external gelatin in the liquid phase of the emulsion is removed by washing the grains with water by centrifugation. After several washings, the external gelatin is essentially gone, leaving, however, an adsorbed layer of gelatin on the surface of the grains. (b) The adsorbed gelatin is then removed by treating the grains three times with a dilute solution of sodium hypobromite. (c) The internal gelatin is released by dissolving the sample in sodium thiosulfate solution. (d) The gelatin is concentrated by use of an ingenious foaming technique, first described by Abribat.[5] In this procedure, air is bubbled into the solution through a fritted disk and the foam produced, which is enriched in gelatin, is allowed to rise through a reflux column and to overflow into a receiving vessel where it coalesces to a liquid. (e) The final detection of gelatin is carried out by use of a modified Zsigmondy gold-number test in which a red-gold sol is added to the foam concentrate. The high concentration of electrolyte (sodium thiosulfate) in this solution causes the color of the sol to change rapidly from wine red to blue-gray. In the presence of gelatin, this color change does not occur, owing to the protective action of the gelatin, and this effect is utilized by Davis as a semiquantitative method for gelatin.

Experimental Procedure

We have studied each of the steps in the Davis procedure, exactly as it is described in the literature,[3] and our findings may be summarized as follows:

(1) The hypobromite treatment is entirely effective as a method for the quantitative removal of the adsorbed or surface gelatin. Electron micrographs indicate that 0.01 *N* hypobromite solution does not have an appreciable solvent action on the grains. There is no significant etching of the grains and the possibility of recrystallization of the silver halides during the hypobromite treatment appears remote.

(2) Gelatin is nearly quantitatively removed from 20% sodium thiosulfate solution by the foaming procedure when approximately 5% of the liquid volume is transferred by the foaming operation.

(3) The gold-sol test is sensitive to about 10 μg of gelatin when the test is applied to a 30% solution of sodium thiosulfate.

Communication No. 1944 from the Kodak Research Laboratories. Received 12 February 1958.

The test, however, failed completely when applied to a foam concentrate prepared according to Davis's directions, i.e., when applied to a solution which contained 20 grams of silver halide dissolved in 250 ml of 20% hypo solution. A solution of this composition rapidly and spontaneously generated silver sulfide particles, as shown by the appearance of a slightly tan color. These silver sulfide particles were concentrated with the gelatin by foaming and apparently were highly effective in coagulating the gold sol, even in the presence of relatively large amounts of added gelatin, viz., 400 μg. Accordingly, the Davis test, when applied as described, invariably showed a negative test for gelatin.

The rate of formation of silver sulfide in a solution of sodium thiosulfate containing dissolved silver halides is strongly dependent upon the ratio of the silver to the thiosulfate concentrations. Under the conditions specified by Davis, a visible discoloration of the solution occurred in a relatively few minutes. When the concentration of silver was limited to approximately one half that specified by Davis, no detectable discoloration occurred during the time needed to carry through the procedure. Under these modified conditions, the gold-sol test retained much of its sensitivity for gelatin in the foam concentrate.

The Davis procedure, modified by reducing the sample size to 10 grams of silver halide, was applied to several commercial-type negative and x-ray emulsions. The foaming apparatus was essentially identical to that described by Davis, except that its capacity was increased to 275 ml so that the entire sample solution could be foamed in a single operation. In every case, a clearly positive test for internal gelatin was obtained. Since there still may have been negative interference from silver sulfide particles, it was not possible to estimate quantitatively the amount of internal gelatin present, but values as high as 0.025 mg of gelatin per gram of silver halide were obtained. Although this work adequately demonstrated the existence of internal gelatin, it seemed appropriate to devise alternate procedures for the quantitative determination.

The Micro-Kjeldahl Method

In this procedure, a conventional micro-Kjeldahl method was used for the final determination of gelatin in the foam concentrate. The preceding steps for the removal of surface gelatin and the concentration of the internal gelatin by foaming were identical with the Davis procedure except that the larger apparatus (275 ml) and a double foaming technique were used. The first foam concentrate was diluted to 250 ml with water containing 10 grams of sodium sulfate, and the solution was refoamed. In this way, the silver and thiosulfate concentrations were substantially reduced. The second foam concentrate was fumed with concentrated sulfuric acid in the presence of copper sulfate as a catalyst, whereby the gelatin nitrogen was converted to ammonium sulfate.

The solution was made alkaline, the ammonia was distilled into boric acid solution and titrated with 0.01 *N* hydrochloric acid, with a mixture of Bromo Cresol Green and Methyl Red[6] as the indicator. With experience, using a microburet, it was possible to reproduce the endpoint to ±0.01 ml of 0.01 *N* acid, which is equivalent to ±0.008 mg of gelatin.

The results obtained by the application of this procedure to four commercial-type emulsions are given in Table I. Replicate results are included to illustrate the reproducibility of the method. The control emulsions reported in this and in succeeding tables were prepared by precipitating silver bromide and growing the grains to 1–2 μ in size in the absence of gelatin. The grains were then suspended in a 3% gelatin solution, and the analytical procedure was applied to these emulsions, which were assumed to be entirely free of internal gelatin. The results show that the hypobromite procedure was entirely effective for removing external gelatin.

TABLE I

Internal Gelatin by Micro-Kjeldahl Method

Milligrams of Gelatin per Gram of Silver Halide

	Bromo-iodide	Chloro-bromide	Bromide	Chloride	Control
	0.033	0.031	0.022	0.015	0.001
	0.041	0.039	0.024	0.040	0.002
	0.046	0.037	0.030	0.037	0.004
	0.037	0.035	0.017	0.016	0.003
	0.041	0.040	0.024	0.040	—
	0.037	0.033	0.022	0.041	—
	0.038	—	—	—	—
Av.	0.040	0.036	0.023	0.032	—

In this, as in all micro-Kjeldahl work, it was necessary to take precautions to avoid the pickup of ammonia fumes from the laboratory atmosphere or the introduction of nitrogen-containing impurities from the reagents used. The largest potential source of nitrogen contamination was the 250 ml of 20% sodium thiosulfate solution used to dissolve the sample, and to concentrate the gelatin by foaming. Ordinary reagent-quality sodium thiosulfate was used and was found to be very low in nitrogen, or at least in nitrogen compounds which can be concentrated by foaming. Blanks representing all the reagents carried through the entire procedure remained at a satisfactory low level for each of the several lots of thiosulfate used and amounted to about 0.2 ml of 0.01 *N* hydrochloric acid. This is equivalent to 0.156 mg of gelatin for a 20-gram sample, or 0.008 mg of gelatin per gram of silver halide. The results reported in the tables have been corrected for the blank.

The Biuret Method

In this procedure, the well-known biuret method[7] commonly used for the determination of proteins was applied to the foam concentrate. As in the micro-Kjeldahl method, a double foaming procedure was used to decrease the concentrations of silver and thio-

sulfate. In order to achieve adequate sensitivity, it was necessary to measure the biuret color using a 10-cm light path. The method was calibrated by adding known amounts of gelatin to solutions containing appropriate concentrations of sodium thiosulfate, sodium sulfate, and dissolved silver bromide, none of which interfered with the successful application of the method.

The method was applied to a commercial-type emulsion and to an emulsion prepared in the laboratory by precipitating the grains in water and by growing them to approximately 1 μ in size in the presence of gelatin. The results obtained are given in Table II, where they are compared with results obtained on the same emulsion by use of the micro-Kjeldahl procedure. Agreement between the two methods is good. The control emulsion again shows essentially no internal gelatin.

TABLE II

Internal Gelatin by Biuret Method

Milligrams of Gelatin per Gram of Silver Halide

Emulsion	Biuret Method	Micro-Kjeldahl Method
Commercial Emulsion	0.030 0.035	0.041 0.036
Laboratory Emulsion	0.039 0.033	0.037 0.033
Control	0.004	—

The Direct Kjeldahl Method

In this procedure, the conventional macro-Kjeldahl method was applied directly to the silver halide grains after the external and surface gelatin had been removed by the usual hypobromite treatment. Instead of releasing the internal gelatin by dissolving the silver halides in sodium thiosulfate solution, the same result was achieved by fuming the entire 20 grams of silver halide with concentrated sulfuric acid for 2 hr. Although the sample was only partially dissolved in this period of time, nearly complete recrystallization of the silver halide apparently did occur, releasing the internal gelatin to the hot acid digest where its nitrogen was converted to ammonium sulfate. The digest was then made alkaline and the ammonia was distilled and titrated in the usual way with 0.01 *N* hydrochloric acid.

TABLE III

Internal Gelatin by Direct Kjeldahl Method

Milligrams of Gelatin per Gram of Silver Halide

Emulsion	Direct Kjeldahl Method	Micro-Kjeldahl Method
A	0.019 0.022	0.023 0.025
B	0.019 0.017	— —
C	0.033 0.045 0.030 0.033	— — — —
Control	0.001 0.001	— —

The results obtained on three commercial-type emulsions are given in Table III, which includes the values obtained in Sample A by use of the micro-Kjeldahl method. If recrystallization of the silver halides in the acid digest were incomplete, the results obtained by use of the method would tend to be low. Agreement with the micro-Kjeldahl method, however, is reasonably good and the results obtained by use of the method are comparable to the values reported in Tables I and II.

Discussion

The hypobromite treatment as described by Davis involves treating the grains, in sequence, with 0.016 *M* sodium hypobromite solution, 0.01 *M* sulfuric acid solution, and distilled water. This sequence of treatments is applied three times to ensure complete removal of the surface gelatin. Davis stated that this treatment does not result in significant recrystallization of silver bromide. Electron micrographs of treated grains, taken in these laboratories, show very little etching or erosion, in agreement with Davis's statements. Although the control experiments listed in Tables I, II, and III demonstrate adequately that the hypobromite solution removes essentially all the surface gelatin, the following experiment was carried out to show that the hypobromite treatment did not attack internal gelatin: A commercial-type emulsion was analyzed for internal gelatin by the micro-Kjeldahl method after application of the usual hypobromite treatments (3 times). In a second experiment, the entire sequence of treatments was applied twice (6 hypobromite treatments). The results, given in Table IV, show that the hypobromite does not reach the internal gelatin by recrystallization or any other mechanism during the time intervals needed for the treatment.

TABLE IV

Effect of Time of Hypobromite Treatment on Amount of Internal Gelatin Found

Milligrams of Gelatin per Gram of Silver Halide

3 Hypobromite Treatments	6 Hypobromite Treatments
0.034 0.032	0.035 0.032

None of the methods reported here is specific for gelatin. The micro-Kjeldahl procedure shows that the silver halide grains contain a nitrogen-containing material which is concentrated by foaming. The positive biuret test indicates that this substance is a peptide, protein, or amino acid, and its protective action on the gold sol strongly suggests that we are

dealing with whole gelatin molecules rather than degraded gelatin fragments.

The data presented in Tables I–IV were obtained, almost entirely, by the analysis of commercial-type emulsions which were prepared with gelatin present during both the precipitation and the ripening steps. Table V gives data representing laboratory emulsions

TABLE V

Internal Gelatin in Laboratory Emulsion Grains Precipitated in the Absence of Gelatin

Milligrams of Gelatin per Gram of Silver Bromide

Experiment	Emulsion Grains	Control
A	0.052	—
B	0.071	—
C[a]	0.048	—
	0.058	—
D[a]	0.035	—
	0.043	—
E[a]	0.032	—
	0.030	—
F	0.037	0.001
	0.033	—
G	0.056	0.002
	0.048	—
H	—	0.003
	—	0.003
I	—	0.001
	—	0.001

[a] Emulsion treated with Takamine prior to removal of external gelatin by washing.

which were prepared with no gelatin present during the precipitation step. The method used for the preparation of the starting silver bromide sol in the absence of a protective colloid was essentially that of Bokinik and Iljina,[8] in which a potassium bromide solution and a silver nitrate solution were run simultaneously into a relatively large quantity of water. Under these conditions, a stable silver bromide suspension was obtained in which the average particle size was approximately 0.06 μ. After precipitation was complete, gelatin was added, as well as some potassium bromide, to increase the solubility of the silver bromide, and the grains were grown to 1–2 μ in size. Grains prepared in this way were analyzed for internal gelatin by the micro-Kjeldahl method.

The data in Table V show clearly that gelatin is incorporated into the grains during the ripening process. The amounts of internal gelatin found in these laboratory emulsions are fully as high as that found in the commercial type.

It would be of considerable interest to ascertain whether the internal gelatin is homogeneously dispersed throughout the silver halide grains, or whether it is present in discrete pockets or occlusions within the grain boundaries. If it is homogeneously distributed, the gelatin would be a much more effective trapping material for either photoelectrons or positive holes. If it exists in the form of discrete occlusions, its effect probably would be equivalent to that of the adsorbed layer of gelatin on the surface of the grain.

Sheppard and Lambert[9] proposed that the silver halide grains in a photographic emulsion grow by a combination of the Ostwald ripening process, and a process of coalescence in which some of the very fine grains touch each other and fuse together. Upon continued growth, such an aggregate of two or more crystals may rearrange and assume one of the regular crystal shapes. Recently, Ammann-Brass[10] has also come to the conclusion that coalescence is an important factor in silver halide grain growth. Based on electron-microscope studies made during the ripening of an emulsion, Ammann-Brass found that there is a sudden decrease in the population of the medium-sized grains which cannot be explained by the simple Ostwald ripening mechanism of grain growth. Observations made in the course of this work on the ripening of laboratory emulsions by conventional methods also suggest that coalescence is involved, at least to some extent, in grain growth. Electron micrographs of the silver halide grains made at various stages in their growth show many irregularly shaped grains, particularly in the early stages of ripening. Relatively few of the grains show the regular crystal shapes that appear in large numbers in the finished emulsion. This suggests that the perfection of the smaller grains is constantly being disturbed by coalescence and that it is only after this process becomes negligible that the crystals achieve a regular crystal shape by ionic deposition. Since it is known that gelatin is tightly adsorbed to the surface of the silver halide grains, it is easy to visualize that the process of coalescence might result in trapping gelatin in the form of occlusions.

Bibliography

1. Trivelli, A. P. H., and Sheppard, S. E., *The Silver Bromide Grain of Photographic Emulsions*, Monograph No. 1, Eastman Kodak Co., D. Van Nostrand Co., New York, N.Y., 1921, pp. 56, 127.
2. Reinders, W., *Kolloid Z., 9:* 10 (1911); *Z. phys. Chem., 77:* 677 (1911).
3. Davis, P., *Proc. Roy. Phot. Soc. Centenary Intern., Confer. on the Science and Applications of Photography, London, Sept. 10–25, 1953*, R. S. Schultze, ed., Roy. Phot. Sci., London, 1955, p. 22.
4. ———, *J. Appl. Chem., 6:* 413 (1956).
5. Abribat, M., *Compt. rend., 209:* 244 (1939).
6. Ma, T. S., and Zuazaga, G., *Ind. Eng. Chem., Anal. Ed., 14:* 280 (1942).
7. Robinson, H. W., and Hogden, C. G., *J. Biol. Chem., 135:* 707 (1940).
8. Bokinik, J. I., and Iljina, Z. A., *Acta Physicochimica U.R.S.S., 3:* 383 (1935).
9. Sheppard, S. E., and Lambert, R. H., *Colloid Symposium Monograph, 6:* 265, Chemical Catalog Co., Inc., New York, N.Y. (1928).
10. Ammann-Brass, H., *Chimia, 10:* 173 (1956).

(*See* Note *on following page.*)

Note on *Internal Gelatin in Photographic Silver Halide Grains*

Having had the privilege of seeing the paper by Ballard, Zuehlke, and Miller on "Internal Gelatin in Photographic Silver Halide Grains" prior to publication, I would like to congratulate them on the work they have described and to make some comments on the difference in results from those I obtained six years ago.[3]

In their paper they suggest formation of silver sulfide in the hypo solution of the silver halide as the explanation of my negative results. This is unlikely as in my work I did several control experiments using 10-μg additions of gelatin either to the silver bromide (after hypobromite treatment) or to the hypo solution. In all cases I got a positive gold sol test with no interference from silver sulfide. Also I had done two experiments on photographic emulsions using lower silver concentrations, as recommended by Ballard *et al.*, and in both cases I got a negative gold sol test.

The difference in results remains unexplained. The evidence indicates that the difference is caused prior to dissolving the silver halide grains in hypo, as addition of gelatin at this stage always gave a positive gold sol test in my experiments.

It is hoped that further work will explain the difference in results. —P. Davis, *Kodak Research Laboratories, Wealdstone, Middlesex, England.*

PHOTOGRAPHIC SCIENCE AND ENGINEERING
Volume 2, Number 4, December 1958

On the Minimum Energy Detectable by Photographic Materials

Part II. Results for Four Current Kodak Films

R. CLARK JONES, *Research Laboratory, Polaroid Corporation, Cambridge, Mass.*

Data are given on the energy detectivity and contrast detectivity of four current Eastman Kodak films: Royal-X, Tri-X, Plus-X, and Panatomic-X. The results are substantially more accurate than those given in Part I because the new Kodak measurements were made on the same batch of each film and the data are based on monochromatic exposures. The minimum energy that can be detected by any detector involves not only the properties of the detector, but also the reliability of the detection, and the number of permitted false alarms. Accordingly, a simpler concept is used, that involves only the properties of the detector: the noise equivalent energy E_N, which is defined as the amount of signal energy that produces a density increment equal to the root-mean-square density fluctuation of the granularity. E_N is shown to be proportional to the diameter of a signal-receiving area A of circular shape, provided the area is large compared with L^2, where L is a length defined in terms of the point spread-function of the film. When the signal-receiving area is large compared with L^2, the detecting ability of the films is suitably described by the figure of merit $M_2 = 3 \times 10^{-4} A^{\frac{1}{2}}/E_N$ (A in square centimeters, E_N in ergs). The value of M_2 is thus independent of the signal area A, and is inversely proportional to the noise equivalent energy E_N. E_N is decreased by suitably pre-exposing the film. Results also are presented on the noise equivalent contrast C_N and its reciprocal, the contrast detectivity $\mathfrak{D}_C$.

1.0 Introduction

The present paper is a continuation of an earlier paper[1] that appeared in *Photographic Science and Technique*. The early paper, which will be referred to as Part I, presented results for four Kodak films made in 1945. The present paper presents results on four current Kodak films.

The results reported here not only cover more recent films, but, more importantly, are based on experimental data obtained from one batch of film. Thus the results are substantially more accurate than those in Part I.

The basic experimental data are the same as those used in a recent article in *PSⅇE*,[2] hereafter referred to as Ref. 2.

As explained in Part I, the actual subject of the papers is the noise equivalent energy of photographic materials. The noise equivalent energy is a purely physical concept, whereas the minimum detectable energy is a more complex concept that involves also the notions of the reliability of the detection, and the permitted fraction of false detections.

The chief results concerning the noise equivalent energy of the four films are given in Sec. 4.0, in Figs. 2 and 3, and in Tables B, C, and I through IV.

Presented at the Annual Conference, Rochester, N.Y., 8 October 1958. Received 27 May 1958.

The important situation where the light image on the film is of the same size or smaller than the minimum possible size of the photographic image is discussed in Part III (see page 198). (The minimum possible size of the silver image is determined primarily by the lateral scattering of the light during the exposing of the film.)

2.0 Experimental Data

The Eastman Kodak Company has very generously provided monochromatic sensitometric data and granularity data on four of its current films.

The four films are defined in Table A, along with

TABLE A
Names and Method of Development of the Four Films

Name	Abbreviation	Time (min)	Developer	Gamma
Kodak Royal-X Pan Film, Code 6128	Royal-X	5	DK-50	0.65
Eastman Tri-X Panchromatic Negative Film, Type 5233	Tri-X	6.5	SD-28	0.54
Eastman Plus-X Panchromatic Negative Film, Type 4231	Plus-X	6.5	SD-28	0.79
Kodak Panatomic-X Film, Code 5240	Pan-X	6	D-76	0.67

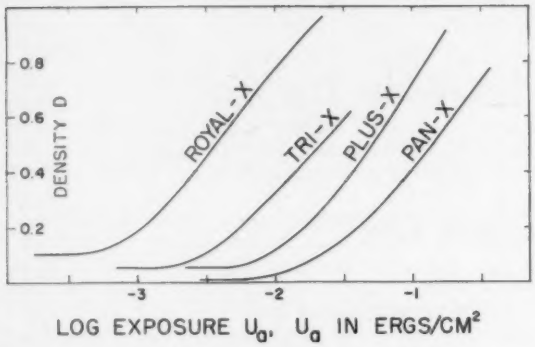

Fig. 1. Optical density of the developed films as a function of the 430 mμ exposure expressed in ergs per square centimeter.

abbreviated names, the conditions of development, and the resulting gammas.

Figure 1 shows the density vs. log exposure curves of the four films. The density D plotted is the density above base, and the exposure U is in ergs per square centimeter of 430 mμ radiation. The data used to plot the curves in Fig. 1 are tabulated in Table B of Ref. 2.

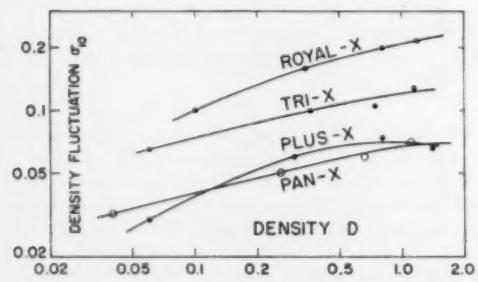

Fig. 2. Root-mean-square density fluctuation as a function of the mean optical density for the four films. The films were uniformly exposed to 430 mμ radiation. The ordinate is the root-mean-square density fluctuation measured with a circular aperture 10 μ in diameter.

Figure 2 shows the root-mean-square fluctuation σ_{10} of the density (measured with an aperture 10 μ in diameter) as a function of the film density. The data used to plot Fig. 2 are tabulated in Table C of Ref. 2. The same tables include evidence that the root-mean-square density fluctuation for other aperture diameters varies inversely as the diameter. This fact will be used in the next section.

The data in Figs. 1 and 2 are representative of the films at the time of manufacture, but it should be recognized that their characteristics can be expected to vary with manufacturing tolerances and may change as improvements are introduced into the products.

The reader will find in Ref. 2 a more detailed discussion of these data.

3.0 Theory

The noise equivalent energy of a photographic film is defined in general as the energy incident on the undeveloped film that produces in the developed film an increase of density equal to the root-mean-square density fluctuation.

The noise equivalent energy for a film that has received no other exposure is much larger than it is for a film that has received a suitable pre-exposure or post-exposure. Accordingly, in this paper we consider the noise equivalent energy as a function of the pre-exposure.

The discussions in this paper are confined to the situation in which the size of the (circular) image that constitutes the signal is large compared with L, where L is a length characteristic of the light-scattering in the undeveloped emulsion. The length L is defined in the following paper. With this restriction, the noise equivalent is proportional to the square root of the area of the signal image, for circular images with a diameter that is large compared with L.

If one measures the density of a uniformly exposed film with a small circular aperture at a number of different places, not all of the measured densities will be the same. They will have a mean value, and a root-mean-square deviation from the mean, which is denoted σ. The scatter in the measured values is due to the grain structure (the granularity) of the developed film. The value of σ depends of course on the kind of film, method of development, and on the amount of pre-exposure. The value of σ depends also on the diameter of the measuring aperture.

Suppose now that a pre-exposed film is exposed also to a circular signal image. This signal image will increase the density of the developed film at the corresponding point. If a photoelectric scanning system scans the surface of the developed film, the output will contain a signal pulse from the signal image, and will contain noise due to the granularity. Always subject to the condition that the signal image is large compared with L, it is easy to see that the ratio of peak signal to root-mean-square noise will have a sharp maximum when the aperture of the scanning system has a diameter equal to that of the signal. Accordingly, in the following paragraphs it is supposed that the density fluctuation that limits the detecting ability of a photographic material is the fluctuation measured with an aperture equal in size to that of the signal.

It is supposed throughout the paper that the density increments produced by the signal and those involved in the granularity are all so small that the derivative dD/dU is substantially constant over the range of densities involved.

In the following development, we shall wish to distinguish between the area A_s of the signal and the area A_a of the aperture used to measure σ. If the two areas are equal, the area will be denoted with both subscripts: A_{sa}.

We now proceed to derive an expression for the noise equivalent energy E_N in terms of the data given in Section 2.0.

We use the symbol σ to denote the mean-square density fluctuation, measured with a circular aperture of the same diameter as the signal image. Then the increase U_N in the exposure U that produces a density increment equal to σ is given by

$$U_N = \sigma dU/dD \tag{3.1}$$

and the energy increment that makes the same density increment is

$$E_N = \sigma A_{sa} dU/dD \tag{3.2}$$

where A_{sa} is the area of the region upon which the energy E_N is incident and is also the area of the aperture used to measure σ, and where dU/dD is the reciprocal of the slope of the D vs. U curve of the film.

The last equation supposes consistent units. With U expressed in ergs per square centimeter, A must be in square centimeters. It is convenient, however, to express the area of the signal image in square microns. We denote areas measured in square microns by $\mathfrak{A}$. The last equation then becomes

$$E_N = 10^{-8} \sigma \mathfrak{A}_{sa} dU/dD \tag{3.3}$$

E_N is in ergs if U is in ergs per square centimeter.

We now introduce explicitly the fact noted in Section 2.0: the root-mean-square density fluctuation σ varies inversely as the square root of the area of the scanned area. Thus one has

$$\sigma = (78.54/\mathfrak{A}_s)^{\frac{1}{2}} \sigma_{10} \tag{3.4}$$

where σ_{10} is the root-mean-square density fluctuation measured with a circular aperture 10 μ in diameter.

Equation (3.3) now becomes

$$E_N = 8.862 \times 10^{-8} \sigma_{10} \mathfrak{A}_{sa}^{\frac{1}{2}} dU/dD, \; A_{sa} \gg L^2 \tag{3.5}$$

In this expression the noise equivalent energy has been expressed in terms of the quantities presented in section 2.0 (σ_{10} and dD/dU) and in terms of the area $\mathfrak{A}_{sa}$ of the signal.

The noise equivalent energy is in some respects an upside-down measure of the detecting ability of a photographic material. The better the detecting ability, the *smaller* is E_N. To escape this difficulty, it has become customary to use the reciprocal of E_N, called the detectivity,[3] or more accurately, the energy detectivity. The detectivity is denoted $\mathfrak{D}$ and is defined by

$$\mathfrak{D} = \frac{1.13 \times 10^7}{\sigma_{10} \mathfrak{A}_{sa}^{\frac{1}{2}}} \frac{dD}{dU} \tag{3.6}$$

The last expression shows that the detectivity varies as the inverse square root of the area $\mathfrak{A}_{sa}$. Many different kinds of detectors, including such diverse kinds as bolometers, thermocouples, photoconductive cells, photoemissive tubes, and image orthicons (and, under suitable restrictions, also human vision and radio antennas) have detectivities that are inversely proportional to the square root of the sensitive area of the detector. In order to obtain a measure of the detectivity that is independent of the area of the detector, the writer introduced[4] in 1949 a figure of merit denoted by M_2 and defined by

$$M_2 = 3 \times 10^{-8} \mathfrak{A}^{\frac{1}{2}} \mathfrak{D} \tag{3.7}$$

where $\mathfrak{A}$ is in square microns, and $\mathfrak{D}$ in reciprocal ergs. (The numerical coefficient was introduced to make M_2 have a value near unity for many detectors.)

By combining the last two equations, one finds

$$M_2 = \frac{0.3385}{\sigma_{10}} \frac{dD}{dU} \tag{3.8}$$

We conclude this discussion of energy detectivity by restating Eqs. (3.5) and (3.6) for an arbitrarily chosen signal that is 50 μ in diameter:

$$E_N(50\,\mu) = 3.927 \times 10^{-6} \sigma_{10} dU/dD \tag{3.9}$$

$$\mathfrak{D}(50\,\mu) = 2.546 \times 10^5 (dD/dU)/\sigma_{10} \tag{3.10}$$

We now derive expressions for the noise equivalent contrast C_N and its reciprocal the contrast detectivity $\mathfrak{D}_c$.

The contrast of a signal is defined in general by

$$C = \Delta U/U \tag{3.11}$$

where ΔU is the exposure increment, and U is the total exposure of the surrounding region of the film.

The noise equivalent value of the contrast is now simply defined as the value of C when ΔU is equal to the noise equivalent value U_N:

$$C_N = \frac{\sigma}{U} \frac{dU}{dD} \tag{3.12}$$

whence

$$\mathfrak{D}_c = \frac{U}{\sigma} \frac{dD}{dU} \tag{3.13}$$

For the arbitrarily selected signal 50 μ in diameter, the last two expressions become

$$C_N(50\,\mu) = \frac{\sigma_{10}}{5U} \frac{dU}{dD} \tag{3.14}$$

and

$$\mathfrak{D}_c(50\,\mu) = \frac{5U}{\sigma_{10}} \frac{dD}{dU} \tag{3.15}$$

We shall now establish an interesting relation between the detectivities (energy and contrast) and the detective quantum efficiency Q that is the subject of Ref. 2. We shall show that if log Q is plotted versus log U, as for example in Fig. 4 of Ref. 2, the point of this curve where the slope is +1 corresponds to the exposure U at which the energy detectivity $\mathfrak{D}$ has its maximum value. We shall show also that the point on this curve where the slope is −1 corresponds to the exposure where the contrast detectivity $\mathfrak{D}_c$ has its maximum value.

Reference 2 gives the following expression for the detective quantum efficiency Q of a photographic film:

$$Q = \frac{\mathcal{E} U}{A} \left(\frac{dD}{\sigma dU} \right)^2 \tag{3.16}$$

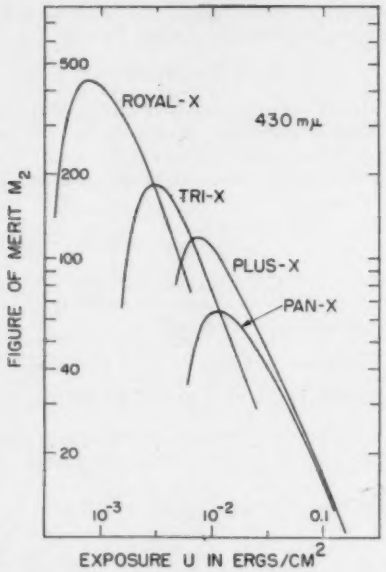

Fig. 3. The figure of merit M_2 of the four films vs. the pre-exposure U in ergs per square centimeter of 430 mμ radiation. The figure of merit M_2 is defined by Eq. (3.7) and is a reciprocal measure of the noise equivalent energy. M_2 is designed to be independent of the area of the signal, provided that the size of the signal is so large that spreading of the image by light scattering in the negative may be ignored. The numerical value of the maximum values of M_2 for each of the films is shown in Table B. M_2 is dimensionless.

where $\mathcal{E}$ denotes the energy of a single photon, and the other symbols are those used in this paper. Logarithmic differentiation then yields

$$\text{Slope} = \frac{d \log \mathcal{Q}}{d \log U} = 1 + 2 \frac{d \log (dD/\sigma dU)}{d \log U} \qquad (3.17)$$

If now the slope is set equal to $+1$, the last equation states

$$\frac{d(dD/\sigma dU)}{dU} = 0 \qquad (3.18)$$

which is just the condition that the energy detectivity $\mathcal{D}$ as given by Eq. (3.6) have a stationary value. If the slope is set equal to -1, Eq. (3.17) states

$$\frac{d(UdD/\sigma dU)}{dU} = 0 \qquad (3.19)$$

which is just the condition that the contrast detectivity $\mathcal{D}_c$ as given by Eq. (3.13) have a stationary value.

Thus if one has a curve of $\mathcal{Q}$ vs. U plotted in logarithmic paper, this curve permits one to determine the exposures corresponding to the maximum value of all three of the most interesting parameters. The conditions for the maximum values of the three parameters can be written in the same form

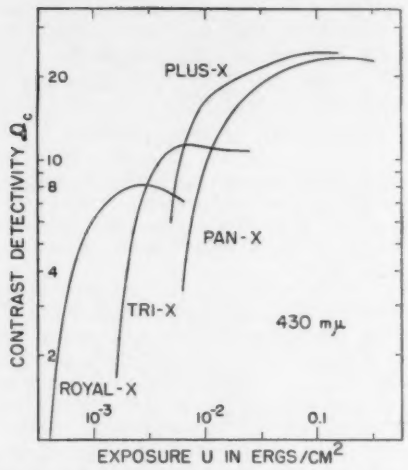

Fig. 4. Showing the contrast detectivity $\mathcal{D}_c$ of the four films vs. the pre-exposure U in ergs per square centimeter of 430 mμ blue light. The data plotted are for a signal image that is 50 μ in diameter. This diameter is arbitrarily chosen, and is assumed to be so large that light spreading in the negative may be ignored. The numerical value of the maximum value of $\mathcal{D}_c$ for each of the four films is shown in Table C. $\mathcal{D}_c$ is dimensionless.

$$\frac{d(U^k dD/\sigma dU)}{dD} = 0 \qquad (3.20)$$

where the exponent k has the values 0, $\frac{1}{2}$, and 1 for the three parameters $\mathcal{D}$, $\mathcal{Q}$, and $\mathcal{D}_c$, respectively.

4.0 Numerical Results

The results of this section are shown in Tables I through IV, each table dealing with one of the four films. Some of the results are plotted in Figs. 3 and 4.

In each of the four tables, the first column shows the value of $\log_{10}U$ for all of the other entries in that row. The second column shows 100 U, and the third shows 100 ΔU, where ΔU is defined as the difference between the values of U at the midpoints of the intervals on either side of the tabulated value of U. ΔU is given by

$$\Delta U = 0.23077\, U \qquad (4.1)$$

The fourth column shows the density D, and the fifth shows 10 ΔD, where ΔD is defined as the difference between the values of D at the midpoints of the interval on either side of the tabulated value of D. Finally, the sixth column shows the root-mean-square density fluctuation σ_{10}. The method of obtaining the entries in the tables from the data supplied by the Eastman Kodak Company is described in detail in Ref. 2.

The ratio $\Delta D/\Delta U$ is the finite-difference approximation to the derivative dD/dU, and is tabulated in the seventh column of the tables. With the help of Eq. (4.1), we find the following expressions:

$$E_N = 3.927 \times 10^{-6}\, \sigma_{10}\Delta 10/\Delta D \qquad (4.2)$$

$$\mathfrak{D}(50\,\mu) = 2.546 \times 10^{5}\, \Delta D/\sigma_{10}\Delta U \qquad (4.3)$$

$$M_2 = 0.3385\, \Delta D/\sigma_{10}\Delta U \qquad (4.4)$$

$$C_N(50\,\mu) = 0.4615\, \sigma_{10}/\Delta D \qquad (4.5)$$

$$\mathfrak{D}_c(50\,\mu) = 21.667\, \Delta D/\sigma_{10} \qquad (4.6)$$

where E_N is in ergs, where $\mathfrak{D}$ is in reciprocal ergs, and the other three quantities are dimensionless. These five quantities are tabulated in the last five columns of Tables I through IV.

In Fig. 3, the figure of merit M_2 is plotted against the logarithm of the exposure U, and in Fig. 4 the contrast detectivity $\mathfrak{D}_c$ for a 50 μ signal is plotted against the logarithm of the exposure.

5.0 Discussion of Results

Probably the most striking aspect of the results shown in Fig. 3 is the existence of a pronounced maximum in the figure of merit for each film at an intermediate value of the exposure. This writer has little doubt that the qualitative explanation for these maxima is the same as that offered for the maxima in the detective quantum efficiency curves in Ref. 2. Each grain requires a finite number of photons to make it developable. A finite exposure of the film is required to supply this number. A larger number of photons does not make that grain any more developable; development of a grain is an all-or-none process. The maximum thus occurs at the exposure where a goodly number of the grains have received the requisite number of quanta. On the basis of this explanation, there would be no relative maximum if the absorption of a single photon were sufficient to make a grain developable; the figure of merit would have its greatest value for zero pre-exposure.

The figure of merit may of course be plotted against any of the other parameters in Tables I-IV. In particular, it may be plotted against the density D, or the gradient $g = dD/d \log U = 10\, \Delta D$. As a practical replacement for such a large number of plots, we show in Table B for each film the values of log U, D, g, γ and g/γ, as well as M_2 itself, for the exposure U that corresponds to the maximum value of M_2.

For the four films discussed in Part I, it was found that at the maximum value of M_2 the ratio of the gradient g to the maximum gradient γ was in every case close to 0.3, and it was there suggested that this might be a working rule valid for many films. The results shown in Table B, however, do not support

TABLE I

Data and Results for Royal-X Film

$\log_{10} U$	100 U (erg/cm²)	100 ΔU (erg/cm²)	D	10 ΔD	σ_{10}	$\Delta D/\Delta U$ (cm²/erg)	$10^9 E_N(50\,\mu)$ (ergs)	$10^{-6}\mathfrak{D}(50\,\mu)$ (erg^{-1})	M_2	$C_N(50\,\mu)$ (per cent)	$\mathfrak{D}_c(50\,\mu)$
−3.4	0.03981	0.009191	0.1075	0.045	0.1040	48.96	8.340	119.9	159.4	106.7	0.9376
−3.3	0.05012	0.01156	0.1155	0.115	0.1070	99.47	4.225	236.7	314.7	42.94	2.329
−3.2	0.06311	0.01456	0.1310	0.197	0.1120	135.3	3.251	307.6	408.9	26.24	3.811
−3.1	0.07944	0.01834	0.1555	0.282	0.1200	153.8	3.065	326.3	433.7	19.64	5.092
−3.0	0.1000	0.02307	0.1885	0.365	0.1294	158.2	3.212	311.3	413.9	16.36	6.112
−2.9	0.1259	0.02910	0.2290	0.444	0.1392	152.6	3.583	279.1	371.0	14.47	6.911
−2.8	0.1585	0.03650	0.2765	0.514	0.1487	140.8	4.148	241.1	320.5	13.35	7.489
−2.7	0.1995	0.04610	0.3310	0.573	0.1575	124.3	4.978	200.9	267.1	12.69	7.883
−2.6	0.2512	0.05791	0.3910	0.618	0.1654	106.7	6.086	164.3	218.4	12.35	8.096
−2.5	0.3162	0.07301	0.4545	0.643	0.1726	88.07	7.698	129.9	172.7	12.39	8.072
−2.4	0.3981	0.09191	0.5195	0.650	0.1790	70.72	9.940	100.6	133.7	12.71	7.868
−2.3	0.5012	0.1156	0.5845	0.644	0.1848	55.70	13.03	76.76	102.0	13.24	7.551
−2.2	0.6311	0.1456	0.6490	0.625	0.1900	42.92	17.39	57.52	76.47	14.03	7.127

TABLE II

Data and Results for Tri-X Film

$\log_{10} U$	100 U (ergs/cm²)	100 ΔU (erg/cm²)	D	10 ΔD	σ_{10}	$\Delta D/\Delta U$ (cm²/erg)	$10^9 E_N(50\,\mu)$ (ergs)	$10^{-6}\mathfrak{D}(50\,\mu)$ (erg^{-1})	M_2	$C_N(50\,\mu)$ (per cent)	$\mathfrak{D}_c(50\,\mu)$
−2.8	0.1585	0.03650	0.0575	0.050	0.0645	13.70	18.49	54.08	71.89	59.52	1.680
−2.7	0.1995	0.04610	0.0665	0.125	0.0667	27.11	9.662	103.5	137.6	24.62	4.061
−2.6	0.2512	0.05791	0.0840	0.210	0.0706	36.27	7.645	130.8	173.9	15.52	6.445
−2.5	0.3162	0.07301	0.1095	0.295	0.0754	40.41	7.326	136.5	181.4	11.80	8.477
−2.4	0.3981	0.09191	0.1425	0.370	0.0804	40.26	7.843	127.5	169.5	10.03	9.971
−2.3	0.5012	0.1156	0.1825	0.430	0.0854	37.19	9.017	110.9	147.4	9.166	10.91
−2.2	0.6311	0.1456	0.2275	0.470	0.0902	32.28	10.97	91.12	121.1	8.857	11.29
−2.1	0.7944	0.1834	0.2755	0.490	0.0946	26.71	13.91	71.91	95.60	8.913	11.22
−2.0	1.000	0.2307	0.3250	0.504	0.0986	21.84	17.72	56.42	74.99	9.025	11.08
−1.9	1.259	0.2910	0.3755	0.515	0.1021	17.70	22.66	44.14	58.67	9.149	10.93
−1.8	1.585	0.3650	0.4270	0.525	0.1051	14.38	28.69	34.85	46.32	9.242	10.82
−1.7	1.995	0.4610	0.4795	0.534	0.1076	11.58	36.48	27.41	36.44	9.302	10.75
−1.6	2.512	0.5791	0.5330	0.540	0.1096	9.325	46.15	21.67	28.80	9.363	10.68

TABLE B

Values of Several Quantities at the Exposure that Maximizes M_2

Film	log U (ergs/cm²)	M_2	D	g	γ	g/γ
Royal-X	−3.12	435	0.150	0.266	0.65	0.41
Tri-X	−2.52	182	0.102	0.278	0.54	0.51
Plus-X	−2.13	120	0.082	0.215	0.79	0.27
Pan-X	−1.95	64	0.033	0.152	0.67	0.23

this hypothesis; the values of g/γ at the maximum of M_2 range from 0.23 to 0.51.

The maxima in the $\mathfrak{D}_c$ vs. log exposure curves of Fig. 4 are by no means as pronounced as the maxima in Fig. 3, but each curve does show a relative maximum. For each film, the curve will of course drop further if it is continued to the right, but for at least one of the films this happens only if the exposure is increased considerably.

TABLE C

Values of Several Quantities at the Exposure that Maximizes $\mathfrak{D}_c$

Film	log U (ergs/cm²)	$\mathfrak{D}_c$	D	g	γ	g/γ
Royal-X	−2.57	8.1	0.410	0.628	0.65	0.96
Tri-X	−2.16	11.3	0.247	0.479	0.54	0.89
Plus-X	−1.00	24.3	0.718	0.790	0.79	1.0
Pan-X	−0.75	23.3	0.565	0.653	0.67	0.97

The contrast detectivity $\mathfrak{D}_c$ may also be plotted against quite a number of different quantities. Table C is offered as a replacement of these plots. It shows the same quantities as in Table B for the exposure that maximizes the contrast detectivity $\mathfrak{D}_c$.

The energy detectivity (as measured by M_2) of Royal-X is more than twice as great as that of Tri-X, and the rank order of the four films for energy detectivity is the same as the rank order of their ASA

TABLE III

Data and Results for Plus-X Film

$\log_{10} U$	100 U (ergs/cm²)	100 ΔU (ergs/cm²)	D	10 ΔD	σ_{10}	$\Delta D/\Delta U$ (cm²/erg)	$10^9 E_N(50\mu)$ (ergs)	$10^{-6}\mathfrak{D}(50\mu)$ (erg^{-1})	M_2	$C_N(50\mu)$ (per cent)	$\mathfrak{D}_c(50\mu)$
−2.3	0.5012	0.1156	0.0585	0.090	0.0295	7.785	14.88	67.20	89.33	15.13	6.610
−2.2	0.6311	0.1456	0.0710	0.162	0.0327	11.12	11.54	86.63	115.2	9.320	10.73
−2.1	0.7944	0.1834	0.0910	0.237	0.0369	12.92	11.21	89.17	118.5	7.184	13.92
−2.0	1.000	0.2307	0.1185	0.312	0.0417	13.52	12.11	82.58	109.8	6.169	16.21
−1.9	1.259	0.2910	0.1535	0.383	0.0467	13.16	13.94	71.76	95.39	5.627	17.77
−1.8	1.585	0.3650	0.1955	0.450	0.0516	12.33	16.44	60.84	80.87	5.291	18.90
−1.7	1.995	0.4610	0.2435	0.512	0.0561	11.10	19.84	50.41	67.01	5.058	19.77
−1.6	2.512	0.5791	0.2975	0.570	0.0600	9.844	23.93	41.78	55.54	4.859	20.58
−1.5	3.162	0.7301	0.3570	0.624	0.0632	8.547	29.04	34.44	45.78	4.675	21.39
−1.4	3.981	0.9191	0.4215	0.673	0.0657	7.322	35.24	28.38	37.73	4.505	22.20
−1.3	5.012	1.156	0.4905	0.716	0.0675	6.193	42.81	23.36	31.06	4.352	22.98
−1.2	6.311	1.456	0.5635	0.752	0.0688	5.164	52.33	19.11	25.41	4.223	23.68
−1.1	7.944	1.834	0.6400	0.776	0.0697	4.231	64.68	15.46	20.55	4.146	24.12
−1.0	10.00	2.307	0.7185	0.790	0.0703	3.424	80.65	12.40	16.49	4.107	24.35
−0.9	12.59	2.910	0.7975	0.790	0.0706	2.714	100.3	9.791	13.02	4.124	24.25
−0.8	15.85	3.650	0.8765	0.790	0.0706	2.164	128.1	7.806	10.38	4.124	24.25

TABLE IV

Data and Results for Pan-X Film

$\log_{10} U$	100 U (ergs/cm²)	100 ΔU (ergs/cm²)	D	10 ΔD	σ_{10}	$\Delta D/\Delta U$ (cm²/erg)	$10^9 E_N(50\mu)$ (ergs)	$10^{-6}\mathfrak{D}(50\mu)$ (erg^{-1})	M_2	$C_N(50\mu)$ (per cent)	$\mathfrak{D}_c(50\mu)$
−2.2	0.6311	0.1456	0.0120	0.040	0.0237	2.747	33.89	29.51	39.23	27.34	3.657
−2.1	0.7944	0.1834	0.0180	0.080	0.0262	4.362	23.59	42.39	56.35	15.11	6.616
−2.0	1.000	0.2307	0.0285	0.126	0.0291	5.461	20.92	47.79	63.53	10.66	9.382
−1.9	1.259	0.2910	0.0445	0.177	0.0323	6.082	20.86	47.95	63.74	8.425	11.87
−1.8	1.585	0.3650	0.0660	0.230	0.0356	6.301	22.19	45.07	59.91	7.143	14.00
−1.7	1.995	0.4610	0.0925	0.283	0.0388	6.138	24.82	40.29	53.55	6.329	15.80
−1.6	2.512	0.5791	0.1240	0.336	0.0419	5.802	28.36	35.26	46.88	5.757	17.37
−1.5	3.162	0.7301	0.1605	0.388	0.0448	5.314	33.10	30.21	40.16	5.328	18.77
−1.4	3.981	0.9191	0.2015	0.437	0.0475	4.755	39.23	25.49	33.88	5.018	19.93
−1.3	5.012	1.156	0.2465	0.483	0.0500	4.178	46.99	21.28	28.28	4.778	20.93
−1.2	6.311	1.456	0.2960	0.524	0.0523	3.598	57.08	17.52	23.29	4.606	21.71
−1.1	7.944	1.834	0.3500	0.562	0.0544	3.064	69.74	14.34	19.07	4.468	22.38
−1.0	10.00	2.307	0.4080	0.595	0.0564	2.579	85.91	11.64	15.48	4.374	22.86
−0.9	12.59	2.910	0.4690	0.623	0.0582	2.141	106.8	9.367	12.45	4.312	23.19
−0.8	15.85	3.650	0.5325	0.645	0.0599	1.767	133.1	7.511	9.985	4.286	23.33
−0.7	19.95	4.610	0.5980	0.661	0.0614	1.434	168.2	5.946	7.904	4.288	23.32
−0.6	25.12	5.791	0.6645	0.670	0.0628	1.157	213.1	4.692	6.237	4.325	23.12
−0.5	31.62	7.301	0.7315	0.670	0.0640	0.9177	273.9	3.651	4.854	4.409	22.68

TABLE D
Figure of Merit M_2 for the Optimum Wavelength

Film	$M_{2,430}$	S_{430} (cm²/erg)	S_m (cm²/erg)	λ_m (mμ)	$M_{2,m}$
Royal-X	435	33.9	35.5	400	456
Tri-X	182	5.45	6.60	605	220
Plus-X	120	0.943	0.965	600	123
Pan-X	64	0.463	0.660	590	91

speeds. The rank order is reversed for contrast detectivity, except that Plus-X comes out slightly higher than Pan-X.

Since the four films rank in opposite order for the two criteria of energy detectivity and contrast detectivity, it is natural to inquire whether there is not some intermediate criterion by which all of the films will be rated equally. The answer, of course, is that there is such a criterion: It is the concept of detective quantum efficiency described in Ref. 2. It is there shown that the maximum detective quantum efficiency of the four films is about the same (about 0.7%), except that Pan-X comes out somewhat lower (about 0.3%).

The results given so far in this section are of course all for the radiation wavelength 430 mμ. Information on the films for other wavelengths is not available for the same batches of emulsion. Data are available, however, for the same types of film, but taken on other batches. The Eastman Kodak Company has kindly supplied information on the absolute sensitivity S of the four films as a function of the wavelength. The sensitivity is defined as the reciprocal of the exposure (measured in ergs per square centimeter) required to produce a density of 1.0 above the gross fog density. The sensitivity of each of the four films is plotted as a function of the wavelength in Fig. 5. To the extent that one may assume (1) that a change of wavelength merely shifts the D vs. log U curves sidewise without changing their shape, and (2) that the granularity at a given density is independent of the wavelength, the figure of merit M_2 will vary with the wavelength in the same way that S does. Thus the data in Fig. 5 may be used to estimate the figure of merit for radiation wavelengths other than 430 mμ. Furthermore, to the extent that these assumptions are true, the contrast detectivity is independent of the wavelength.

With the help of the data in Fig. 5 and the assumption stated above, we may compute the value of M_2 that is a maximum with respect to both pre-exposure and wavelength. The details are shown in Table D. The second column shows the value of M_2 at 430 mμ at the optimum pre-exposure indicated in Table B; the third column shows the sensitivity S at 430 mμ; the fourth column indicates the maximum value of S;

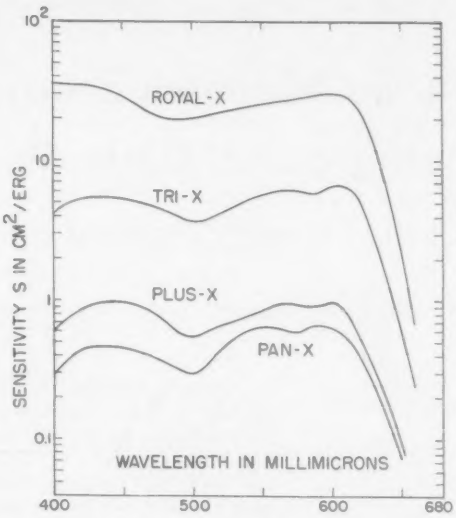

Fig. 5. Sensitivity S vs. the wavelength λ. S is measured in square centimeters per erg and λ is measured in millimicrons. S is defined as the exposure required to produce a density of 1.0 above the gross fog density. On the basis of suitable assumptions discussed in the text, M_2 varies with wavelength in the same way as S, and thus the data in this figure may be used to estimate the value of M_2 for wavelengths other than 430 mμ (see Table D).

the fifth column shows the wavelength at which it occurs; and, finally, the last column shows the figure of merit M_2 for the wavelength in the fifth column, computed by the relation

$$M_{2,m} = M_{2,430} S_m / S_{430} \qquad (5.1)$$

Acknowledgment

The writer wishes again to thank the Eastman Kodak Company for their generosity in supplying the unpublished data on their current films. He is particularly indebted to George C. Higgins and Hans J. Zweig for many stimulating discussions about the subject of this paper.

References

1. Jones, R. Clark, "On the Minimum Energy Detectable by Photographic Negatives," *Phot. Sci. & Tech.*, 2: 56 (1955).
2. ———, "On the Quantum Efficiency of Photographic Negatives," *Phot. Sci. & Eng.*, 2: 57 (1958).
3. ———, "Detectivity: The Reciprocal of Noise Equivalent Input of Radiation," *Nature*, 170: 937 (1952).
4. ———, "Factors of Merit for Radiation Detectors," *J. Opt. Soc. Am.*, 39: 344 (1949). M_2 is described also in an article by the same author, "Performance of Detectors for Visible and Infrared Radiation," in *Adv. in Electronics*, Vol. 5, Academic Press, New York, 1953, pp. 1–96.

PHOTOGRAPHIC SCIENCE AND ENGINEERING
Volume 2, Number 4, December 1958

On the Minimum Energy Detectable by Photographic Materials

Part III. Energy Incident on a Microscopic Area of the Film

R. CLARK JONES, *Research Laboratory, Polaroid Corporation, Cambridge, Mass.*

A method is described for evaluating rigorously the minimum energy that is detectable by a photographic film when the energy to be detected is incident on a very small area of the film. The method is applied to four current Kodak films: Royal-X, Tri-X, Plus-X, and Panatomic-X; values ($\times 10^{-9}$) of 1.47, 3.04, 5.39, and 4.12 ergs, respectively, are found at the wavelength that maximizes the energy detectivity $\mathfrak{D}$ of the film. In deriving the results given, it was necessary to start with the line spread-functions measured by Zweig, Higgins, and MacAdam, and to derive the point spread-functions of the films. This was done by finding an analytic representation of the line spread-functions measured by these authors.

The expression derived for the noise equivalent energy holds whenever the diameter of the light-image is small compared with a length L, which is a measure of the diameter of the developed image when the light is incident on a point of the film. The length L is defined in terms of the point spread-function of the film. Comparison of the expression found in this paper with that found in Part II, where the opposite assumption was made (that the area A of the light-image was large compared with L^2) shows that the noise equivalent energy is identical with that found in Part II, except that the area A is replaced by L^2. A sketch is given of the relation between the noise equivalent energies for light-images small and large compared with L.

1.0 Introduction

The noise equivalent energies found in Part II (see page 191) are valid only if the signal-receiving area is so large that one may ignore the spreading of the developed image by light scattering during the exposing of the film.

In this paper we consider the opposite situation, i.e., the situation in which the size of the developed image is so small that it is determined primarily by the light scattering in the undeveloped film.

The situation discussed here is of course very important if we wish to know the smallest possible value of the noise equivalent energy. Since the noise equivalent energy for large signal areas has been shown to vary as the square root of the area, it is clear that to minimize the noise equivalent energy, one will reduce the area of the signal. As the area is decreased, it ceases to be large compared with L^2, and the theory given in Part II breaks down.

The relation between the noise equivalent energy E_N and the area A of the illuminated region of the film is sketched in Fig. 1. For areas A large compared with L, the noise equivalent energy is proportional to $A^{1/2}$, as indicated by the diagonal line in Fig. 1. As the area decreases, however, the noise equivalent energy fails to follow the line and approaches a finite value as the area approaches zero. The value of $A^{1/2}$ at which the horizontal dashed line crosses the diagonal line is equal to L.

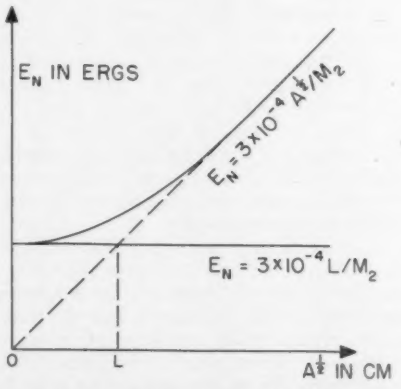

Fig. 1. A sketch suggesting the way that the noise equivalent energy E_N depends on the illuminated area A of the film. When the area is large compared with L^2, the value of E_N is proportional to $A^{\frac{1}{2}}$, as indicated by the diagonal line and by the diagonal equation, which is derived from Eq. (3.7) of Part II. When, however, the area is small compared with L^2, the value of E_N is independent of the area A, as indicated by the horizontal line and the horizontal equation, which is derived from Eq. (2.13) of this paper. The length L corresponds to the intersection of the two lines.

Presented at the Annual Conference, Rochester, N.Y., 8 October 1958. Received 27 May 1958; revised 11 August 1958.

The importance of the noise equivalent energy when the energy is incident on a microscopically small area of the film has been very properly emphasized in a paper by Zweig, Higgins, and MacAdam.[1] The treatment in the cited paper emphasizes the physical concepts, and is less than rigorous in the mathematical evaluation of the problem.

The theory developed in Sec. 2.0 is applied in Sec. 3.0 to the four Kodak films discussed in Part II, and described in Table A of that paper (see page 191).

2.0 Theory

The density distribution produced by a point light-image is called the point spread-function, and is here denoted by $Q(r)$, where r is the radial distance. $Q(r)$ is here defined as the density increment produced at the distance r from the point image when the point image contains the energy E. (The amount of the energy E is of course limited by the condition that the density increment it produces may not effect more than a small change in the derivative dD/dU.) One then finds that the integral of $Q(r)$ over the surface of the film is equal to E times dD/dU.

$$EdD/dU = 2\pi \int_0^\infty Q(r) r dr \qquad (2.1)$$

This equation is easily derived by considering a uniform image as a superposition of a large number of point images.

Suppose now that we scan the film with a densitometer equipped with a small aperture, and consider the ratio of the peak signal voltage S to the root-mean-square noise voltage N that is produced by scanning over the granularity. This situation is considered in detail by the writer in a 1955 article,[2] where it is shown that an upper bound to S/N is given by

$$\left(\frac{S}{N}\right)^2 \leqslant \int_\infty \int \frac{|\theta(k_1,k_2)|^2}{n(k_1,k_2)}\, dk_1 dk_2 \qquad (2.2)$$

where $\theta(k_1,k_2)$ is the two dimensional Fourier transform of $Q(r)$, and where $n(k_1,k_2)$ is the noise spectrum of the granularity of the film. The upper bound is in fact achieved if and only if the shape of the scanning aperture is such that its Fourier transform $v(k_1,k_2)$ is given by

$$v(k_1,k_2) = \text{const.}\,\theta^*(k_1,k_2)/n(k_1,k_2) \qquad (2.3)$$

where θ^* is the complex conjugate of θ.

Zweig[2] has recently shown that it is a reasonable approximation to his granularity data to require that the noise spectrum $n(k_1,k_2)$ be a constant independent of k_1 and k_2.

This fact has three consequences. First, n is given by

$$n = A_a \sigma^2 \qquad (2.4)$$

where σ is the root-mean-square density fluctuation measured with an aperture of area A_a. Second, the filter function v is a constant multiple of θ^*, from which it follows that the function $u(r)$ that describes the transmittance of the scanning aperture at the radius r is proportional to $Q(r)$:

$$u(r) = \text{const.}\,Q(r) \qquad (2.5)$$

In words, the shape of the scanning aperture must be the same as the shape of the point spread-function. Third, Eq. (2.2) becomes

$$(S/N)^2 \leqslant (A_a\sigma^2)^{-1} \int_\infty \int |\theta(k_1,k_2)|^2 dk_1 k_2 \qquad (2.6)$$

The integral on the right may be transformed by Plancherel's theorem thus:

$$(S/N)^2 \leqslant (2\pi/A_a\sigma^2) \int_0^\infty Q^2(r) r dr \qquad (2.7)$$

Henceforth, it is supposed that the optimum aperture is in fact used, so that the equality holds in the last expression.

We now combine Eqs. (2.1) and (2.7), with the result

$$\frac{S}{N} = \frac{E}{A_a^{1/2}\sigma L}\frac{dD}{dU} \qquad (2.8)$$

where the length L is defined by

$$L = \frac{2\pi \int Q(r) r dr}{[2\pi \int Q^2(r) r dr]^{1/2}} \qquad (2.9)$$

The value of E that makes $S = N$ is of course the noise equivalent energy E_N. Thus one finds

$$E_N = A_a^{1/2}\sigma L dU/dD \qquad (2.10)$$

Just as in Part II, we now prefer to have A and L measured in microns instead of centimeters; we denote the quantities so measured as $\mathfrak{A}$ and $\mathfrak{L}$. We also recall that $A_a\sigma^2$ is independent of A_a, whence

$$\mathfrak{A}_a\sigma^2 = 78.54\sigma_{10}^2 \qquad (2.11)$$

Equation (2.10) then becomes

$$E_N = 8.862 \times 10^{-8}\, \sigma_{10} \mathfrak{L} dU/dD,\ A_a \ll L^2 \qquad (2.12)$$

We compare the last equation with Eq. (3.5) of Part II, and note that they differ only in that $\mathfrak{L}$ occurs in (2.12) where $\mathfrak{A}_{sa}^{1/2}$ occurs in (3.5). In order to obtain the noise equivalent value for a point signal-image from the noise equivalent value for large signal diameters, one simply replaces $\mathfrak{A}_{sa}^{1/2}$ in (3.5) by the length $\mathfrak{L}$.

This result may be expressed in another form. The preceding paper contains numerical information about the figure of merit M_2 of the four films. If we know not only M_2, but also the length $\mathfrak{L}$, the noise equivalent energy E_N or its reciprocal $\mathfrak{D}$ for a point signal is given by

$$E_N^{-1} = \mathfrak{D} = \frac{M_2}{3 \times 10^{-5}\mathfrak{L}} \qquad (2.13)$$

It is clear from examination of the expression (2.9) that the value of L is independent of the normalization of $Q(r)$. In the calculation of L it is convenient to normalize $Q(r)$ by the requirement $Q(0) = 1$. Then

the integrals in the numerator and denominator are both areas that satisfy the condition

$$L^2 \geqslant A_1 \geqslant A_2 \tag{2.14}$$

where A_1 and A_2 are defined by

$$A_1 = 2\pi \int Q(r) r dr \tag{2.15}$$

and

$$A_2 = 2\pi \int Q^2(r) r dr \tag{2.16}$$

L itself is then given by

$$L = A_1 / A_2^{1/2} \tag{2.17}$$

3.0 Results for the Four Films

The data of Zweig, Higgins, and MacAdam[1] provide the (experimentally-determined) line spread-functions of the four films, reproduced in Fig. 5. But the theory developed in Sec. 2.0 is based on the point spread-function. Accordingly, it is necessary to compute the point spread-function $Q(r)$ from the line spread function $A(x)$.

The relations between these two functions and between these functions and the transfer function (alternately called the spatial frequency response) are the subject of a recent article.[4] Six relations exist among the three functions, such that given any one function, the other two may be calculated. The six relations are

$$A(x) = \int_{-\infty}^{\infty} T(k) \cos 2\pi kx \, dk \tag{I}$$

$$T(k) = \int_{-\infty}^{\infty} A(x) \cos 2\pi kx \, dx \tag{II}$$

$$Q(r) = 2\pi \int_0^{\infty} T(k) J_0(2\pi kr) k dk \tag{III}$$

$$T(k) = 2\pi \int_0^{\infty} Q(r) J_0(2\pi kr) r dr \tag{IV}$$

$$A(x) = 2 \int_x^{\infty} Q(r)(r^2 - x^2)^{-1/2} r dr \tag{V}$$

$$Q(r) = -\frac{1}{\pi} \frac{d}{dr} \int_r^{\infty} \frac{A(x) dx}{x(x^2 - r^2)^{1/2}} \tag{VI}$$

where the transfer function is denoted by $T(k)$ and where all three of the functions are normalized by the condition that $T(0)$ is unity. It follows that the $Q(r)$ and $A(x)$ satisfy the conditions:

$$\int_{-\infty}^{\infty} A(x) dx = 1 \tag{3.1}$$

$$2\pi \int_0^{\infty} Q(r) r dr = 1 \tag{3.2}$$

The function J_0 is the usual Bessel function of the first kind.

The relation (VI) that gives the point spread-function $Q(r)$ in terms of the line spread-function $A(x)$ is not a relation that is easily adapted to numerical integration. Accordingly, the writer has chosen to employ an analytic function that is a reasonably close approximation to the experimental line spread-functions.

The photographic literature suggests several possible analytic functions. Schade measured the transfer function of three Kodak films and reported[5] in 1948 that all three films could be represented by the relation

$$T(k) = e^{-2\pi a|k|} \tag{3.3}$$

where a is length, and is different for each of the films. (See Ref. 4 for further details.) Ingelstam, Djurle, and Sjögren[6] have suggested a line spread-function of the form

$$A(x) = A_0 e^{-2\pi b|x|} \tag{3.4}$$

and Sayanagi[7] has suggested a point spread-function of the form

$$Q(r) = Q_0 e^{-2\pi cr} \tag{3.5}$$

He has shown that this function represents the experimental data of Ingelstam et al. for Panatomic-X film.

The three functions $T(k)$, $A(x)$, and $Q(r)$ for each of these suggestions are as follows:

Exponential transfer function:

$$T(k) = e^{-2\pi a|k|} \tag{3.6}$$

$$A(x) = \frac{a}{\pi(a^2 + x^2)} \tag{3.7}$$

$$Q(r) = \frac{a}{2\pi(a^2 + r^2)^{3/2}} \tag{3.8}$$

Exponential line spread-function:

$$T(k) = b^2/(b^2 + k^2) \tag{3.9}$$

$$A(x) = \pi b e^{-2\pi b|x|} \tag{3.10}$$

$$Q(r) = 2\pi b^2 K_0(2\pi br) \tag{3.11}$$

Exponential point spread-function:

$$T(k) = c^3/(c^2 + k^2)^{3/2} \tag{3.12}$$

$$A(x) = 4\pi c^2 |x| K_1(2\pi c|x|) \tag{3.13}$$

$$Q(r) = 2\pi c^2 e^{-2\pi cr} \tag{3.14}$$

In these expressions K_0 and K_1 are Bessel functions of the third kind with imaginary argument.[8]

The integrals that result from substituting Eqs. (3.6) through (3.8) in Eqs. (I) through (VI) are evaluated in the references indicated: (I) Dwight's *Table of Integrals* (Macmillan, 1934), Eq. 863.2. (II) Dwight, Eq. 859.3. (III) Watson (Ref. 8), Eq. (6), p. 386. (IV) Watson, Eq. (2), p. 434. (VI) Dwight, Eq. 856.8.

Equation (3.9) is obtained from (3.10) and (II) by Eq. 863.2 of Dwight, and Eqs. (3.9) and (III) yield (3.11) by Eq. (5) on p. 425 of Watson.

Equation (3.12) is obtained from (IV) and 3.14 by Eq. (6), p. 386, Watson. The result of substituting (3.12) in (I) is a more difficult integral; it may be evaluated by a transformation of Eq. (10) on p. 388 of Watson, or more directly by Eq. 558.5 in Campbell and Foster, *Fourier Integrals* (D. Van Nostrand Company, Inc., New York, 1948).

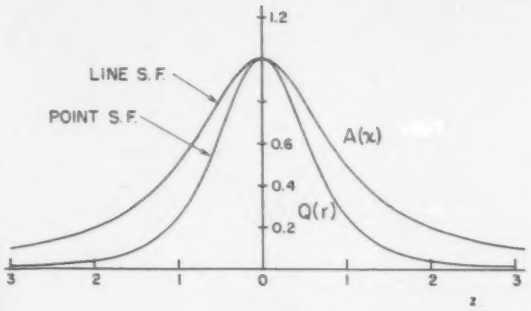

Fig. 2. The shapes of the point and line spread-functions when the transfer function is assumed to have an exponential form. Both functions are here normalized to a maximum value of unity, and the abscissa is a dimensionless coordinate z representing either r or x: $z = 2\pi a|x|$ for the normalized line spread-function $A(x) = a^2/(a^2+z^2)$, and $z = 2\pi ar$ for the normalized point spread-function $Q(r) = a^3/(a^2+z^2)^{3/2}$.

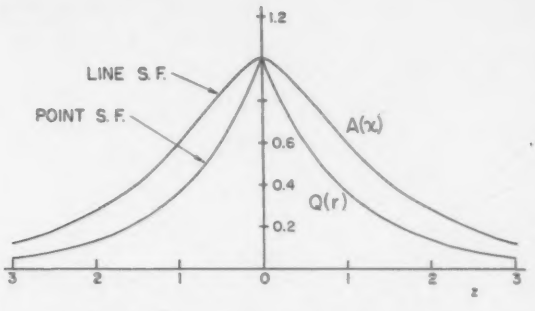

Fig. 3. The shapes of the point and line spread-functions, when the point spread-function is assumed to have an exponential form. Both functions are normalized to a maximum value of unity. The normalized line spread-function is $A(x) = xK_1(x)$, and the normalized point spread-function $Q(r) = e^{-z}$.

The line and spread functions corresponding to these three cases are plotted in Figs. 2, 3, and 4. Inspection of the figures shows that the point spread-function $Q(r)$ is always more sharply peaked than the line spread-function $A(x)$; in fact, the point spread-function (3.11) becomes infinite at the origin; this fact indicates that the exponential line spread-function cannot be exactly correct for any real film. In reference to Eq. (3.13), the function $K_1(z)$ varies as $1/z$ for small values of z, whence it follows that $A(x)$ as given by Eq. (3.13) approaches the value $2c$ as z approaches 0; the slope $dA(x)/dx$ is 0 at the origin, but the second derivative is negatively infinite.

In the following, we shall use the point spread-function given by Eq. (3.7) in the form in which it normalized to a maximum value of unity:

$$Q(r) = a^3/(a^2 + r^2)^{3/2} \qquad (3.15)$$

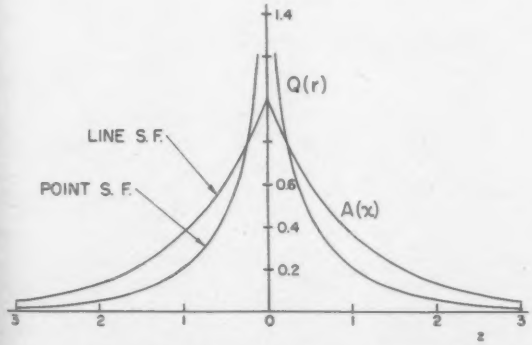

Fig. 4. The shapes of the point and line spread-functions when the line spread-function is assumed to have an exponential form. The line spread-function is normalized to a maximum value of unity, but the point spread-function has a maximum value that is infinite, so that its normalization has been chosen arbitrarily. The normalized line spread-function is $A(x) = e^{-z}$, and the point spread-function is $Q(r) = \frac{1}{2}K_0(z)$.

For this function, the areas A_1 and A_2 are given by

$$A_1 = 2\pi a^2 \qquad (3.16)$$

and

$$A_2 = {}^1/_2\pi a^2 \qquad (3.17)$$

Henceforth, and in all of the figures, all of the spread functions are normalized to a maximum value of unity.

The Kodak line spread-functions for the four Kodak films are shown in Fig. 5, which is reproduced with permission.[1] These line spread-functions were examined to determine which, if any, of the analytic functions (3.15), (3.10), and (3.13) would provide a good fit. The results: The data for the Royal-X and Tri-X films are fitted perfectly by the function (3.15), with the length a equal to 4.45 μ for both films. Equation (3.15) does not fit perfectly the data for the Plus-X and Pan-X films, but the fit is distinctly better than was obtainable with either (3.10) or (3.13), and also better than was obtainable with a line spread-function of Gaussian shape. The best

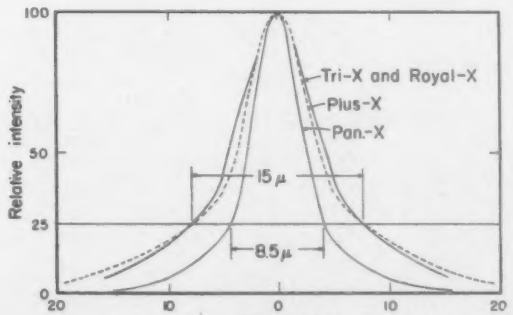

Fig. 5. The experimental line spread-functions of the four films, as determined by Zweig, Higgins, and MacAdam. The functions are normalized to a maximum value of unity, and the abscissa is the distance x in microns.

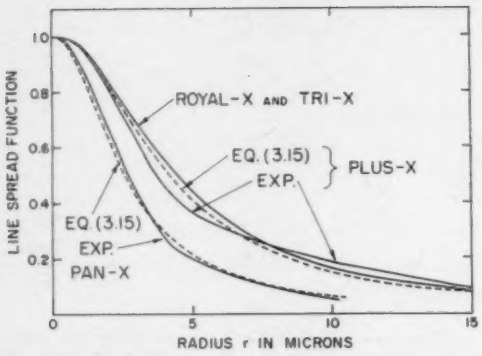

Fig. 6. This figure compares the experimentally determined line spread-functions, and the best fitting representation by Eq. (3.15). The fit for the Royal-X and Tri-X films is so good that one line can be drawn to represent both curves. For the Plus-X and Pan-X films, the experimental curves are the solid curves, and the best fitting curves of the form (3.15) are the dashed curves. Note that the Plus-X and Pan-X curves diverge from the best fitting curves in opposite directions.

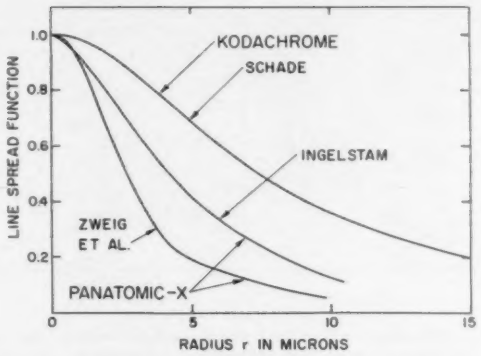

Fig. 7. This figure compares three different line spread-functions, two for Panatomic-X film, and one for Kodachrome film. The lowest curve is the experimental curve for Panatomic-X shown in Fig. 5. The middle curve represents the experimental results for Panatomic-X film as measured by Ingelstam and as interpreted by Sayanagi. The upper curve represents the experimental results for Kodachrome film as measured by Schade and as interpreted by Jones.

fit is given by $a = 4.2\ \mu$ for Plus-X and $a = 2.6\ \mu$ for Pan-X.

The nature of the fit between the experimental data and Eq. (3.15) is shown in Fig. 6. For the Royal-X and Tri-X films, the fit is so good that the fitting error cannot be shown in the figure; the curve in Fig. 6 represents both the data and the experimental results. For the other two films, the experimental curves are drawn with solid lines, and the best fitting form of Eq. (3.15) is shown by a dashed curve. The author judges the fit to be good.

It is possible, however, to obtain a slightly better over-all result as follows: From Eqs. (2.15) and (2.16) one notes that A_1 involves an integral of $Q(r)$, but that A_2 involves an integral of $Q^2(r)$. Thus one may expect that an improved value of $\mathfrak{L}$ will result if one uses to calculate A_1 the best fitting curves obtained above, and if one uses to compute A_2 the line spread-function (squared) that gives the best fit to $A^2(x)$. The values of a stated above are listed in Table I and are denoted a_1. Another set of a values, obtained by fitting the square of line spread-function (3.15) to $A^2(x)$, are also shown in Table I and are denoted by a_2.

From Eqs. (3.16) and (3.17) one then has $A_1 = 2\pi a_1^2$ and $A_2 = {}^1/_2\pi a_2^2$, whence

$$\mathfrak{L} = 2^{3/2}\pi^{1/2}a_1^2/a_2 \qquad (3.18)$$

where a_1 and a_2 are in microns. The length $\mathfrak{L}$ for each of the films is also tabulated in Table I.

TABLE I

Characteristic Lengths, in Microns

Film	a_1	a_2	$\mathfrak{L}$	L
Royal-X	4.45	4.45	22.3	13.3
Tri-X	4.45	4.45	22.3	13.3
Plus-X	4.2	4.0	22.1	13.3
Pan-X	2.6	2.7	12.5	7.54

In the paper by Zweig, Higgins, and MacAdam,[1] an approximate method is used to evaluate a length that is equivalent to $\mathfrak{L}$. Their method is equivalent to setting $\mathfrak{L}^2$ equal to the area of a circle whose diameter is equal to the width of the line spread-function where it has 0.25 of its maximum value. The values of $\mathfrak{L}$ determined by this method are here denoted L and are tabulated in the last column of Table I.

Let us now compare the line spread-functions that have been obtained by various authors. Ingelstam et al. have measured the transfer function of Panatomic-X film, and Sayanagi[7] showed that Ingelstam's results are in good agreement with the transfer function indicated by Eq. (3.12) above, with a value of $1/(2\pi c) = 3.4\ \mu$.* The corresponding line spread-function as given Eq. (3.13) is plotted in Fig. 7. Of the three films (Super-XX, Kodachrome, and Micro-file) whose transfer functions were measured by Schade,[5] the present writer judges that Kodachrome has a resolution most nearly comparable with Panatomic-X. Schade's measured transfer function for Kodachrome accords with Eq. (3.6) with $a = 7.43\ \mu$. The corresponding line spread-function as given by Eq. (3.16) is plotted in Fig. 7. Finally, the line spread-function for Panatomic-X film as measured by Zweig, Higgins, and MacAdam[1] is also plotted in Fig. 7.

Figure 7 indicates a wide divergence among the results obtained by different investigators on similar films. Obviously there are many possible reasons for the divergence. Nearly every conceivable imperfection of measuring apparatus or technique will tend to widen the spread function. Thus, a priori, one tends to give greater weight to the narrower of the reported spread functions.

* The value of $1/(2\pi c)$ given in Ref. 7 is 6.4 μ, but Sayanagi has confirmed in a personal communication that this is a misprint for 3.4 μ. The curve in his Fig. 1 uses the value 3.4 μ.

Noise Equivalent Energies

With the value of £ known for each of the films, it is now straightforward to calculate the noise equivalent energy for an exposure with a diameter small compared with £. Since the smallest value of £ is about 30 times the wavelength of the exposing light (430 mμ), a lens of moderate numerical aperture is sufficient to produce a light-image whose diameter is small compared with £.

TABLE II

Performance at Wavelength 430 mμ

Film	£ (μ)	M_2	$\mathfrak{D}$ ($ergs^{-1}$)	E_N (ergs)	N (photons)
Royal-X	22.3	435	6.50×10^8	1.54×10^{-9}	334
Tri-X	22.3	182	2.72×10^8	3.68×10^{-9}	798
Plus-X	22.1	120	1.81×10^8	5.52×10^{-9}	1200
Pan-X	12.5	64	1.71×10^8	5.86×10^{-9}	1272

Table II lists the values of £ and of the figure of merit M_2 for the wavelength 430 mμ and the optimum pre-exposure. The values of the noise equivalent energy E_N and its reciprocal $\mathfrak{D}$ are calculated by Eq. (2.13). The last column in Table II shows the noise equivalent energy in terms of the number of photons N whose total energy is equal to E_N:

$$N = E_N/E_{h\nu} \qquad (3.19)$$

where $E_{h\nu} = 4.61 \times 10^{-12}$ erg is the energy of a 430-mμ photon.

Figure 8 shows the noise equivalent energy E_N for each of the films plotted versus the amount of pre-exposure for radiation of wavelength 430 mμ.

TABLE III

Performance at Wavelength That Maximizes M_2 and $\mathfrak{D}$

Film	λ (mμ)	£ (μ)	M_2	$\mathfrak{D}$ ($ergs^{-1}$)	E_N (ergs)
Royal-X	400	22.3	456	6.81×10^8	1.47×10^{-9}
Tri-X	605	22.3	220	3.29×10^8	3.04×10^{-9}
Plus-X	600	22.1	123	1.855×10^8	5.39×10^{-9}
Pan-X	590	12.5	91	2.42×10^8	4.12×10^{-9}

Table III shows the values of E_N and $\mathfrak{D}$ for the optimum pre-exposure and for the wavelength that maximizes the figure of merit M_2. Since the wavelengths indicated in Table III are quite different for the four films, the noise equivalent number of photons N is not tabulated; intercomparison of the values would be misleading.

4.0 Discussion

Detectivity $\mathfrak{D}$ as defined in this paper is formally identical with the "informational sensitivity," I, introduced by Zweig, Higgins, and MacAdam.[1] In the numerical evaluation, however, $\mathfrak{D}$ and I differ

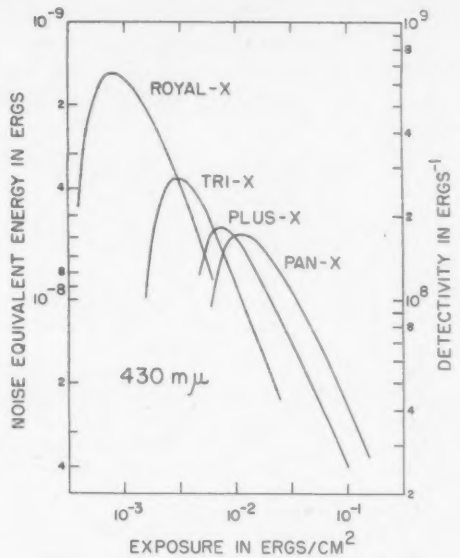

Fig. 8. The noise equivalent energy E_N in ergs on the left, and the detectivity in reciprocal ergs on the right, plotted against the pre-exposure U in ergs/cm². The results are for a wavelength of 430 mμ. The values at the peak of each curve are given in Table II. These data are for a light-image of diameter small compared with £. These results may be compared with those in Fig. 3 of Part II, which hold for a light image of diameter large compared with £.

because different measures of the effective area are employed. Zweig, Higgins, and MacAdam employ a length **L** (see Table I) that is approximately proportional to the length £ defined by formula (2.9). From the table, one easily finds that the ratio of **L** to £ is 0.60 for all the films. Accordingly, so long as one is interested only in *relative* values of the informational sensitivity — and this is the interest of Zweig et al. — the use of **L** is just as appropriate as the use of £. The results of the present paper have thus confirmed the propriety of the method used by Zweig et al. to assign arbitrary relative diameters to the point spread-function. If, however, one is interested in evaluating the detectivity on an absolute basis, one must use the length £. Use of **L** would lead to a value of the detectivity too high by the factor 1.67.

Among the quantities discussed in this and in the preceding paper (M_2, $\mathfrak{D}$, £, and the detective quantum efficiency Q), it is tempting to inquire, are there any invariants — that is to say, quantities that are nearly the same for the four films? Q is a good candidate, as suggested in Part II, and the ratio $Q/$£ is even better. The ratio of the largest to the smallest value of M_2 for the four films, according to Table III, is 456/91 = 5.01. For the detectivity $\mathfrak{D}$, the ratio is 6.81/1.885 = 3.67. Neither of these ratios is as small as the ratio for the detective quantum efficiency Q; according to Ref. 2, the ratio is 0.895/0.295 = 3.03. In this connection, it is of some interest, but probably of no fundamental importance, that the ratio $Q/$£ has a numerical value that is more nearly the same for all

TABLE IV
The Ratio Q/£ at 430 mμ

Film	Q_{max} (per cent)	£ (μ)	$Q_{max}/£$ (cm^{-1})
Royal-X	0.895	22.3	4.01
Tri-X	0.588	22.3	2.64
Plus-X	0.618	22.1	2.80
Pan-X	0.295	12.5	2.34

the films. The values of Q_{max}, £, and the ratio $Q_{max}/£$ are given for each of the films in Table IV, where it is seen that the ratio of the greatest to the smallest value of $Q_{max}/£$ is only 1.7.

Among the four films in Table II, Royal-X has the greatest detectivity. The noise equivalent energy is equal to the energy of 334 photons. If we multiply this number by the detective quantum efficiency of this film, which is 0.00895 (Ref. 9), the result is 3.0 photons.

On the basis of the results of Webb[10], it was estimated in Part I that about $^1/_{40}$ of the incident photons contribute to formation of the latent image; 334 divided by 40 is 8.3 photons.

The results of the two preceding paragraphs may be compared with the currently accepted belief that a single grain must absorb effectively 3 (Ref. 11) through 8 (Ref. 12) photons to make the grain developable.

The closeness of the agreement is perhaps misleading, and is at least in part fortuitous. The result, 3.0 photons based on the detective quantum efficiency, involves not only the response of the film, but also the statistics of the grain distribution as expressed in the granularity. On the other hand, the results of Refs. 11 and 12 are concerned only with the response of individual grains, and thus take no account of the statistics of the grain distribution.

Acknowledgment

The writer is much indebted to H. J. Zweig, G. C. Higgins, and D. L. MacAdam[1] for communicating a copy of their manuscript in advance of publication, and also for permission to use their data as given in Fig. 5.

References

1. Zweig, H. J., Higgins, G. C., and MacAdam, D. L., "On the Information-Detecting Capacity of Photographic Emulsions," *J. Opt. Soc. Am.*, *48:* 926 (1958).
2. Jones, R. Clark, "New Method of Describing and Measuring the Granularity of Photographic Materials," *ibid.*, *45:* 799 (1955).
3. Zweig, Hans J., "Autocorrelation and Granularity," *ibid.*, *46:* 805 (1956).
4. Jones, R. Clark, "On the Point and Line Spread Functions of Photographic Images," *ibid.*, *48:* 934 (1958).
5. Schade, Otto H., "Electro-optical Characteristics of Television Systems," *RCA Rev.*, *9:* 7, 246, 491, 653 (1948).
6. Ingelstam, Djurle, and Sjögren, "Contrast-Transmission Functions Determined Experimentally for Asymmetrical Images and for the Combination of Lens and Photographic Emulsion," *J. Opt. Soc. Am.*, *46:* 707 (1956).
7. Sayanagi, Kazuo, "On the Light Distribution in the Photographic Image," *ibid.*, *47:* 566 (1957).
8. Watson, G. N., *Bessel Functions*, Cambridge University Press, 1944, 2nd ed., pp. 78–80.
9. Jones, R. Clark, "On the Quantum Efficiency of Photographic Negatives," *Phot. Sci. & Eng.*, *2:* 57 (1958).
10. Webb, J. H., "Absolute Sensitivity Measurements on Single-Grain Layer Photographic Plates for Different Wavelengths," *J. Opt. Soc. Am.*, *38:* 312 (1948).
11. Mitchell, J. W., and Mott, N. F., "Nature of Formation of the Photographic Latent Image," *Phil. Mag.* (*8*), *2:* 1149 (1957).
12. Webb, J. H., "Low Intensity Reciprocity-Law Failure," *J. Opt. Soc. Am.*, *40:* 3, 197 (1950).

PHOTOGRAPHIC SCIENCE AND ENGINEERING
Volume 2, Number 4, December 1958

Analysis of the Variability Among Density-Log Exposure Curves of Black-and-White Negative Films by the Method of Principal Components

J. L. SIMONDS, *Research Laboratories, Eastman Kodak Company, Rochester, N.Y.*

It is shown that the *D*-log *E* characteristic curves of a wide variety of black-and-white negative films vary from the mean of these curves in only four basically different ways. A complete description of the shape of any of the characteristic curves can be given by four numbers, which are the amounts of each of the four component types of variability which combine to produce the shape differences between the sample curve and the mean curve. The system of analysis described offers a precise and efficient parametric representation of the information contained in the sensitometric curve.

In sensitometric studies of black-and-white films, the results are often expressed graphically in the form of the density-log exposure curve, also known as the H & D curve. The shape and position of the *D*-log *E* curve for a particular material provide useful information about the pictorial results one may expect from its use.

Two methods have been used to describe *D*-log *E* curves numerically. One method is that of sensitometric parameters. Parameters such as speed, exposure scale, fog, gamma, D_{max}, etc., are graphically derived from the *D*-log *E* curve in order to provide information about the photographic characteristics of a film. A further use of the parametric data is to reduce the description of the sensitometric characteristics of a film to a few numbers which provide a concise description of the shape and position of portions of the characteristic curve.

The other method describes the entire *D*-log *E* curve by a mathematical function which approximately fits *D*-log *E* curves of a variety of films. The mathematical functions are based on the assumption that *D*-log *E* curves vary in only a few unique ways which are accommodated by changing the constants and coefficients of the function.

Both methods have basic shortcomings. The parametric data do not describe the entire curve from which they are derived but only selected parts of it. In addition, sensitometric parameters which require graphical methods cannot be determined precisely in the presence of small, random densitometry errors in portions of the *D*-log *E* curves.

The mathematical functions which have been used to fit *D*-log *E* curves have not been entirely satisfactory for routine sensitometric studies. Many of the proposed functions fit only a small group of simple films and are not adequate representations of the curves of more complex emulsions. Also, the parameters of the mathematical functions generally are not simply or precisely determinable.

A new approach to the description of a wide variety of *D*-log *E* curves in terms of a limited number of parameters is provided by the method of principal components, described in a paper by H. Hotelling.[1] The system of multivariate analysis described by Hotelling can be used to determine the number and type of characteristic ways in which *D*-log *E* curves vary from one another.*

A study of this kind has been made on data from 101 samples of roll- and sheet-film emulsions, from ten manufacturers in six countries. It shows that all significant differences in shapes of their H & D curves can be described completely by only four empirically determined functions which, like the H & D curve itself, treat density as a function of log exposure.

A. *Principal-Component Analysis of a Wide Variety of D-log E Curves*

The black-and-white negative films chosen for analysis were:

a. The films used by Jones and Nelson[2,3] in their

Communication No. 1962 from the Kodak Research Laboratories. Received 26 May 1958.

* The application of Hotelling's principal-component analysis to photographic response data is due to R. H. Morris, head of the Scientific Computing Department, Eastman Kodak Company, Rochester, N.Y. Mr. Morris recognized the power of the method for expressing continuous functions, such as *D*-log *E* functions, as linear combinations of basic empirical functions. Hotelling's analysis was primarily concerned with the analysis of a complex of dissimilar variables.

original work which specified the fractional-gradient criterion as a measure of speed.

b. The film-developer combinations used by Nelson and Simonds[4] to investigate simple approximations to fractional-gradient speed. These film-developer combinations represent currently available Kodak films developed in five developers for times ranging from 3 to 18 min.

c. The 54 roll and sheet films used by Simonds[5] in comparing ASA and DIN speeds of current films of foreign and domestic manufacture. These films were produced by ten manufacturers located in six countries.

It is felt that these 101 film-developer combinations exemplify the variety of curve shapes which may be encountered in roll and sheet films for black-and-white photography (excluding graphic arts films, x-ray films, and other special types).

Density data were obtained at sixteen levels of exposure, the exposures of contiguous levels or steps being in the ratio of $\sqrt{2}$ to 1 ($\Delta \log E = 0.15$). The exposure steps were chosen so that the density at the twelfth step is equal to fog density* plus 0.7. Ascending step numbers indicate ascending exposures. The sixteen densities are considered to be an essentially complete description of the shape of the curve over the log exposure range from which they were derived. The position of the curve along the log exposure axis must be reported separately as, for example, the log exposure of the twelfth step.

By the technique described by Hotelling and in some detail in a following section of this paper, the four most characteristic independent kinds of variation among the 101 materials have been found. They are shown graphically in Fig. 1, and their individual effects are illustrated in Fig. 2 by showing the influence each would have on an average curve.

B. *Characteristic Vectors: General Description*

A rigorous description of a multivariate analysis of a family of response curves is necessarily mathematically complex. In order to simplify the discussion, an attempt will be made to report the results of the analysis with a minimum of mathematical details. A more detailed description of the mathematics of the analysis is given in Hotelling's paper.

The sensitometric data used in the analysis are the density data obtained from r steps of exposure as previously described, the exposures of any two contiguous steps being in a constant ratio ($\Delta \log E$ = constant). For each characteristic curve the r densities are considered to be an essentially complete description of the shape of the curve over the log exposure range from which they were derived.

Consider that data are derived from a family of n characteristic curves representing n different films. An n-row, r-column matrix of densities can be formed, each row of which contains the r densities for one of the n films. Each row is called a "density vector." The mean density vector can be computed by finding the average density at each of the r steps. The mean vector is, therefore, the average D-log E curve of the n films.

It is possible to find a set of p vectors, called "characteristic vectors," which, when added in the proper amounts, step by step, to the mean density vector, will adequately approximate any density vector in the original family of n density vectors. The characteristic vectors, like the density vectors themselves, are sets of r numbers. Mathematically stated, the densities of each step of any film are given by Eq. (1):

$$\left.\begin{aligned}
d_{\text{step }1} &= \bar{D}_{\text{step }1} + Y_1V_{1,\text{ step }1} + Y_2V_{2,\text{step }1} + Y_3V_{3,\text{step }1} \\
&\quad + \ldots\ Y_pY_{p,\text{step }1} \\
d_{\text{step }2} &= \bar{D}_{\text{step }2} + Y_1V_{1,\text{step }2} + Y_2V_{2,\text{step }2} + Y_3V_{3,\text{step }2} \\
&\quad + \ldots\ Y_pV_{p,\text{step }2} \\
&\vdots \\
d_{\text{step }r} &= \bar{D}_{\text{step }r} + Y_1V_{1,\text{step }r} + Y_2V_{2,\text{step }r} + Y_3V_{3,\text{step }r} \\
&\quad + \ldots\ Y_pV_{p,\text{step }r} \\
&\quad (p \le r \le n)
\end{aligned}\right\} \quad (1)$$

The Y's are the amounts of the characteristic vectors which must be added to the mean density vector in order to produce the sample density vector. The characteristic vectors, V_i, are uniquely determined for a given family of curves—in this case, a family of D-log E curves. The characteristic vectors are invariant for all films belonging to the original family from which the vectors are derived. The values of $Y_1, Y_2, Y_3 \ldots . Y_p$ vary from film sample to film sample. The Y's, therefore, are a complete specification of the density vector to which they apply. Together with the uniquely determined characteristic vectors and mean density vector, the Y's are sufficient information with which to reconstruct the density vector from which they were derived.

The number of characteristic vectors required to explain all the differences among a family of curves, each represented by r densities, will be equal to or less than r. For a perfect fit to all the density vectors, r characteristic vectors may be required. The probability is strong, however, that a large percentage of the variability among the family of density vectors may be explained by using only a few characteristic vectors.

The following statements are given without proof:

(1) The p characteristic vectors are orthogonal; that is, they represent statistically independent types of density variability. Mathematically stated:

$$\sum_{i=1}^{r} V_{a,\text{ step }i}\, V_{b,\text{ step }i} = 0, \quad a \neq b.$$

(2) The Y's, called "scalar multiples," can be determined for each sample density vector as a linear combination of the densities for all r steps. Hence,

* In this paper, fog density is defined as the density of an unexposed, processed portion of the film.

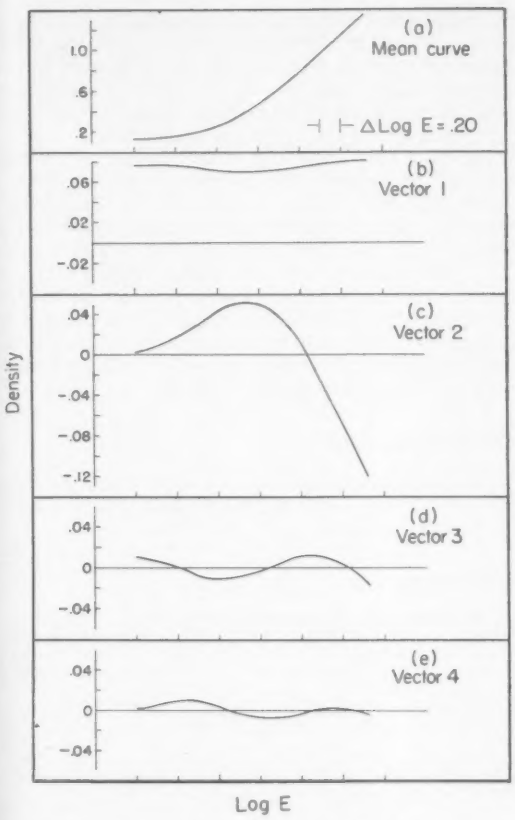

Fig. 1. Plot of the mean *D*-log *E* curve and of the four characteristic vectors of density variability.

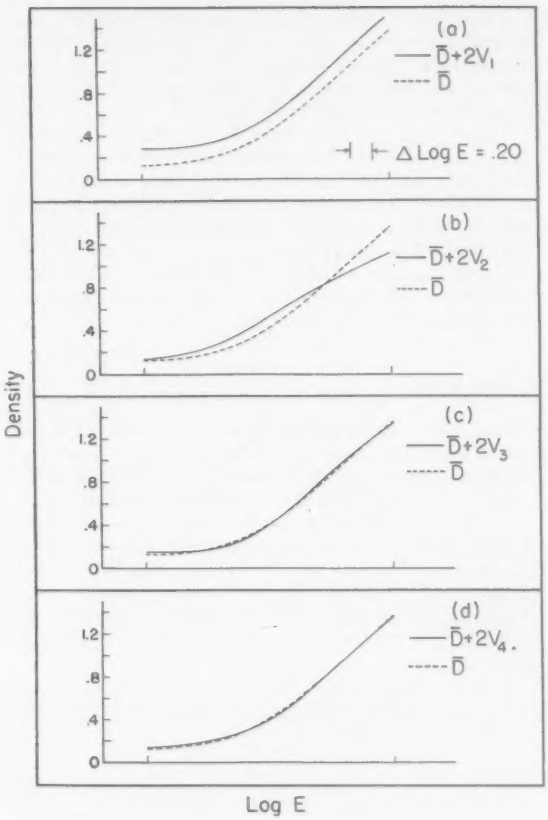

Fig. 2. Plot of the mean *D*-log *E* curve and of combinations of the mean curve with each of the four characteristic vectors.

$$\left.\begin{aligned} &= W_{1,0} + W_{1,1}d_{\text{step }1} + W_{1,2}d_{\text{step }2} + \cdots W_{1,r}d_{\text{step }r} \\ &= W_{2,0} + W_{2,1}d_{\text{step }1} + W_{2,2}d_{\text{step }2} + \cdots W_{2,r}d_{\text{step }r} \\ &\quad\vdots \\ &= W_{p,0} + W_{p,1}d_{\text{step }1} + W_{p,2}d_{\text{step }2} + \cdots W_{p,r}d_{\text{step }r} \end{aligned}\right\} \quad (2)$$

where the W's are uniquely determined for a particular set of vectors (see Appendix).

(3) It is possible to normalize each of the characteristic vectors in such a way that the standard deviation of the scalar multiples is unity.

Since theoretical representations of characteristic curves indicate that curves differ in only a few ways, it is reasonable to assume that a small number of characteristic vectors are required to explain the differences among the 101 film curves of Section A. It was actually found that only four vectors are required to give essentially perfect reconstitution of the density data for all of the 101 curves. In Table I are listed the mean density vector and the four characteristic vectors derived (1-sigma amounts of each).

TABLE I

Mean and Four Characteristic Vectors of 101 Films

Step	Mean Curve	V_1	V_2	V_3	V_4
1	0.13	0.076	0.002	0.010	0.001
2	0.13	0.076	0.006	0.008	0.003
3	0.14	0.076	0.012	0.003	0.007
4	0.16	0.075	0.020	−0.002	0.008
5	0.19	0.073	0.029	−0.008	0.008
6	0.23	0.072	0.040	−0.011	0.004
7	0.29	0.069	0.048	−0.011	−0.001
8	0.37	0.069	0.052	−0.009	−0.005
9	0.47	0.070	0.050	−0.004	−0.007
10	0.58	0.071	0.041	0.002	−0.007
11	0.70	0.073	0.026	0.009	−0.008
12	0.83	0.076	0.000	0.012	−0.001
13	0.96	0.078	−0.027	0.011	0.000
14	1.10	0.078	−0.057	0.006	0.001
15	1.23	0.079	−0.089	−0.004	−0.001
16	1.36	0.080	−0.121	−0.015	−0.004

Figure 1 is a plot of the data in Table I.

Figure 2 is a plot of the mean density vector, $\bar{D}$, and of the following combinations: (a) $\bar{D} + 2V_1$; (b) $\bar{D} + 2V_2$; (c) $\bar{D} + 2V_3$; (d) $\bar{D} + 2V_4$.

The effect of adding V_1 to the mean density vector is basically a fog adjustment. The second vector represents a contrast change. The effects of the other two vectors are not so easily interpreted on the basis of established sensitometric parameters.

These characteristic vectors represent the most characteristic ways in which these film curves vary. Since only four vectors, together with a mean density vector, are necessary for reconstitution of the original density data, a complete description of the shape of each of the 101 curves is given by the values of Y_1, Y_2, Y_3, and Y_4, the amounts of the vectors which must be added to the mean vector in order to reconstitute the original density data.

Conclusions

It has been demonstrated that the curve-shape differences among a family of characteristic curves of black-and-white negative films can be represented by combinations of four uniquely determined characteristic vectors. The curve-shape differences between a sample density vector and the mean density vector can be described completely by four numbers, called "scalar multiples," which specify the amounts of the characteristic vectors which must be added to the mean density vector in order to synthesize the sample density vector.

If the characteristic vectors cannot be used to reconstitute, with accuracy, the original density data for samples not included in the original study, it can be stated that the film-developer combination represented by these data is basically different from any of the films studied thus far. Hence, poor reconstitution is indicative of films which depart radically from those films from which the vectors were derived.

The fact that only four characteristic vectors are required to explain the differences among such a variety of curve shapes indicates that the variations in materials and manufacturing techniques employed in producing the 101 films result in curves which vary in only four basically different ways. Hence, the domain of probable curve shapes in black-and-white negative roll and sheet films appears to be limited to those curves which can be generated by combining the four characteristic vectors in all possible combinations with the mean density vector.

Acknowledgment

The writer is indebted to J. L. Tupper for initiating this project and to R. H. Morris and F. C. Williams for valuable counsel.

References

1. Hotelling, H., *J. Educational Psychology*, *24:* 417 (1933).
2. Jones, L. A., and Nelson, C. N., *J. Opt. Soc. Am.*, *30:* 93 (1940).
3. *Ibid.*, *31:* 10 (1941).
4. Nelson, C. N., and Simonds, J. L., *J. Opt. Soc. Am.*, *46:* 324 (1956).
5. Simonds, J. L., *Phot. Sci. and Eng.*, *1:* 28 (1957).

APPENDIX

The following is an example of the computation of the scalar multiples of the characteristic vectors listed in Table I for a sample set of density data.

The weighting factors, $W_{i,j}$, for the computation of the Y's from Eq. (2) are given in Table II. The weighting factors are proportional to the characteristic vectors themselves. The constants, $W_{i,0}$, are found by multiplying the weighting factors in Table II, step by step, by the mean density vector.

Consider the sample density data from an actual curve as given in Column (a) of Table III.

TABLE II

Weighting Factors for Computation of Scalar Multiples

Step	W_1	W_2	W_3	W_4
1	0.8536	0.0582	8.5309	2.6138
2	0.8553	0.1391	6.7199	7.8623
3	0.8604	0.2993	2.4175	16.2341
4	0.8419	0.4970	−1.4931	20.2086
5	0.8202	0.7378	−6.5010	19.2205
6	0.8050	1.0232	−9.1557	9.0339
7	0.7847	1.2199	−9.2437	−2.7038
8	0.7757	1.3176	−7.0178	−11.7549
9	0.7876	1.2580	−3.5765	−16.4137
10	0.8040	1.0363	1.7515	−17.7939
11	0.8254	0.6556	7.5894	−18.2892
12	0.8563	0.0021	9.3832	−2.2187
13	0.8790	−0.6805	9.2496	0.8731
14	0.8790	−1.4294	4.8038	2.9087
15	0.8933	−2.2553	−3.0956	−2.2586
16	0.8997	−3.0574	−12.1484	−9.7969

$W_{1,0} = -7.5914$ $W_{3,0} = +0.2793$

$W_{2,0} = +6.1234$ $W_{4,0} = +37.2535$

TABLE III

Original Density Data and Reconstituted Data for a Sample Computation

Step	(a) Sample Density Data	(b) Reconstituted Data Using Eq. (1)	(c) Differences Between Actual and Reconstituted Densities
1	0.06	0.07	−0.01
2	0.07	0.07	0.00
3	0.09	0.09	0.00
4	0.11	0.11	0.00
5	0.15	0.15	0.00
6	0.21	0.20	0.01
7	0.27	0.27	0.00
8	0.34	0.34	0.00
9	0.43	0.43	0.00
10	0.53	0.53	0.00
11	0.64	0.64	0.00
12	0.76	0.76	0.00
13	0.89	0.89	0.00
14	1.03	1.03	0.00
15	1.17	1.17	0.00
16	1.30	1.31	−0.01

The scalar multiples for the sample curve are given by:

$$Y_1 = -7.5914 + (0.8536)(0.06) + (0.8553)(0.07) + \ldots . (0.8997)(1.30) = -0.70$$
$$Y_2 = 6.1234 + (0.0582)(0.06) + (0.1391)(0.07) + \ldots . (-3.0574)(1.30) = 0.14$$
$$Y_3 = 0.2793 + (8.5309)(0.06) + (6.7199)(0.07) + \ldots . (-12.1484)(1.30) = -1.32$$
$$Y_4 = 37.2535 + (2.6138)(0.06) + (7.8623)(0.07) + \ldots . (-9.7969)(1.30) = 0.21$$

In order to determine how accurate a reconstruction of the original density data can be obtained by using the Y's, substitute the above values of the Y's into Eq. (1) to obtain the reconstituted density data.

The reconstituted densities are given in Column (b) of Table III. In Column (c) of Table III are listed the differences between the original densities and the reconstituted densities.

$$d_{\text{step 1}} = 0.13 + (-0.70)(0.076) + (0.14)(0.002) + (-1.32)(0.010) + (0.21)(0.001) = 0.07$$
$$d_{\text{step 2}} = 0.13 + (-0.70)(0.076) + (0.14)(0.006) + (-1.32)(0.008) + (0.21)(0.003) = 0.07$$
$$\vdots$$
$$d_{\text{step 16}} = 1.36 + (-0.70)(0.080) + (0.14)(-0.121) + (-1.32)(-0.015) + (0.21)(-0.004) = 1.31$$

PHOTOGRAPHIC SCIENCE AND ENGINEERING
Volume 2, Number 4, December 1958

The Use of Principal-Component Description of *D*-log *E* Curves in a Study of the ASA-DIN Speed Relationships

J. L. SIMONDS, *Research Laboratories, Eastman Kodak Company, Rochester, N.Y.*

The description of *D*-log *E* curves by the method of principal components has been used to study the relation between fixed-density (0.1) speed and fractional-gradient speed for black-and-white negative roll and sheet films. The analysis shows that the log exposure difference between the two speed points is not constant, but is predictable for most films from simple measurements made on the *D*-log *E* curve. The special cases for which the log *E* differences are not simply predicted are discussed.

In an earlier paper,[1] it was shown that the density-log exposure curves of a wide variety of black-and-white negative films vary from the mean of the family of curves in only four basically different ways. A complete description of the shape of any of the characteristic curves within the family can be given by four numbers, called "scalar multiples," which are the amounts of each of the four component types of variability which combine to produce the shape differences between the sample curve and the mean curve.

The shape of the *D*-log *E* curve of a black-and-white film is known to be correlated with the photographic tone-reproduction qualities of the film. The ability to describe the shape of the *D*-log *E* curve with only four scalar multiples leads to the hope that the scalar multiples may be simply correlated with photographic tone-reproduction qualities of films. This paper is concerned with a study of the relation between two measures of photographic speed and of how this relation is affected by changes in the shape of the *D*-log *E* curve as represented by the scalar-multiple description.

The American[2] and British[3] standards of speed determination specify the 0.3 $\bar{G}$ fractional-gradient criterion because experimental studies have shown that it gives speed values for negative films which correlate more closely with subjective appraisals of photographic speeds than do the speeds obtained by any other known sensitometric criterion. The speed value is equal to the reciprocal of the exposure, in meter-candle-seconds, at which the slope of the curve is three-tenths of the average gradient measured over a log exposure interval of 1.5 extending from the speed point over higher exposures.

A simpler sensitometric method of speed specification is given in the German standard.[4] Speed is there defined as a linear function of the common logarithm of the exposure required to produce a density of 0.1 above fog. A criticism of the German criterion is that it does not correlate with print-judgment speed as well as the fractional-gradient speed criterion does.

Nelson and Simonds[5] showed that a simple relation exists between the density (above fog) resulting from an exposure equal to 20 times the exposure required for a density of 0.1 (above fog) and ΔX, the difference in log exposure between the log *E* required to produce a density of 0.1 above fog and the log *E* of the fractional-gradient speed point.

Figure 1 is a plot of the empirically determined relation between ΔX and ΔD, the difference between fog density plus 0.1 and the density resulting from an exposure 20 times greater than that required for a density of 0.1 above fog.

In this report, the scalar-multiple characterization of

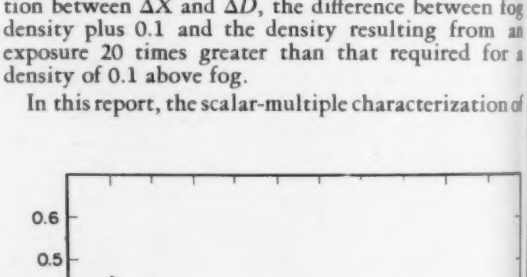

Fig. 1. Empirically derived relation between ΔX and ΔD.

Communication No. 1965 from the Kodak Research Laboratories. Received 9 June 1958.

the shape of *D*-log *E* curves, as described in the previous paper, is used to show that:

(a) ΔX is predictable by a simple linear function of the scalar multiples;

(b) the choice of a density measurement made at an exposure 20 times greater than the exposure required for a density of 0.1 above fog as a means of predicting ΔX is well justified for the domain of films represented by the family of 101 film–exposure–development combinations studied in the previous paper;

(c) the domain of probable shapes of *D*-log *E* curves of black-and-white negative films, sampled by adding the four characteristic vectors of density variability in a variety of combinations to the mean *D*-log *E* curve of the family of 101 curves, contains one small region in which prediction of ΔX from a simple density measurement is not accurate. The reasons for the inability to predict ΔX for these curves are discussed.

A. *Prediction of ΔX by a Linear Function of Scalar Multiples*

Scalar multiples of the vectors of density variability for the family of 101 curves studied in the earlier paper were computed for each of the 101 films.

The method of least squares was used to compute a linear transformation from the four scalar multiples to the value of ΔX which was graphically derived from the *D*-log *E* curves of the 101 films. The resulting equation is

$$\Delta X = 0.248 + 0.005Y_1 + 0.066Y_2 - 0.015Y_3 + 0.004Y_4 \quad (1)$$

The standard deviation of the differences between the measured values of ΔX and the values of ΔX predicted by the use of Eq. (1) is

$$\sigma_{\text{residual}} = 0.022.$$

B. *Examination of the Density-Weighting Function for Predicting ΔX by a Linear Function of Density*

Since each scalar multiple is computed as a linear combination of densities resulting from a geometric progression of exposures, then ΔX is also predictable as a linear combination of the same density data. Mathematically stated, this is

$$\Delta X = a_0 + a_1 d_{\text{step } 1} + a_2 d_{\text{step } 2} + \cdots\cdots a_n d_{\text{step } n} \quad (2)$$

The densities in Eq. (2) are those resulting from a series of 16 exposures, the exposures of any two contiguous steps being in the ratio of $\sqrt{2}$ to 1.

Figure 2a is a plot of the mean *D*-log *E* curve of the original set of 101 films. Figure 2b is a plot of the coefficients, a_i, in Eq. (2) vs. log exposure (step number).

Examination of Fig. 2b shows that the densities which are to be weighted most heavily in predicting ΔX are those resulting from an exposure (point *A*) approximately equal to that which is required for a density of 0.1 above fog and from an exposure (point *B*) separated from the former by 1.05 in log *E*.

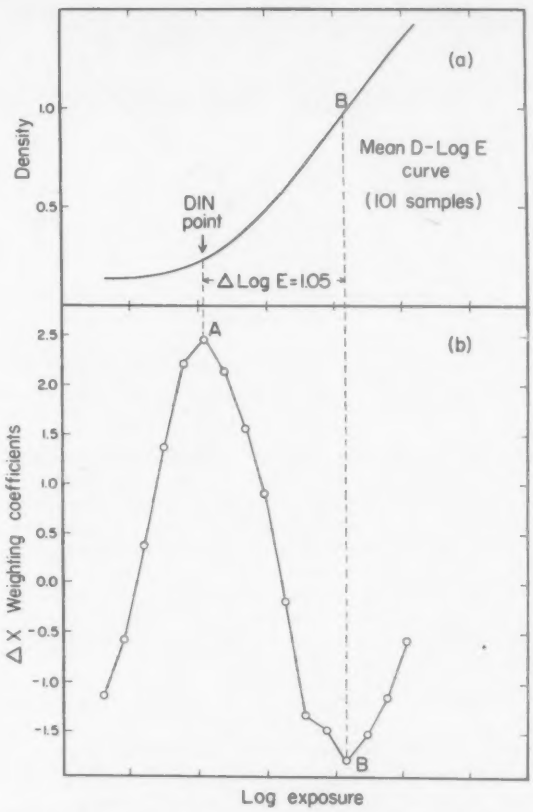

Fig. 2. (a) Mean *D*-log *E* curve of original group of 101 films. (b) Plot of coefficients, a_i, in Eq. (2).

Nelson and Simonds[5] reported the empirical finding that ΔX is correlated with ΔD. The density weighting suggested by Nelson and Simonds to predict ΔX is similar to the density weighting shown in Fig. 2. The Nelson and Simonds weighting gives equal (but opposite in sign) weights to the densities resulting from the exposure required to produce 0.1 above fog and from an exposure 20 times greater than the former (Δ log E = 1.30). The similarity between the ΔD weighting and the weighting shown in Fig. 2b indicates that the choice of ΔD as a predictor of ΔX is well justified for the domain of films represented by the family of 101 film–exposure–development combinations.

C. *A Study of the ΔX-ΔD Relationship*

An advantage of the characteristic vector description of the *D*-log *E* curves is that it is possible to sample systematically the domain of curve shapes represented by the 101 films studied in the previous paper. A set of *D*-log *E* curves was artificially generated by adding to the mean *D*-log *E* curve all possible combinations of the four characteristic vec-

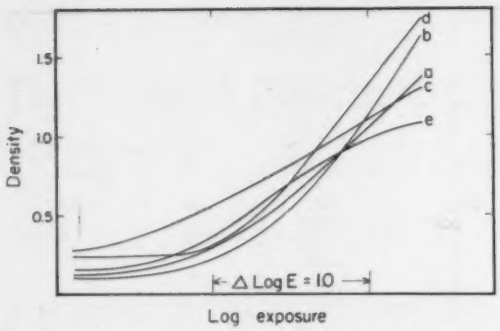

Fig. 3. Five *D*-log *E* curves generated by adding the characteristic vectors of density variability to the mean curve in various amounts, as listed in Table I.

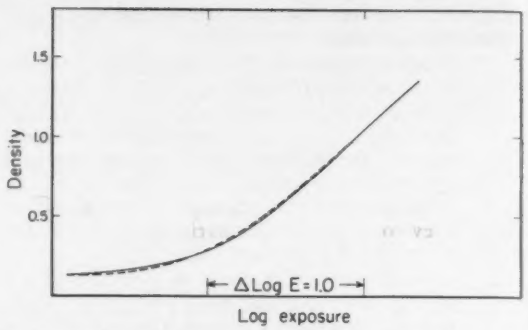

Fig. 4. Solid curve is the mean density vector plus a 2-sigma amount of the fourth characteristic vector of density variability. Dashed curve is the mean curve itself.

tors in zero, plus 2-sigma and minus 2-sigma amounts. These curves are a comprehensive sampling of the domain of curve shapes likely to be encountered in black-and-white negative roll and sheet films.

Five of the 81 possible combinations are given in Fig. 3 to illustrate the wide variety of curve shapes which can be generated in this manner. The amounts of the characteristic vectors (i.e., the scalar multiples) which were added to the mean curve to produce the five curves are listed in Table I.

TABLE I

Scalar Multiples of the Curves in Fig. 3

Curve	Y_1	Y_2	Y_3	Y_4
a	0	0	0	0
b	0	−2	−2	0
c	2	2	−2	2
d	0	−2	2	−2
e	0	2	2	0

The *D*-log *E* curve of each of the 81 combinations was plotted and ΔX and ΔD were measured graphically. The relation between ΔX and ΔD found by Nelson and Simonds is

$$\Delta X = 0.83 - 0.86\,\Delta D + 0.24\,(\Delta D)^2 \qquad (3)$$

The values of ΔX for the 81 curves were predicted from ΔD. The standard deviation of the differences between the measured values of ΔX and the predicted values of ΔX was only 0.026 in log *E*.

The only curve for which ΔX was not predicted accurately from ΔD was one which was generated by adding to the mean curve the fourth vector alone in a plus 2-sigma amount. The curve of this combination is given in Fig. 4.

An actual practical photographic test of the effective speed difference between two films having *D*-log *E* curves as shown in Fig. 4 has not been made, because the solid curve represents a wholly imaginary type of film. The characteristic vector study has, nevertheless, indicated that it is a curve shape which may conceivably be encountered. There is no evidence, however, that the fractional-gradient criterion is superior to the fixed-density criterion in evaluating the effective speed of such a film.

If the one case just mentioned (in which the fractional-gradient criterion itself is suspect) is omitted from the computation of the standard deviation of the differences between the measured and predicted values of ΔX, the standard deviation would become considerably smaller, thus providing further evidence that the empirically derived relation between ΔX and ΔD is a most accurate means of relating one speed point to the other over the entire domain of curve shapes which may be encountered in black-and-white photography.

Conclusions

The characteristic vector description of *D*-log *E* curves is useful in studying the effects of curve-shape changes on the ASA–DIN speed relationship.

The family of curves generated by adding various amounts of the characteristic vectors to the mean curve is a comprehensive sampling of the domain of *D*-log *E* curves which may be encountered in black-and-white photography. Since the characteristic vectors are mutually orthogonal, each of the vector combinations is dissimilar from all other combinations.

It was shown that the scalar multiples are correlated with ΔX, the log *E* difference between the DIN and ASA speed points. It is possible that the scalar multiples may be correlated equally well with sensitometric parameters other than ΔX, and even with subjective appraisals of quality. Investigations of such correlations are now in progress.

References

1. Simonds, J. L., *Phot. Sci. & Eng.*, 2: 205 (1958).
2. American Standard PH2.5-1954, *Method for Determining Photographic Speed and Exposure Index*, American Standards Association, 70 East 45th Street, New York 17, N. Y.
3. *British Standard Method of Determining Speed and Exposure Index of Photographic Negative Materials*, BS 1380.
4. German Standard DIN 4512, Blatt 1, November 1957.
5. Nelson, C. N., and Simonds, J. L., *J. Opt. Soc. Am.*, 46: 324 (1956).

PHOTOGRAPHIC SCIENCE AND ENGINEERING
Volume 2, Number 4, December 1958

Degradation of Phenidone in Developer Solutions During Storage

G. C. ALLETAG, *Photographic Research Laboratory, Philip A. Hunt Company, Palisades Park, N.J.*

Phenidone (1-phenyl-3-pyrazolidone) has received much attention in the literature during the past eight years. It has been employed as a development agent, mainly as a replacement for Metol, because of several technical and economic advantages. It is now widely used in prepared liquid developers, many of which are highly alkaline. In such solutions, however, it tends to decompose upon prolonged storage, especially at high temperatures. Studies of three typical formulas are presented which relate the rate of degradation to developer alkalinity and storage temperature. The conclusion is reached that all liquid Phenidone developers have strict limitations as to the temperature and duration of storage. The mechanism of degradation is discussed, and reference is made to preliminary studies of Phenidone-B (1-phenyl-4-methyl-3-pyrazolidone).

Phenidone* (1-phenyl-3-pyrazolidone) has received much attention in the literature since its discovery as a developing agent in 1940[1] and particularly since its commercial introduction in Great Britain in 1951.[2] Since becoming available commercially in the United States in 1953, it has become the third most widely-used developing agent in black-and-white photography in this country, outranked only by hydroquinone and Metol.

While Phenidone can be employed as the sole developing agent in certain types of developer, its principal use has been in conjunction with hydroquinone where it exhibits a superadditivity similar to that obtained in Metol-hydroquinone developers.[3]

The rapid commercial acceptance and application of Phenidone can be easily understood when several of the advantages claimed for it are considered. Its activity is less affected by increases in bromide concentration than that of Metol.[4] This characteristic allows the preparation of developers having improved working lives, and it may make possible the formulation of Phenidone developers which operate at somewhat lower pH's than Metol formulas of comparable activity. Phenidone developers tend to discolor less in use than those made with Metol. They are also usually satisfactory for use by those persons who are allergic to Metol and aromatic diamines.

Phenidone is also attractive from an economic standpoint. Its higher initial cost is more than offset by the fact that only one-fifth to one-tenth as much Phenidone as Metol is normally required in a given formula.

Presented at the Annual Conference, Rochester, N.Y., 9 October 1958. Received 12 September 1958.
*Registered trade-mark of Ilford, Ltd.

Since much smaller quantities of Phenidone are required than Metol, and also because Phenidone is not salted out of solution to the extent that Metol is, there has been widespread use of Phenidone in concentrated liquid developers.[5] Indeed, Phenidone has led to the introduction of more concentrated developers than were possible with Metol. Thus, concentrates have appeared which are commonly diluted as much as 1:20 for certain uses. Many such concentrates are highly alkaline, with pH's ranging to 11.5 and higher, in order to take advantage of maximum hydroquinone and sulfite solubilities.

It is in such highly alkaline liquid developer concentrates that the first serious disadvantage of Phenidone has been encountered. Experience has shown that upon prolonged storage in such solutions Phenidone tends to decompose and lose its photographic activity.

This paper summarizes the results of a study of Phenidone degradation conducted in the Research Laboratories of the Philip A. Hunt Company. It is not presented as a finished study, since further work is under way and much more remains to be learned on the subject. It was decided, however, that, in view of the serious losses in photographic quality that Phenidone degradation can cause in certain circumstances, the results of this work should be made available now, even though incomplete, and despite the fact that certain exact relationships have not yet been clearly established.

The Problem of Storage in the Field

When developing solutions are prepared by the user, either by weighing and dissolving dry ingre-

dients or by dissolving prepared powder products, they are generally not stored for long periods before use. Developers which are marketed as prepared solutions, however, are subject to storage periods ranging from a few weeks to several years, depending not only on the distribution system of the manufacturer and his dealers, but also on the user's promptness in using stock on hand. It is highly desirable, therefore, that such prepared liquid developers possess adequate stability characteristics to insure that they will function satisfactorily after maximum storage periods.

The conditions of storage are not always ideal. It is not uncommon for temperatures during transportation and storage to reach 120 F or higher in the United States. Similarly, temperatures may fall as low in transit and storage as the lowest outside temperatures encountered. Such temperature variations impose further demands on the storage stability of liquid developers.

Many prepared liquid developers have become available over the years in various photographic fields, and, as a general rule, their storage stability has been excellent. Cold weather problems such as crystallization and precipitation have been troublesome at times, but lack of chemical stability has not been an important problem, even at high temperatures.

With the introduction of Phenidone developers, however, this situation has changed. Upon prolonged storage, especially at high temperatures, such solutions often lose activity and contrast. This instability, which has been traced to Phenidone degradation, also seriously shortens the working life of the developer.

As an example, a prepared concentrated liquid developer containing Phenidone was procured on the open market for testing in the Hunt Research Laboratories, and was found to function very satisfactorily as a paper developer at high dilution when first obtained. The concentrate was then stored at laboratory room temperature in full, tightly-stoppered amber bottles. After 16 months storage it would not develop a satisfactory image at its normal dilution or even when used without dilution.

As another example, an experimental liquid developer was prepared in the Hunt laboratories which had excellent activity, contrast, and exhaustion characteristics when freshly mixed. After six months storage at room temperature, however, its activity and contrast had decreased noticeably, and its useful life was reduced by approximately 50%.

As a result of such observations, a research program was initiated to study the influence of various conditions of storage on the rate of Phenidone degradation.

Test Formulas

Three developer formulas were selected for study. It was felt that these represented the range of alkalinity and concentration of developers containing Phenidone which have become available during the past several years.

(1) Ilford ID-68, a published formula, is a buffered borax-type fine-grain film developer of low pH (9.0) which is normally prepared at working strength.

(2) Ilford ID-67, a published formula, is a carbonate-type film and paper developer of moderately high pH (10.3) which is normally prepared in concentrated form and requires dilution of 1:2 for tray development.

(3) Hunt G-6 is an experimental formula. This is a carbonate-hydroxide-type of high pH (10.8) which is highly concentrated and normally diluted 1:7 for tray development of paper. It contains 1.20 grams of Phenidone per liter of concentrated solution in addition to hydroquinone.

Equivalent Metol formulas were also included in the test as control developers for sensitometric purposes. Ilford ID-11, a published formula, was used as the control for ID-68. Ilford ID-2, a published formula, was used as the control for ID-67. A variation of Hunt G-6, containing 12.0 grams of Metol per liter of concentrated solution in place of Phenidone, was used as the control for G-6. The Metol variation of G-6 was supersaturated at room temperature.

Sensitometric Test Methods

Sensitometric control strips used throughout the test were exposed using a nonintermittent-type intensity-scale sensitometer with a wedge density increment of 0.15.

Control strips for ID-68 and ID-67 were exposed on commercial film and developed at 20 C. Developing times were 9 min for ID-68 and $4^1/_2$ min for ID-67, using standard agitation techniques.

Control strips for the G-6 developer were exposed on a fast bromide paper and developed at 20 C for 60 sec.

Toe speed was measured as the relative log E required to produce a density 0.10 above fog. Contrast was measured as gamma.

Test Storage Conditions

All developers used in the test were prepared at the same time. Uniform samples of each were stored in full, sealed amber glass bottles. One set of samples was stored at room temperature (20-30 C), another at 50 C, and a third at 95 C. Sets contained sufficient samples of each developer so that full bottles could be withdrawn at intervals, tested, and disposed of.

The 50 C storage temperature is considered the most useful accelerated test condition, since it results in a convenient degradation interval which extends over several weeks, making periodic testing practical and minimizing test errors introduced by the original heating of the solution to oven temperature and the subsequent cooling to processing temperature. The 50 C temperature also provides more meaningful information since it represents the

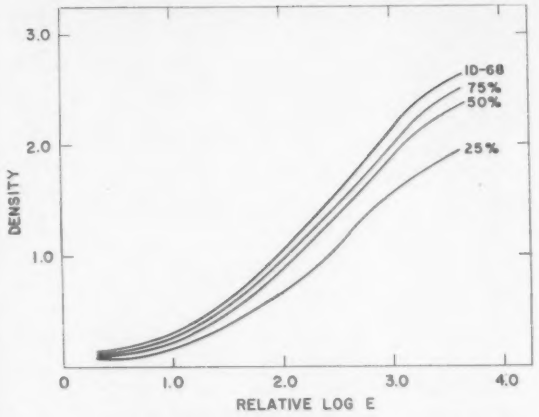

Fig. 1. Characteristic curve for test developer ID-68 and variations caused by reduction of formula weight of Phenidone.

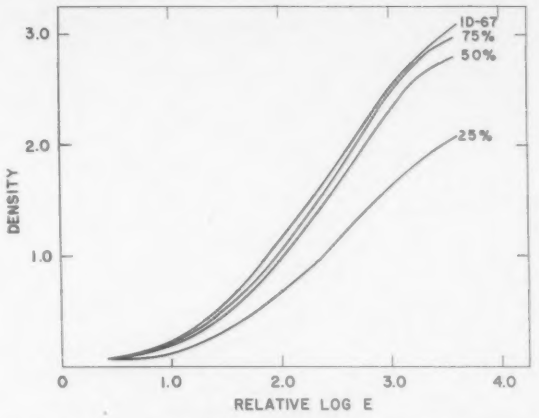

Fig. 2. Characteristic curve for test developer ID-67 and variations caused by reduction of formula weight of Phenidone.

approximate maximum temperature encountered under field conditions of transit and storage in the United States.

The samples stored at 50 C and 95 C were in total darkness. The room-temperature samples were stored in subdued room lighting.

Reference Developers

No method is yet known by which Phenidone degradation may be measured by the analysis of developer solutions. Methods which require the acidification and/or heating of the solution involve the risk of further Phenidone degradation or of the regeneration of Phenidone from the degradation product. Methods involving the extraction and oxidation of Phenidone are not sufficiently precise and also do not always appear to be selective between Phenidone and its degradation product.

In order to interpret sensitometric results in terms of Phenidone degradation, therefore, variations of the three test developers were prepared beforehand which contained 75%, 50%, 25%, and 0% of the Phenidone called for by each formula. The pH of each solution was adjusted to that of the standard test formula.

Characteristic curves for the three test developers and variations resulting from reduction of Phenidone are illustrated in Figs. 1, 2, and 3. It should be noted that in all three formulas the reduction of Phenidone to 75% of its standard formula weight causes relatively small differences in the characteristic curves. Reductions to 50 or 25% of the standard formula weight of Phenidone are required to cause marked differences in the activities of the fresh developers. Since the rate of exhaustion of a developer depends largely on the amount of Phenidone present, however, the effects of Phenidone reduction are much more serious in developers where working life is an important consideration, and even small reductions in

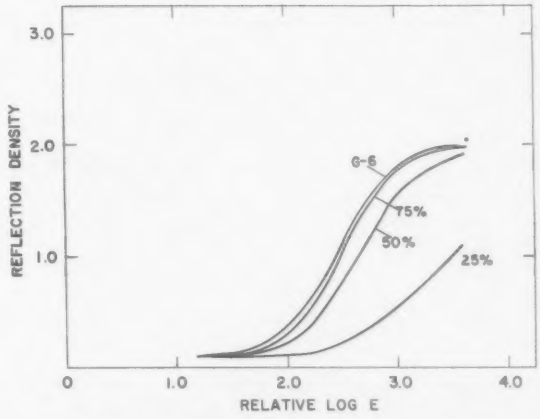

Fig. 3. Characteristic curve for test developer G-6 and variations caused by reduction of formula weight of Phenidone.

Phenidone content will cause noticeable losses in developer life.

In all three formulas the total elimination of Phenidone resulted in no density being produced over fog.

The loss of toe speed caused by Phenidone reduction in the three reference test developers has been plotted in Fig. 4, and the effect on gamma is shown in Fig. 5. The toe speed curves were used to estimate the extent of Phenidone degradation in storage tests.

Storage Test Results

The Metol control developers showed no significant changes in fog level, toe speed, or gamma after four weeks storage at room temperature, four weeks storage at 50 C, or 20 hours storage at 95 C. The Metol control formulas were considered stable, there-

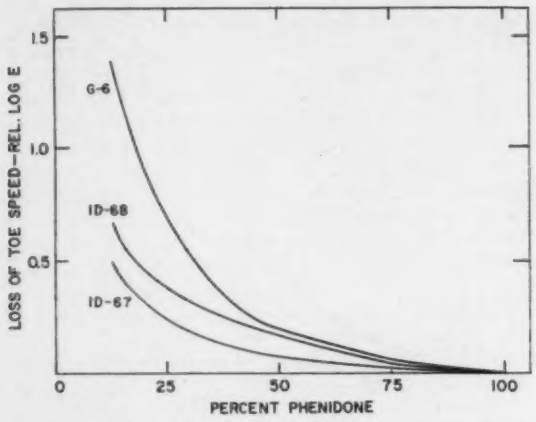

Fig. 4. Loss of toe speed in reference test developers as a function of percentage of formula weight of Phenidone present.

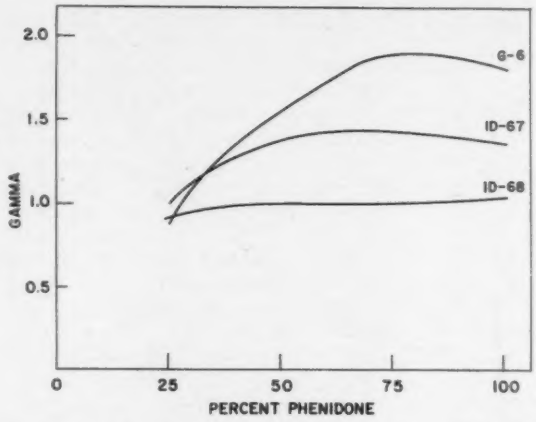

Fig. 5. Gamma of reference test developers as a function of percentage of formula weight of Phenidone present.

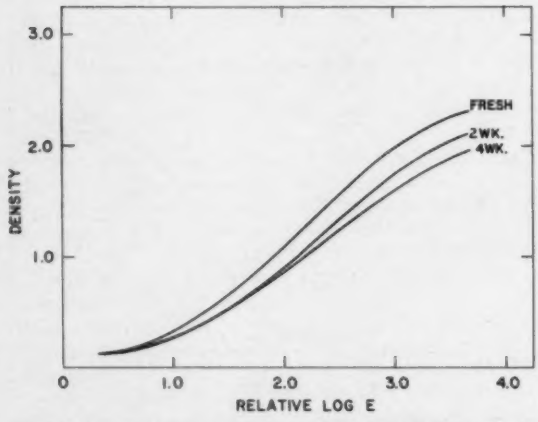

Fig. 6. Changes in characteristic curve of test developer ID-68 after various periods of storage at 50 C.

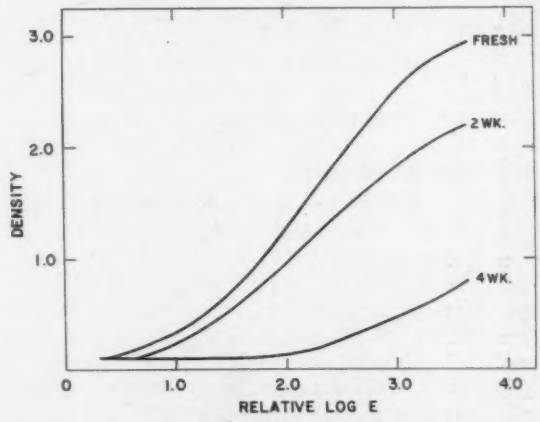

Fig. 7. Changes in characteristic curve of test developer ID-67 after various periods of storage at 50 C.

fore, and used primarily to monitor processing conditions during the test.

Samples of the three test developers stored at room temperature were tested after three days, one week, two weeks, and four weeks, and showed no significant changes in activity after four weeks storage.

Samples of the three test developers stored at 50 C all showed evidence of Phenidone degradation after various intervals, as follows:

Formula ID-68 (Fig. 6) exhibited a slight loss in toe speed after one week at 50 C, and this had become more pronounced at the end of four weeks. This formula also showed a loss of contrast which became steadily worse.

The results of degradation in ID-67 at 50 C (Fig. 7) were more striking. After one week, toe speed and contrast fell off slightly, and after two weeks the developer was judged unsatisfactory for use. At the end of four weeks at 50 C this formula was essentially inactive.

Formula G-6 (Fig. 8) showed an even more rapid loss of activity at 50 C. After three days, it was considered unsuitable for use as a paper developer, and the activity fell off steadily after two and four weeks storage.

After 20 hours storage at 95 C, all three test developers exhibited a loss in activity which was appreciably greater than that observed after four weeks at 50 C.

Losses in toe speed were determined for each of the three test developers after the various storage intervals at 50 C, and from these the extent of Phenidone degradation was estimated, using the previously established reference curves (Fig. 4). This is based on the assumption that the total loss of activity is a

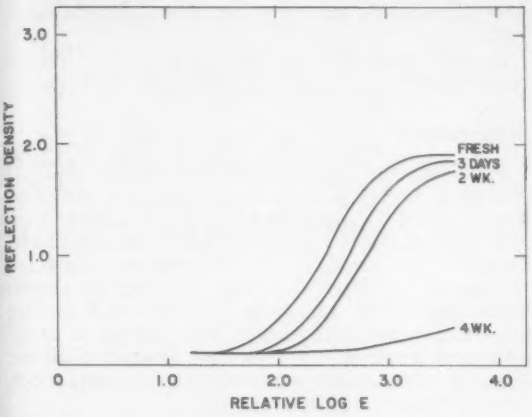

Fig. 8. Changes in characteristic curve of test developer G-6 after various periods of storage at 50 C.

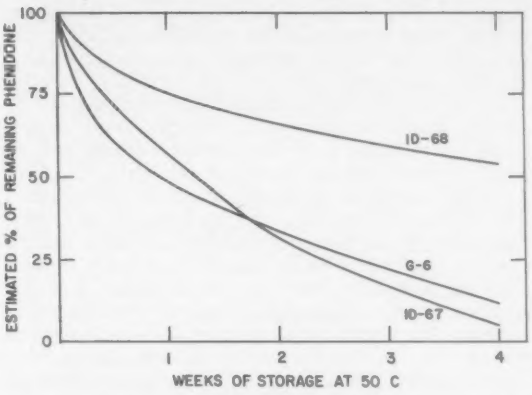

Fig. 9. Estimated Phenidone degradation in test formulas stored at 50 C based on loss of toe speed.

result of Phenidone degradation. The results were plotted, and are presented in Fig. 9.

Other Tests

In order to establish further that Phenidone degradation was the direct cause of the loss of activity noted in the field and in the above tests, a simple solution of Phenidone (0.0075 *M*) and sodium metabisulfite (0.05 *M*) was prepared (pH 4.5). Three aliquots of this solution were taken and their pH's adjusted to 7.0, 9.0 and 11.0 respectively with NaOH. Samples of these solutions were stored at room temperature, 50 C, and 95 C. After intervals of 20 hours, two weeks, and four weeks, appropriate volumes of these solutions were used to prepare small quantities of the ID-68, ID-67, and G-6 test developers, and the developers were tested sensitometrically.

Developers prepared from all samples of Phenidone solution which had been stored at room temperature for four weeks showed no loss of activity. Developers prepared from samples of Phenidone solution having pH's of 9.0 and 11.0 which had been stored at 50 C exhibited losses of activity which were similar to those observed in the test developers stored under the same conditions. Similar results were also observed in developers prepared from Phenidone solutions of pH 9.0 and 11.0 which had been stored at 95 C for 20 hours. No significant losses of activity were noted in developers prepared from Phenidone solutions of pH 7.0 which had been stored at the two elevated temperatures.

Storage Temperature Correlations

On the basis of these and similar tests, in addition to numerous observations made in the field, a correlation has been developed relating the rate of Phenidone degradation to storage temperature.

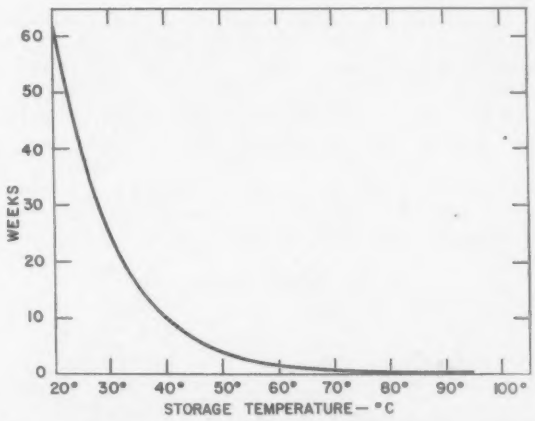

Fig. 10. Approximate relationship of storage time to storage temperature in Phenidone degradation studies.

While this is subject to further refinement, it is offered as an aid in the interpretation of accelerated storage tests. The rate of degradation appears to increase by a factor of about 2.5 with each 10 C rise in storage temperature. Thus, four weeks of storage at 50 C, or 12 hours at 95 C, is equivalent to about 14 months at 20 C. This relationship is illustrated in Fig. 10.

Conclusions

Phenidone degradation apparently occurs to some extent in all alkaline Phenidone developers. The rate at which degradation takes place depends primarily on the alkalinity of the developer and on the storage temperature. The loss of activity caused by Phenidone degradation depends on the characteristics of the developer, such as the original concentration of developing agents present and the alkali-restrainer

balance. The effects of Phenidone degradation are usually more pronounced on the working life of the developer than in the changes in characteristics of the fresh solution.

In practice, Phenidone degradation should cause no significant loss of quality in developer solutions prepared by the user from dry chemical ingredients or from prepared powder products, providing solutions are used at normal temperatures and in a period of a few weeks after mixing. Prepared liquid developers containing Phenidone, especially those with moderate and high pH's have limited shelf life. Precautions are advisable regarding the maximum duration and temperature of storage, unless ways are found to stabilize Phenidone or to compensate for its degradation.

Accelerated storage tests may be conducted at high temperatures and used to predict the shelf life of a product.

Mechanism of Degradation

It has been established that Phenidone degradation is not caused by oxidation or by reaction with other developer ingredients except, of course, the alkali. Kendall* states that the loss of activity is apparently due to a gradual opening of the pyrazolidone ring to form the sodium salt of phenyl hydrazinopropionic acid.

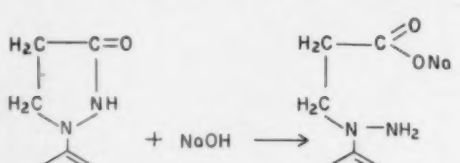

*Private communication

Experimental evidence supports such a hydrolysis mechanism.

Phenidone-B

Phenidone-B (1-phenyl-4-methyl-3-pyrazolidone) has been proposed as having improved stability. Tests similar to those described above confirm this. The improvement is relatively small in magnitude, however, and probably not sufficient to allow the unrestricted storage of highly alkaline developers formulated with this agent. Phenidone-B is also less soluble than Phenidone, and this tends to reduce its advantage in highly concentrated solutions. No field experience is yet available on Phenidone-B, however.

Acknowledgments

The author gratefully acknowledges the permission of the Philip A. Hunt Company to publish this work and also the assistance of his colleagues in the preparation of the article and illustrations. J. D. Kendall of Ilford, Ltd., has been most cooperative in furnishing information and suggestions on the subject of this study. Thomas T. Hill, formerly associated with the Hunt Research Laboratories, initiated many of the original inquiries which became the basis of this work.

References

1. Kendall, J. D., Brit. Pat. 542,502, May 28, 1941; ———, U.S. Pat. 2,289,367, July 14, 1942.
2. ———, *Brit. J. Phot.*, *100:* 56 (Jan. 30, 1953).
3. Axford, A. J., and Kendall, J. D., *J. Phot. Sci.*, *2:* 1 (1954).
4. ———, *Brit. J. Phot.*, *103:* 272 (June 8, 1956).
5. Kendall, J. D., and Axford, A. J., (Ilford, Ltd.), Brit. Pat. 708,479, May 5, 1954.

PHOTOGRAPHIC SCIENCE AND ENGINEERING
Volume 2, Number 4, December 1958

Some Simplified Shutter, Flash Synchronization, and Motion-Picture Camera Tests

SAMUEL L. LOVE, *National Camera Repair School, Inc., Englewood, Colorado*

An overlay grid technique is adapted to oscillographic testing of camera shutter speeds and flashlamp synchronization. The details are described as they apply to a particular test instrument, but are basically applicable to other cathode-ray tube instrumentation. Along with a beam-splitting device designed to facilitate measurement of "inaccessible" shutter action, the methods are outlined with particular emphasis on the value of fast and precise test procedures to the user, rather than to the designer of photographic equipment.

When a special test is to be made on a single piece of photographic apparatus, or when a single test is to be repeated on many identical units moving along a production line, the extensive setup time and costly special apparatus that may be needed are relatively unimportant. On the other hand, when it is desired to perform frequent and varied tests on a multitude of existing photographic apparatus, somewhat different requirements arise. One approach toward accomplishing many tests easily and quickly resulted in the development of the ServiShops Motion Analyzer.[1] With this instrument, widely different levels of precision can be attained to suit the test being made and the requirements of the user.

Unfortunately, an attempt to bring test procedures to a practical and simplified level often results in the degeneration of testing procedure from a quantitative to a qualitative plateau. The aim of the procedures and test accessories to be described here was to reduce the need for calculation or extra steps while still leading to dependable, quantitative test answers.

Some of the techniques herein described can also be used with other, more conventional, oscillograph test setups. However, certain dissimilarities between the setup of the ServiShops Motion Analyzer and that of conventional instruments may nullify the advantages of these simplified procedures.

Oscillograph Screen Overlays

Given dependable linearity of both the horizontal sweep and vertical deflection, transparent grids can be used over the screen of the cathode-ray tube (CRT) for direct reading of a number of variables. An overlay grid for determining shutter speeds which has been found very useful in several ways is reproduced in Fig. 1.

The design of the grid is self-evident. The length of the horizontal sweep is adjusted so that it is $^1/_2$ in. shorter than the total width of the visible screen. This sweep width is then allowed to represent 140% of true exposure time. The horizontal distance is calibrated lineally at 100% and ±10, 20 and 30%.

In order to use the chart for rapid tests, the following assumption must be made and proven: the shutter to be tested will require approximately the same amount of time to open as it does to close. The failure of any particular shutter to conform to this pattern is immediately revealed when the trace indicating shutter action appears on the screen, because in such an event the opening and closing slopes are

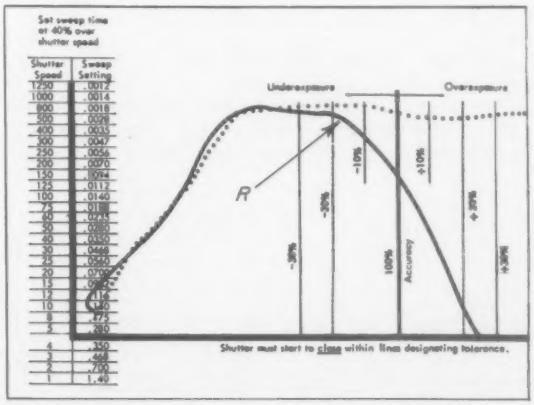

Fig. 1. A simple, transparent overlay which may be placed on the face of the cathode-ray tube to permit direct shutter-speed readings in percentage of error. When the sweep-time can be predetermined, mere linear calibration provides adequate accuracy for many tests. *Solid curve:* Trace as seen on the shutter-speed tolerance chart when shutter is tripped. Providing that opening time and closing time appear equal, good accuracy may be obtained by taking a reading at a point where the shutter starts to close (arrow marked R). The shutter speed measured here indicates an underexposure at the test aperture of approximately 18%. *Dotted curve:* Trace obtained with a shutter that delivers an overexposure greater than 40%. (Charts copyrighted by National Camera Repair School, Inc.)

Received 10 December 1957.

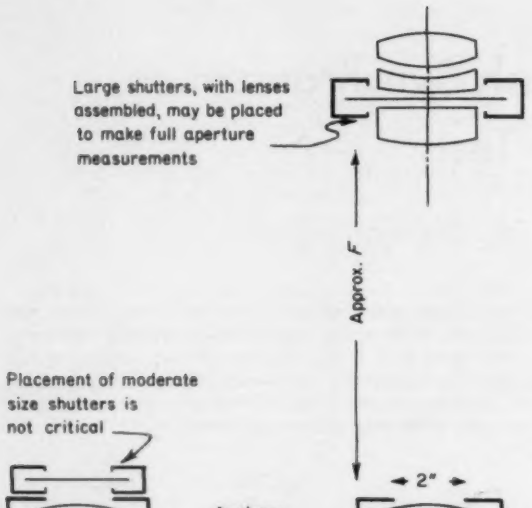
Large shutters, with lenses assembled, may be placed to make full aperture measurements
Approx. F
Placement of moderate size shutters is not critical
2"
Analyzer Optical System

Fig. 2. Diagram showing how examinations of the efficiency of between-the-lens shutters can be made effectively only if all the light passing through the aperture can be examined integrally. A small shutter (with a maximum aperture of 2 in. or less) is measured by direct placement over the optical system of the Analyzer. A shutter of unlimited size may be similarly measured by incorporating its assembled lenses into the optical system of the Analyzer.

not similar. Further tests may then be necessary for precise quantitative evaluation.

The test procedure using the chart relies on the averaging of the opening and closing times of a shutter, as indicated in the following equation:

$$\frac{T_o + T_c}{2} + T_w = E_t$$

Where T_o is opening time,
T_c is closing time,
T_w is time wide open, and
E_t is effective exposure.

But when

$$T_o = T_c$$

the equation may be reduced to the form:

$$T_o + T_w = E_t.$$

The two conditions under which the use of this simplified formula is not permissible are easily recognized from the shape of the trace that appears on the screen of the cathode-ray tube: the traces indicating the opening and closing phases of the shutter are either dissimilar or distorted.

At the same time, if either T_o or T_w is no more than 50% greater than the other, the error introduced in the term $\frac{T_o + T_c}{2}$ is 25% or less. But, a difference of 50% between opening and closing times is readily visible and indicates that more precise measurements should be made.

In order to apply the equation to practice, the sweep time on the Analyzer is set at 140% of the indicated exposure time that is to be verified. The grid overlay which includes a table of sweep times required for most common shutter speeds is placed over the screen of the CRT. When the shutter is tripped, a trace is obtained similar to that shown by the solid line in Fig. 1. If any negative error or a positive error of less than 40% exists, the trace that appears will show at least part of the closing cycle of the shutter. If the shutter remains open in excess of 140% of the indicated time period a trace similar to that shown by the dashed line in Fig. 1 will result. Two procedures for further measurement may then be followed. Individual measurements of opening, wide open, and closing time may be made and the effective exposure calculated therefrom; or an arbitrary longer exposure may be chosen and the effective exposure determined by comparison. Thus, the exposure trace shown by the dashed line (Fig. 1) resulted at a sweep time of 0.0070 sec, testing a calibrated exposure of 1/200 sec. A logical new test could be made at a sweep time of 0.0112 sec, considering that the shutter may be delivering an effective exposure approximating 1/125 sec.

The percentage of error may be determined by noting the point at which the shutter begins to close. This is indicated by the arrow (R) in Fig. 1. This error value can be interpolated easily to within 3% of the correct value; moreover, erratic shutter performance can be noted by repeated tripping of the shutter and observation of the resulting traces.

The use of the chart eliminates resetting of sweep times unless shutter speed measurements are desirable within less than 3% accuracy. Measurements which establish the exposure provided by a shutter relative to the ASA tolerances[2,3] are easily made within seconds.

The speeds of either between-the-lens type shutters or focal-plane type shutters may be measured, using the same chart, and with identical sweep-time settings.

Further Interpretation of Shutter Tests

Because the vertical deflection of the sweeping spot of the ServiShops Motion Analyzer is linear, some additional conclusions can be rapidly drawn from tests made at a particular *f*-stop and one instrument setup. An increase by a factor of two in the amount of light striking the instrument's photocell causes the height of the tracing spot to double. Similarly, a decrease by a factor of two in the amount of light striking the photocell will lower the tracing spot halfway toward its base line.

In order to take maximum advantage of this linearity, the circuit of the Analyzer is designed to prevent saturation of the photocell. The design of the optical system permits the completion of efficiency tests of between-the-lens shutters having a clear aperture of almost 2 in. Shutters of larger size having lenses

assembled to them may be tested by making these lenses part of the light-gathering system (see Fig. 2).

In instances when the linear performance characteristics of the Analyzer can be used to advantage, the sweep is adjusted to correspond with the chart "base" line at zero vertical deflection (Fig. 3) and the rise control is adjusted to place the trace at the height "O" when the shutter is open at the desired test aperture.

Additional guide lines on the shutter-speed-measurement grid (Fig. 3) permit direct reading of exposure changes that will take place as the *f*-stop of a between-the-lens shutter is changed. Two horizontal dotted lines are labeled "One *f*-stop" and "Two *f*-stops" respectively. By observing the intersection of the shutter-closing trace with either of these two lines, it is possible to predict the true exposure that will be delivered when the diaphragm is stopped down one or two stops from the point at which the test is being made.

Two facts can be determined quite rapidly through this simple test procedure: (1) how large a change in exposure will take place when the aperture is varied; and (2) the aperture at which the speeds of a particular shutter should be measured so that aperture choice would have minimum effect on exposure. The percentage of change in exposure that occurs when the diaphragm of a particular shutter is closed either one or two *f*-stops may be read directly. If, then, an aperture is selected so that *any* diaphragm change would affect exposure less than 30%, no practical exposure error correction is needed.

Routine tests of many shutters have revealed that a shutter speed measurement made at one to two *f*-stops smaller than maximum lens aperture is adequate for predicting shutter performance at other apertures. Although many commercial shutters are within ASA tolerances when tested at maximum aperture, a one *f*-stop change sometimes results in very large changes in effective shutter speed. This is true since a shutter delivering plus 30% of rated exposure is within tolerance at maximum aperture. A 30% further change at one *f*-stop below maximum means that the shutter is then exposing 60% longer than the calibrated exposure setting.

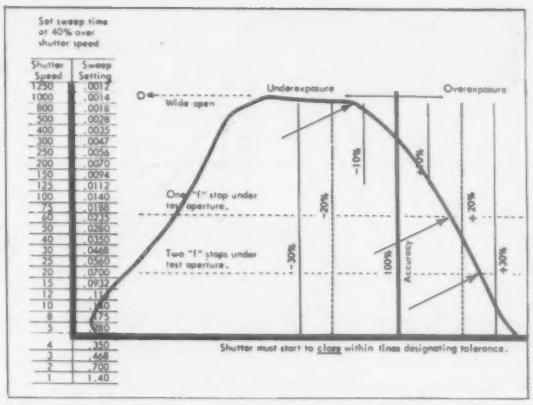

Fig. 3. The standard shutter speed overlay chart modified with additional horizontal lines to indicate the changes that will occur as the shutter is decreased in aperture. Curve shown is for special sealed-beam lamp. Although direct current would provide the most uniform light source, the lamp used here produces only a small amount of vertical ripple, due to the heating and cooling effect on the ac-powered filament.

An Overlay-Chart Flash-Synchronization Test

A further adaptation of the overlay idea greatly simplifies the analysis of the synchronization between shutter operation and the firing of a flashlamp.

A series of charts has been prepared from data obtained with the Analyzer and from specifications supplied by lamp manufacturers. On these charts the vertical scale of the curve is adjusted to fit the light output of each flashlamp within the desired screen area of the analyzer. The horizontal scale of the curve is chosen to fit the burning time of the flashlamp

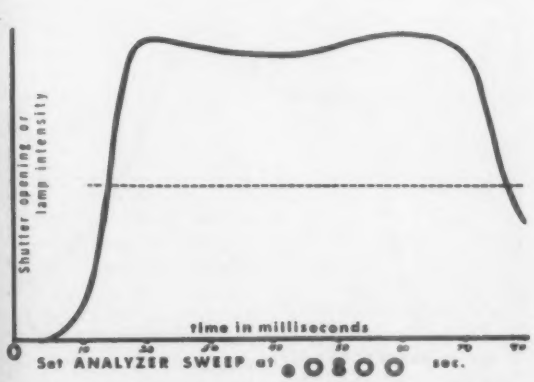

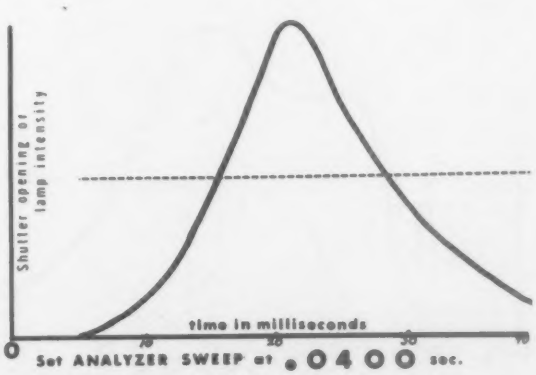

Fig. 4. Two samples of charts prepared for typical flashlamps. The choice of vertical scale and horizontal sweep time depends on the particular flashlamp for which a synchronization test is planned. The half peak line on each chart provides a guide to tolerance permissible in the checking or adjusting of any type of synchronization. (Charts copyrighted by National Camera Repair School, Inc.)

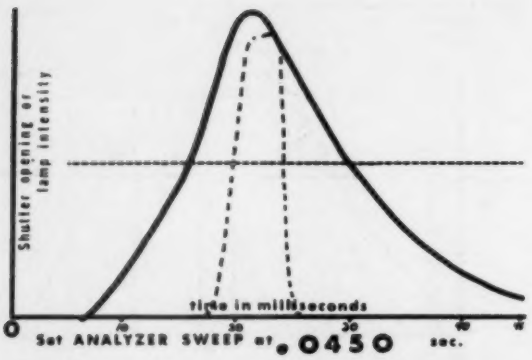

Fig. 5. Shutter opening trace superimposed on a flash chart such as is shown in Fig. 4, quantitatively revealing the quality of synchronization. Even at the short exposure used to make this test, the opening and closing traces indicate that almost half the usable flashlamp output could be utilized with the diaphragm closed two stops below maximum aperture.

and is easily matched by setting the chosen sweep time on the instrument.

Figure 4 shows two samples of charts prepared for typical flashlamps. Each chart is labeled with the proper sweep time in order to make one-test analysis possible. A synchronization test is then made in the usual way[1] except that the sweep time is governed by the chart in use. The choice of the setup is determined by the type of synchronizer being checked. Operation of the shutter and synchronizer yields a trace similar to that shown in Fig. 5, from which it is immediately evident whether or not the shutter opens during the time that the lamp is at half peak or brighter.

With this technique, a rapid quantitative synchronization test is achieved and with a typical shutter-synchronizer combination, the following facts can be quickly revealed:

(1) Adequate synchronization is possible with either one or two flashlamps at all shutter speeds.

(2) An exposure setting of longer than 1/100 sec will not yield an increase in negative density.

(3) Exposures made at the fastest shutter speed and with the lens aperture one *f*-stop smaller than maximum, rather than "wide open," would mean the difference between positive synchronization and possible failure.

There are many instances when synchronization between particular shutter units and a marginal lamp (3 to 18 msec to peak) becomes possible only when the *f*-stop is carefully chosen.

When the synchronization of a flashlamp and a focal-plane shutter is tested, check measurements must be made at various phases of the lamp burning and curtain travel cycles. The dotted lines in Fig. 6A show the appearance of a series of tests made at the leading, central, and trailing parts of the focal plane, with a focal-plane shutter in which synchronization is satisfactory. A shutter that would not provide satisfactory synchronization is revealed in Fig. 6B; here the margin of the focal plane uncovered last by the traveling shutter would not receive sufficient light from the flashlamp. The need for a lamp having a "longer" peak is clearly apparent in this case.

The test patterns may be permanently recorded on a tissue replica of the CRT screen overlay or by photographic techniques. Most technically uninformed users can easily understand and use this type of graphic representation without extensive explanation.

"Inaccessible" Shutter Tests

At least two types of photographic equipment employ shutters which cannot conveniently be used to transmit light to a test instrument:

(1) Enclosed-back cameras of the Leica type, and

(2) Motion picture cameras that either have a focal plane which is not easily accessible, or should be tested with the body closed and the film in position in order to gain precision.

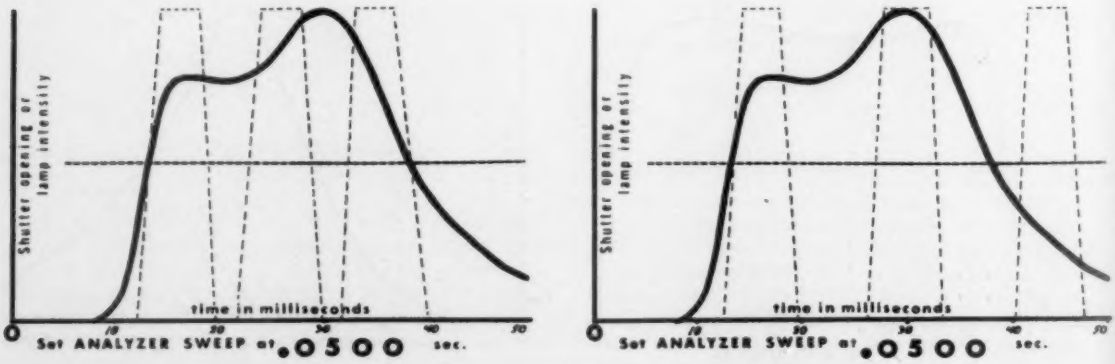

Fig. 6. A synchronization test of a focal-plane shutter and lamp. These differ but slightly from similar tests with between-the-lens shutters. The slit mask is used in the Analyzer optical system.

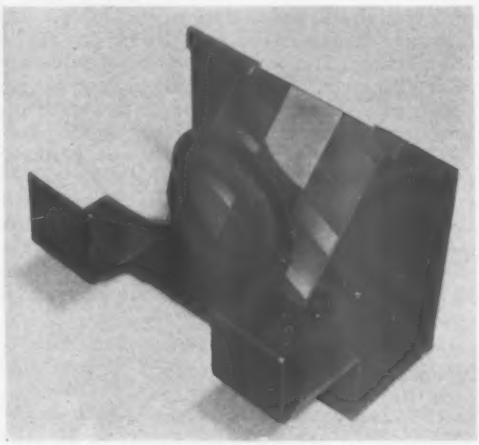

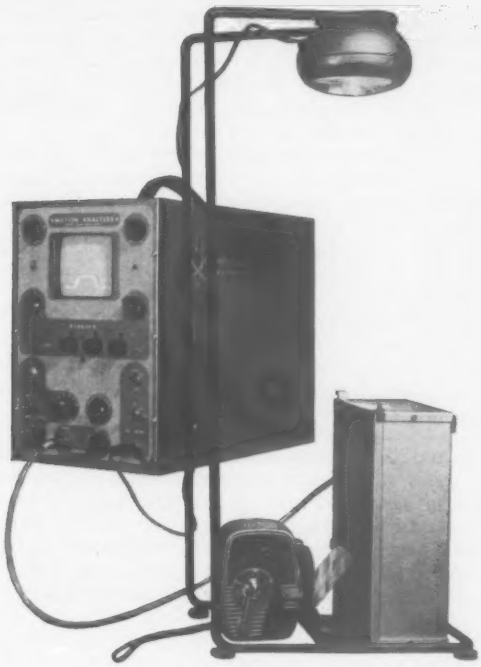

Fig. 7. Beam-splitter adapter used for measurement of still-picture-camera shutter speed and motion-picture-camera picture-sequence time intervals having otherwise inaccessible shutters.

Above: The beam-splitter adapter. The adapter attaches firmly to the standard ServiShops Analyzer photocell housing.

Right: The beam-splitter adapter placed into optimum position during a test. The open design of the light stand permits flexible setup arrangements with such special adapters.

With both types of cameras a measuring technique may be used in which light is reflected from all or part of the focal plane. A simple unit was designed for this purpose. It may be attached to the ServiShops Motion Analyzer photocell housing by means of a clip which slides into the mask-slot (see Fig. 7). A schematic diagram indicating the path of the light rays is shown in Fig. 8. The unit incorporates a special reflector that is fitted in the focal plane of the Leica-type camera and occupies the position normally taken by the film. The reflector consists of two slit-like mirror surfaces, oriented perpendicular to the direction of curtain travel. Only one at a time may be slid into position, either at the leading or the trailing edge of the focal plane. The reflector is made of a triple lamination of black paper on each side of a foil filling, in order to eliminate any danger of damage to the aperture plate or pressure pad of the camera. Light passed by the slit in the traveling focal-plane shutter and reflected from the mirror then triggers the instrument for a shutter speed measurement that may be made in the normal way.

The beam-splitter used in the reflector unit is silvered along two strips located on either side of an unsilvered central area. The choice of this type of beam-splitter was governed by the following factors:

(1) The desire for a reflecting surface in the focal plane having a minimum area;

(2) The small amount of light that could be reflected from such a surface;

(3) The amount of light loss incurred by double reflection from a semitransparent beam splitter.

The sensitivity of the Analyzer coupled with this beam-splitter design is sufficient to permit differentiation between uncontrollable scatter reflection and the reflection from a good reflective surface that measures 0.030 by 0.75 in. As a result, measurements can

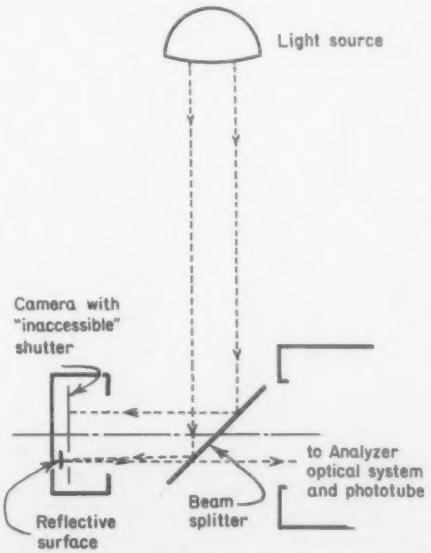

Fig. 8. Diagram showing the light path provided by the beam-splitter attachment.

be made of light reflected from the pressure pad or from film passing through an 8mm motion picture camera. In this case it is only necessary to mask all polished surfaces which might decrease the signal-to-noise ratio. With adequate masking (which may be accomplished with the use of black-paper tape) the difference between the light reflected from the surface of a shutter blade and that reflected from a film surface is easily observed and can be used to time the picture-sequence interval of the camera. Cameras larger than 8mm have enough film area so that the reflection difference is quite great and therefore far less care is needed in eliminating scatter reflection.

The advantages of being able to time a camera that is closed, loaded, and in ordinary operating condition, are obvious. The errors so introduced are measurable.

Conclusions

Although the simplification of precision test procedures is clearly advantageous to field-service men, other advantages should not be overlooked. Whereas the manufacturer may design and use special test procedures for production work and the engineer may have unlimited facilities for essential tests, a test that may be made more quickly or clearly may be both economically advisable and analytically desirable. Rapid quantitative testing makes it possible for the user of the photographic apparatus to predict his result more intelligently. Every control factor that is removed from its questionable status means that the creative, artistic, or scientific purpose of the photographer may be more completely or easily fulfilled. Careless use of a simple qualitative test procedure may only tend to discredit the manufacturer of the equipment. On the other hand, intelligent use of a simple quantitative test procedure will provide any photographer with facts which will permit him to make far better use of equipment which he more fully understands.

References

1. Love, S. L., and Blackwell, L. L., "A New Approach to Photographic Apparatus Testing," *Phot. Sci. and Tech.* (II), 4:13 (1956).
2. *American Standard Exposure-Time Markings for Between-The-Lens Shutters Used in Still Picture Cameras*, PH3.5–1952, American Standards Association, New York, 1952.
3. *American Standard Exposure-Time Markings for Focal-Plane Shutters Used in Still Picture Cameras*, PH3.3-1952, American Standards Association, New York, 1952.
4. Tyroler, J. F., and Smith, C. L., "New Computer Method for Obtaining Optimum Area," *Rev. Sci. Instr.*, 27: 397 (1956).

PHOTOGRAPHIC SCIENCE AND ENGINEERING
Volume 2, Number 4, December 1958

System Analysis and Performance of a Feedback Scanning Printer

L. L. Blackmer and J. C. Marchant, *Research Laboratories, Eastman Kodak Company, Rochester, N.Y.*

Contact printing is carried out by means of a moving spot of light optically projected from the face of a cathode-ray tube onto the printing plane. The spot intensity is instantaneously varied in accordance with local densities of the negative in such a way that a wide-range, linear compression of effective density scale in the negative is obtained. The electrical transfer characteristics are discussed and their performance is analyzed in equivalent photographic terms.

Pictorial negatives generally exhibit wide variations in over-all density and in density scale. To print the gamut of such negatives satisfactorily on conventional printing papers, several grades of paper are frequently required. For routine printing operations involving large numbers of negatives, it would be desirable for economy's sake to make all prints on a single grade of paper.

One approach involves the use of either dodging or masking to compress the effective printing range of the negative by a suitable amount.[1] Photographic masking techniques are useful in certain cases, but they are not economically practical when only a few prints are to be made from each of a large number of negatives.

A similar problem exists in the television industry when flying-spot scanners are used for the transmission of pictures recorded on film. Theile and McGhee[2] showed that the effective tonal scale of a negative can be compressed within the range of the television system by the application of over-all negative feedback from the output of the photoelectric pickup to the control grid of the scanning tube. The net result is equivalent to that obtained by photographic unsharp masking but is accomplished automatically.

By placing photographic paper in the image plane of the optical system between the negative and the photoelectric pickup, Craig[3,4] applied the same principles to photographic printing. For a large scanning spot, however, the result more nearly resembles dodging than masking. The present discussion is concerned with the electrical transfer characteristics required to produce wide-range linear compression of density scales and the photographic performance achieved in contact printing.

Communication No. 1974 from the Kodak Research Laboratories.
Received 22 July 1958.

Apparatus

The principal elements of the printer used for this investigation are outlined in Fig. 1. Except for the addition of a nonlinear amplifier, the arrangement is essentially the same as that described by Craig.

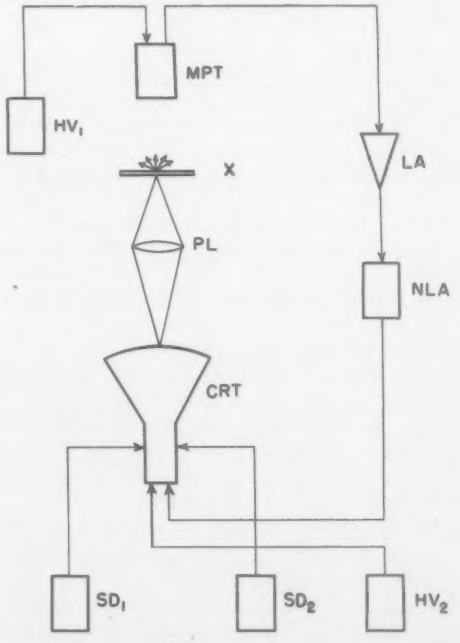

Fig. 1. Block diagram of scanning system. CRT, cathode-ray tube; PL, projection lens; X, printing frame with negative and positive stock; MPT, multiplier phototube; HV_1 and HV_2, high-voltage supplies; LA, linear amplifier; NLA, nonlinear amplifier; SD_1 and SD_2, sweep drivers.

A radiant spot on the face of the cathode-ray tube (hereafter referred to as the CRT), moving in an isotropic pattern as described by Kovasznay, Joseph, and Newman,[5] is optically projected to the plane of the negative X by an anastigmatic lens, PL, of 135mm focal length. At $f/4.5$ and approximately unit magnification, the spot diameter at the printing plane is $^1/_8$ in. This light provides the printing exposure. Some of the light passes through the negative and positive stock and reaches the multiplier phototube, MPT, mounted above the platen. The transmittance of the photographic paper is sufficiently uniform for the instantaneous output of the phototube to be proportional to the transmittance of the negative for each position of the spot. After suitable amplification the resulting electrical signal is applied to the control grid of the CRT in such a manner that the spot intensity is instantaneously and proportionately decreased whenever the spot passes into areas of low density in the negative.

The electrical circuits are not given in detail because they do not involve any novel features. Nevertheless, they must fulfill certain requirements:

(1) In order to make the static measurements, described in the next section, the radiance of the spot in the CRT must be uniquely related to the density of the negative on which the spot is focused. This means that the potential of the CRT control grid must be proportional, not to the change in the amount of light incident on the phototube as the negative is scanned, but to the instantaneous value of the density itself. The electrical circuits are, therefore, directly coupled throughout.

(2) The radiance of the CRT is a power function of control-grid voltage. If compression is to be linear with density, this transfer function must be matched to the logarithmic absorption characteristic of the negative in a proper manner. That is, the logarithm of the radiance must be instantaneously proportional to the density over the printing spot. This is achieved by using a direct-coupled, nonlinear amplifier, NLA, such as a remote cutoff pentode, between the main amplifier, LA, and the CRT. The procedure for aligning the amplifiers will be discussed in detail in the next section.

(3) The amplifiers must have a flat frequency response up to the maximum frequency generated by the particular combination of spot size and spot velocity used. In the present case, this amounts to a sine-wave response of 100 kc/sec for a $2^1/_4 \times 3^1/_4$-in. negative. This requirement is easily fulfilled by several commercially available amplifiers.

(4) Owing to the phosphor persistence of the CRT screen, the phototube receives light not only from the point over the scanning spot but also from the integrated light emitted from areas of the screen previously scanned. This phenomenon causes defects in the picture similar to those produced by poor high-frequency response and is discussed at length by Theile and McGhee. In the present apparatus, the effects of phosphor afterglow are minimized by making the reciprocal of scanning velocity large compared with the phosphor decay time.

(5) While closed-loop circuits normally exhibit a high degree of stability, spurious transients and other externally caused variations will be reproduced as variations in print density. It is therefore important that power supplies HV_1 and HV_2 be adequately regulated. This is particularly true of the phototube supply, because gain is a power function of the dynode potentials.

Analysis of the System

The radiance characteristic of the CRT is readily obtained in terms of the output voltage signal of the multiplier phototube. Since the response of the phototube is linear, its output is directly proportional to the illumination at the printing plane. If feedback loop is opened and a negative potential e_g is applied to the CRT control grid, the output signal is approximately

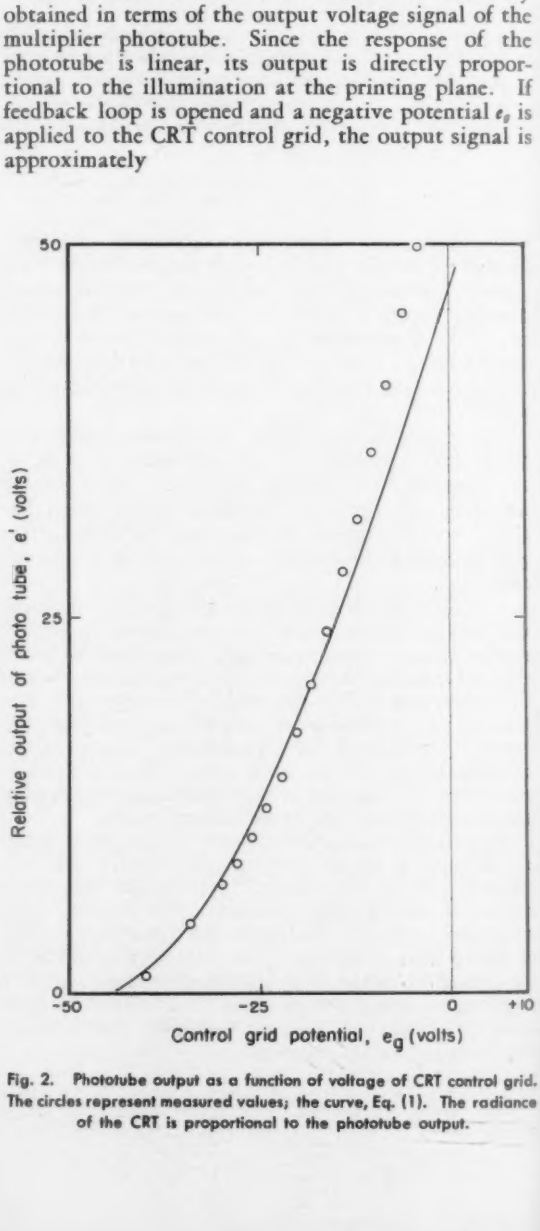

Fig. 2. Phototube output as a function of voltage of CRT control grid. The circles represent measured values; the curve, Eq. (1). The radiance of the CRT is proportional to the phototube output.

$$e' = a(b + e_g)^n, \qquad (1)$$

where a, b, and n are constants. The exponent n has a value of about 1.5 and is fairly constant for tubes of a given type operated under the same conditions; b relates to the grid cutoff potential and exhibits considerable variation from tube to tube.[6] In the curve of Fig. 2, e' is plotted against e_g for $a = 0.14$, $b = 44$, and $n = 1.54$. These values were chosen to give the best fit to the circled points which represent measured values. Although the calculated values depart somewhat from the measured values at high potentials, the equation is quite adequate for the present discussion.

A third-order equation derived by the method of least squares produces better correlation with the measured points. However, it is too unwieldy for the mathematical manipulations described below.

When the feedback loop is closed, its effect can be expressed in terms of what is known as the "masking coefficient." Before discussing the final system, it is instructive to examine the somewhat simpler case in which the nonlinear amplifier is omitted. The density of the negative is D and the output signal at the phototube is e, where the prime has been removed to show that the control grid is now associated with the output of the phototube. Then, as shown in the Appendix, the electronic masking coefficient for constant amplifier gain G is

$$\frac{\Delta \log e}{\Delta D} = \frac{Ge - C_o}{(n-1)\,Ge + C_o}. \qquad (2)$$

Here C_o is a constant related to the output voltage level of the amplifier and amounts approximately to the grid cutoff potential of the CRT. The constant n comes directly from Eq. (1); the constant b in the latter equation is included in C_o, while a has dropped out.

Equation (2) is plotted in Fig. 3 for one value of constant amplifier gain, the experimental points being indicated by the small circles. The precision is low at the higher densities because of stray light and small signal-amplitude, but the correspondence with the theoretical curve is close enough to indicate the practical usefulness of Eq. (2).

By definition, $\Delta \log E/\Delta D$ is the photographic masking coefficient where E is the printing exposure. Since $E = I \cdot t$ (printing flux times exposure duration) and t is a constant for any given spot size and spot velocity, then E is directly proportional to I. But e, the output signal of the photocell, is also proportional to I; hence, Eq. (2) can be written as

$$\frac{\Delta \log E}{\Delta D} = \frac{Ge - C_o}{(n-1)\,Ge + C_o}. \qquad (3)$$

This equation expresses the relationship, then, between the photographic masking coefficient and the electronic parameters of the system.

This ratio indicates the change in log exposure of the positive material corresponding to a change in density of the negative as the spot moves across the printing plane. When its value is unity, the exposure is unmodified; the feedback circuit is open, and the masking is zero. If the value of the ratio were zero, the density variations of the negative would be fully compensated by the variations in the radiance of the CRT; except for edge effects, the developed print would have a uniform density and the masking would be 100%.

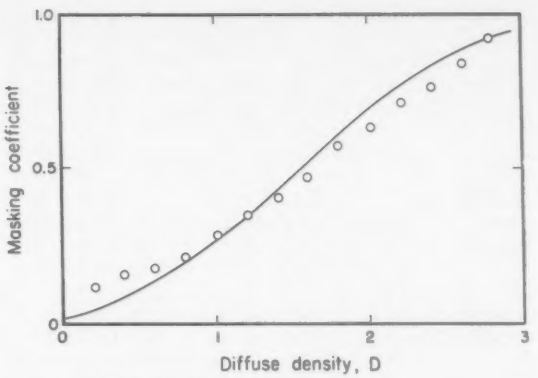

Fig. 3. Masking coefficient as a function of the density of the negative. The circles represent experimental values; the curve, Eq. (2).

If the relative tonal scale of the print is to be undistorted, the masking coefficient must be constant with density, or

$$\frac{\Delta \log E}{\Delta D} = K. \qquad (4)$$

Figure 3 shows that this condition is far from being fulfilled with a linear amplifier alone.

A practical method of maintaining constancy of the coefficient is to control the amplifier gain G in accordance with density of the negative. It is easy to show that the coefficient will be constant if

$$G = \frac{(K+1)\,C_o}{(1-n)\,K + 1} \cdot \frac{1}{e}. \qquad (5)$$

This method fails in the trivial case of $C_o = 0$, but, in practice, this does not happen.

Equation (5) describes the characteristics of the nonlinear amplifier, but the amplifier is most easily adjusted by using an empirical approach. Equation (1) indicates the relation between the output signal e of the phototube and the control grid potential e_g on the CRT, while it can be seen from Eq. (4) and the relation $\Delta \log e = \Delta \log E$ that

$$\log e = -KD + \text{constant}. \qquad (6)$$

The procedure is to find the values of e_g required to produce the values of e given by this equation over the desired range of density when K is constant. With the feedback loop open and no negative in place, e_g is adjusted to make e just slightly greater than zero. The logarithm of this value of e represents the constant in Eq. (6). A curve of e_g against e can then be plotted by inserting successively a graded series of

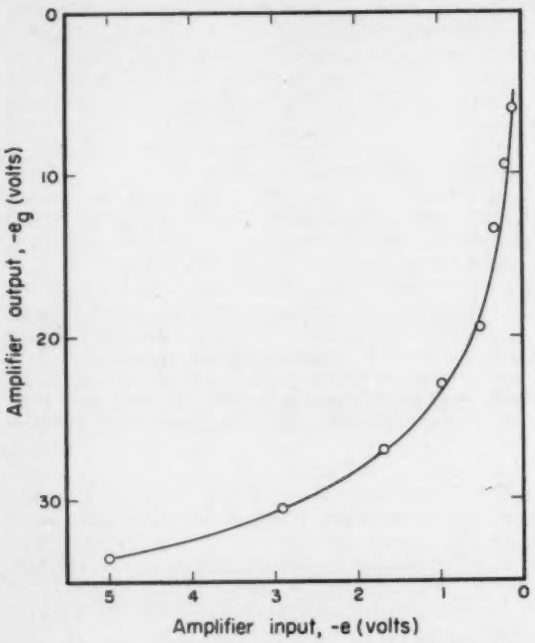

Fig. 4. Characteristic of nonlinear amplifier required for 40% linear masking.

neutral filters in the printing frame and determining the values of e_g that are necessary to fulfill Eq. (6). Such a plot is shown in Fig. 4 for $K = 0.6$.

The curve just obtained is then transferred to the face of a cathode-ray oscilloscope arranged to have a horizontal time base. A linear sawtooth signal is applied across the input to the amplifier, and if the vertical plates of the oscilloscope are connected to these terminals, the upper trace in Fig. 5 results. The oscilloscope is then transferred to the output terminals of the nonlinear amplifier and the operating point and gain of this amplifier are manipulated until the trace coincides with the desired curve drawn on the face of the screen, as shown by the lower trace in the figure. The nonlinear amplifier should now be in a condition to compensate for the nonlinearity of the rest of the system.

When the feedback path is closed, the constancy of the masking coefficient can be determined by placing a graded series of neutral filters successively in the printing frame and measuring the output of the phototube. When $\log e$ is plotted against D, the electronic masking coefficient $\Delta \log e/\Delta D$ is constant if the points fall on a straight line. The slope of this line is the value of the coefficient. Since $\Delta \log e = \Delta \log E$, the same graph indicates the constancy of the photographic masking coefficient and also its numerical value.

The final adjustments to the nonlinear amplifier are made by plotting the graph of $\log e$ against D (Fig. 6). This figure shows by the small circles how closely the apparatus fulfills the linear condition expressed by the solid line. This line corresponds to a masking coefficient of 0.6, which is commonly referred to as 40% masking. The sloping broken line of unit slope represents a masking coefficient of unity, which is equivalent to no feedback or zero masking, while the horizontal broken line represents a masking coefficient of zero, which is equivalent to full compensation or 100% masking.

Photographic Performance

The effect of unsharp masking is to compress density differences of gross details in the negative. The density range in areas smaller than the printing spot, of course, remains unchanged. Since the print is the final result, masking may also be considered as modifying the characteristic curve for large area detail.

When the masking coefficient is constant, the characteristic curve of the print should have the same form as the characteristic curve of the printing stock itself, but the gradient, at any given density, is less in the masked curve than in the unmasked curve by a proportional amount. Figure 7 shows, by the solid line, the curve obtained with no feedback, which is the curve ordinarily obtained. The broken line represents the way in which a gray scale is reproduced on the same grade of paper with 40% masking and the exposure adjusted to give a general density level equal to that of the unmodified print.

In deriving the curves of Fig. 7, direct coupling was used throughout the feedback path. Once the nonlinear characteristic of the amplifier has been established, identical results may be obtained with conventional resistance-capacitance coupling of adequate time constant. In this case, the operating point of the CRT, and thus the average radiance, is determined by the average density of the negative.

It would be desirable for the scanning spot to be

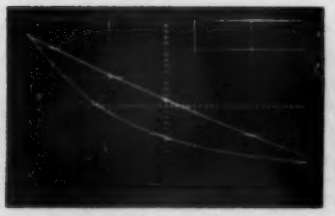

5A

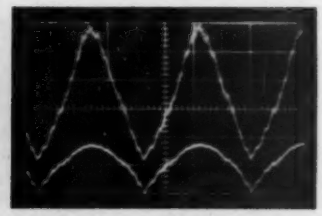

5B

Fig. 5A. Characteristic of nonlinear amplifier as displayed on cathode-ray oscilloscope. Upper trace, linear sawtooth input; lower trace, nonlinear output warped to compensate for remainder of system. Horizontal scale, time from right to left.

Fig. 5B. Effect of scanning gray scale of uniform density increments. Upper trace, output of nonlinear amplifier; lower trace, output of phototube. Horizontal scale, time from right to left.

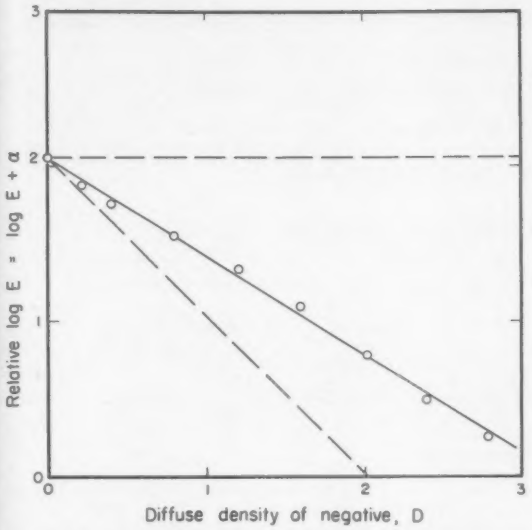

Fig. 6. Test of linearity of masking. The logarithm of the phototube output, which is proportional to printing exposure, is plotted against the density of the negative. The circles represent experimental points; solid curve, condition for 40% linear masking; sloping broken line, zero masking; horizontal broken line, 100% masking.

modulated instantly when it traverses a sharp boundary between regions of different density, but since the spot necessarily has a finite size, a certain amount of edge effect is produced. This effect increases in magnitude as the percent masking increases. It enhances the apparent sharpness of the picture,[5] but if it is very pronounced, the appearance is most unpleasant for some scenes. Although the effect is present, it is generally not objectionable if masking is held below about 50%.

While masking cannot increase the effective printing scale of the negative (or conversely decrease the log exposure scale of the printing medium), the method just described may be used to devise other curve shapes. For example, if the feedback amplifier is linear, the masking coefficient varies with density, as shown in Fig. 3. The way in which a gray scale is reproduced on Grade F2 Kodabromide Paper under these conditions is shown in Fig. 8. The highest curve is the ordinary characteristic curve that would be obtained by simple contact-printing. The lower curves represent increasing amounts of amplifier gain, constant in each case. The increasing distortion in the region of high print densities (the shadow region) is striking. This type of control over the shape of the paper curve might sometimes be desirable. If the curve shape is to be preserved, however, the masking coefficient, as distinguished from the amplifier gain or any other circuit parameter, must be held constant.

Appendix

Derivation of the loop equations

Equation (2) of the text can be derived by considering Fig. 9, where the cathode-ray tube, *CRT*, sends light to a multiplier phototube, *MPT*. When the negative, *Neg*, is out of the beam and the switch, *SW*, is connected to a potential source, *V*, as shown, the output potential of the phototube e' is related to the control-grid potential e_g of the CRT by the relation

$$e' = a(b + e_g)^n, \qquad \text{(A1)}$$

as shown by Fig. 4. As in Eq. (1) of the text, a, b, and n are constants. In this case, the flux L on the phototube equals the flux B emerging from the CRT, but, when a negative of transmittance T is introduced, $L = TB$. Hence, $e = Te'$ and the phototube output becomes

$$e = 10^{-D}a(b + e_g)^n, \qquad \text{(A2)}$$

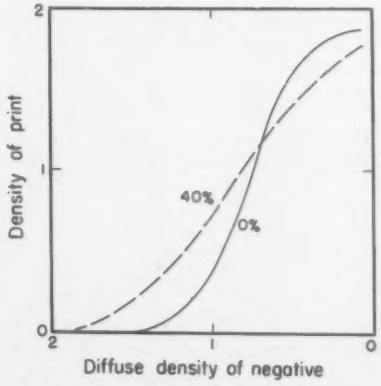

Fig. 7. Characteristic curves of Kodabromide Paper, Grade F4, made in scanning printer with no masking and with linear masking of 40%.

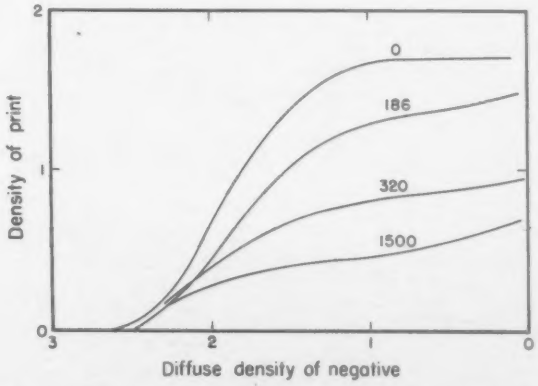

Fig. 8. Characteristic curves of Kodabromide Paper, Grade F2, made in scanning printer with various amounts of feedback through a linear amplifier. The relative gain of the amplifier is indicated on each curve.

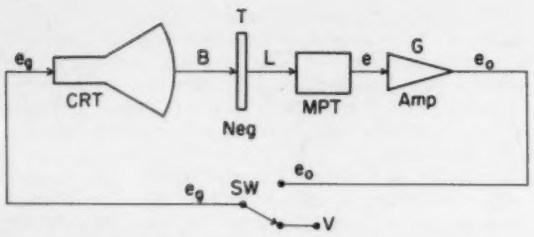

Fig. 9. Simplified block diagram of scanning system. CRT, cathode-ray tube; Neg, negative being printed or neutral filter used for testing; MPT, multiplier phototube; Amp, nonlinear amplifier; SW, switch to control feedback circuit.

where, for convenience, the transmittance T has been written in terms of density D. The output of the amplifier is

$$e_o = C_1 - Ge, \tag{A3}$$

where C_1 is the d-c level of the output signal and G is the gain of the amplifier. When the switch SW in the feedback circuit is thrown up, the control-grid voltage e_g must be equal to the output signal e_o from the amplifier. The value of e_o from Eq. (A3) can be substituted for e_g in Eq. (A2) to give

$$10^{D}e = a(C_o - Ge)^n, \tag{A4}$$

where $C_o = C_1 + b$. Taking the logarithms of both sides gives

$$\log_{10}e + D = \log_{10}a + \frac{n}{\ln 10}\ln (C_o - Ge), \tag{A5}$$

which, when differentiated, gives

$$\frac{d \log_{10} e}{dD} + 1 = -\frac{nG}{\ln 10}\frac{de}{dD}(C_o - Ge)^{-1}. \tag{A6}$$

If the numerator of the right-hand side is multiplied and then divided by e, and it is remembered that $d \ln e = de/e$, it can be shown that

$$\frac{d \log_{10}e}{dD} + 1 = -nGe\frac{d \log_{10}e}{dD}(C_o - Ge)^{-1}. \tag{A7}$$

The terms can now be rearranged to give

$$\frac{d \log e}{dD} = \frac{Ge - C_o}{Ge\ (n-1) + C_o} \tag{A8}$$

which is Eq. (2) in the text.

References

1. Eden, J. A., "The Unsharp Masking Technique of Printing Aerial Negatives," *Photogram. Record, 1:* 5–26 (1955).
2. Theile, R., and McGhee, H., "The Application of Negative Feedback to Flying Spot Scanners," *J. Brit. Inst. of Radio Eng., 12:* 325–329 (1951).
3. Craig, D. R., "The LogEtron: A Fully Automatic, Servo-Controlled Scanning Light Source for Printing," *Phot. Eng., 5:* 219–226 (1954).
4. ———, "LogEtronics," *Photogram. Eng., 21:* 556–563 (1955).
5. Kovasznay, L. S. G., Joseph, H. M., and Newman, N., *Image Processing,* National Bureau of Standards Report No. 4108, June 1955.
6. Soller, T., Starr, M. A., and Valley, G. E., Jr. (editors), *Cathode-Ray Tube Displays,* McGraw-Hill Book Co., New York, 1948, p. 75.

PHOTOGRAPHIC SCIENCE AND ENGINEERING
Volume 2, Number 4, December 1958

Quantitative Estimation of Photographic Kink Susceptibility

BEAT MEERKÄMPER, *Photo Products Department, Research Division, E. I. du Pont de Nemours & Company, Inc., Parlin, N.J.*

The sensitization or densitization of a photographic emulsion following a bend or kink can be a troublesome practical problem. A simple device is described which provides a quantitative estimate of the tendency to kink sensitization or desensitization in terms of the radius of curvature of the film bend. Practical and theoretical implications are discussed.

The desensitization or fog formation of a photographic emulsion following a bend or kink can be a troublesome practical problem. For practical purposes the kink susceptibility of a photographic material is the combined effect of three factors; first, the physical strain on the grains when the film is kinked; second, the photographic response of the grains to the strain inflicted on them; and third, the mechanical characteristics of the film structure which determine its tendency to form a kink under "normal" handling conditions. The test method to be described measures the photographic response to controlled deformations of the film (i.e. a product of the first two factors) such as occurs very frequently in a great number of photographic devices. It does not consider the forces necessary to cause this deformation and consequently gives no information concerning the ease with which a kink is formed in a given film.

Experimental Apparatus

The problem was to devise an apparatus which would deform photographic films in a controlled manner to simulate kinking. It was also desired that the uniformly deformed areas be large enough for quantitative measurement with a densitometer. A schematic diagram of the apparatus designed to fulfill these requirements is shown a Fig. 1. It consists of two plates, Plate 1, which is in a fixed position, and Plate 2, which is guided along rails at a defined distance parallel to Plate 1 (Fig. 1a) or at an angle to Plate 1 (Fig. 1b). In performing the test, one end of the 3.5 × 25-cm test strip is fixed at Point A of Plate 1 and the other end at Point B of Plate 2. Then Plate 2 is moved rapidly and uniformly from start to end position, thus forcing the film to roll from Plate 1 to Plate 2 while describing a circular 180° bend with a radius given by the distance between the two plates. Interference of abrasion effects is avoided as the test film never slides on any surface.

Experimental Results

Several types of test can be performed with this apparatus. The most complete picture of the response of a photographic emulsion to bending at low radius is obtained with the parallel arrangement (Fig. 1a). In this case, the whole length of the strip is bent with the same radius (which can be varied from strip to strip), making it possible to expose a sensitometric wedge on the strip either before or after bending. Figures 2 and 3 show H & D curves of two sets of data obtained with two different double-coated experimental emulsions. Each set contains seven strips, the control (exposure only), three bent (with the radii 2, 2.6 and 4 mm) before and three after sensitometric exposure. These two sets are illustrated because the two emulsions show

(a) Constant radius

(b) Variable radius

Fig. 1. Quantitative "Kink Tester." (a) Parallel arrangement of plates; film (– – –) is bent with constant radius. (b) Plate 2 at a 5° angle in respect to Plate 1; film (– – –) is bent with continuously decreasing radius.

Presented at the Annual Conference, N.Y., 8 October 1958. Received 12 September 1958.

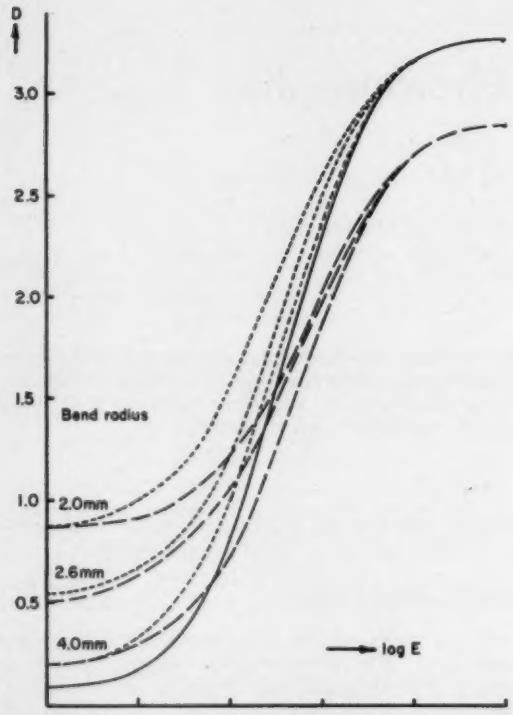

Fig. 2. H & D curves of Emulsion A (—), bent before (– – –) and after (···) exposure.

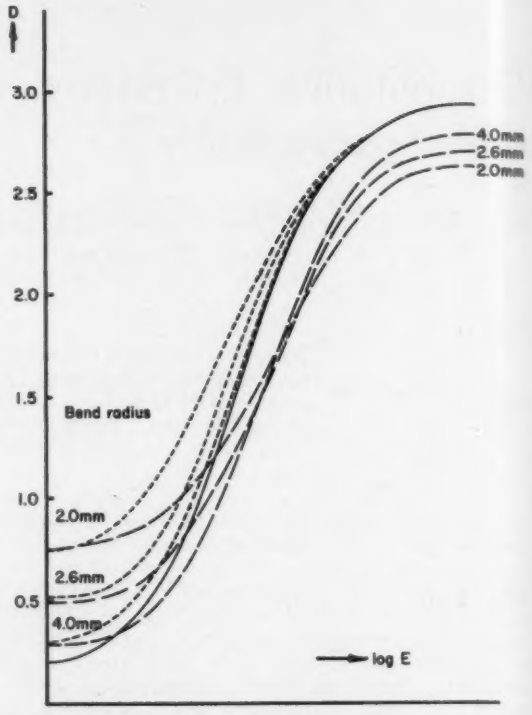

Fig. 3. H & D curves of Emulsion B (—), bent before (– – –) and after (···) exposure.

characteristic differences in their response to this type of mechanical strain. Both emulsions exhibit an increase in fog depending on the bending radius. As can be expected, there is little difference in the fog response whether an exposure is made before or after bending. The desensitization is observed only when bending precedes the exposure. Both emulsions show the decrease in maximum density which is characteristic for the densitization. In the case of Emulsion A (Fig. 2), the desensitization is independent of the bending radius, i.e. of the forces inflicted on the grains within the limits of the experiment. Emulsion B (Fig. 3) shows a loss in D_{max} which is a function of the bending radius. In addition, the entire curve of Emulsion B is shifted toward higher exposure. This parallel shift of the H & D curve is not observed in Emulsion A.

Discussion

It would go beyond the scope of this paper to correlate these observations with other emulsion characteristics and to draw conclusions on the mechanism of these phenomena. The discussion is therefore restricted to observations on how to characterize the mechanical sensitivity of photographic emulsions. It appears that the most significant conclusion that can be drawn from the illustrations cited above is that it is not possible to characterize the kink susceptibility of an emulsion by only one parameter. Fog formation and desensitization must be characterized separately because different groups of grains are involved in the two responses. This is particularly evident with Emulsion A, which appears to contain a class of grains which has an order of magnitude higher sensitivity toward mechanical strain in respect to desensitization. The same grains do not show this high sensitivity toward fog formation.

Based on these observations a simplified method for routine analysis was devised. It was found to be practical to use the arrangement shown in Fig. 1b in which the bending radius varies across the length of the test strip. Separate strips are required to test "kink fog" and desensitization. The strips for both tests are bent in the same way. Those used to characterize the desensitization, together with a control of the same film, are then flash exposed to maximum density. The exposure required to reach maximum density must be predetermined. All the test strips are then processed by a procedure recommended for the product being tested. The densities are then measured across the strip and may be plotted

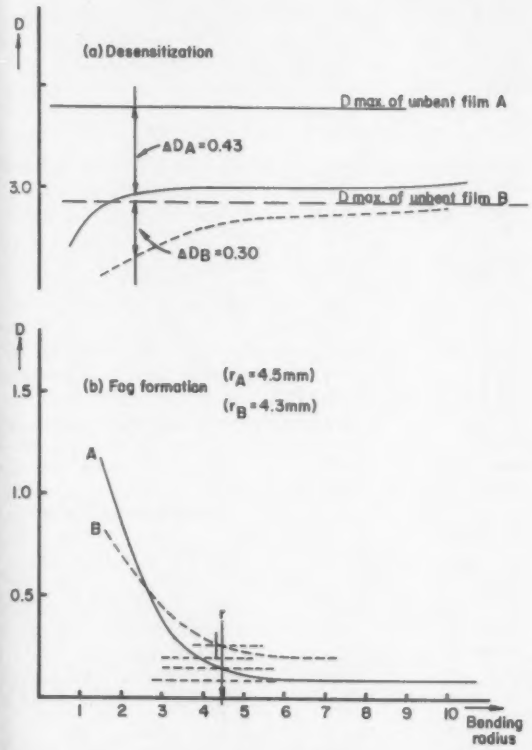

Fig. 4. Practical rating of "kink susceptibility." (a) Desensitization: ΔD_{max} at bending radius, r = 2.3 mm (b) Fog formation: radius at which fog increases, 0.05.

vs. the bending radius, as shown in Fig. 4. The emulsions represented in Fig. 4 are the same as were used for Figs. 2 and 3.

From the unexposed strips, the "kink fog susceptibility" can be characterized by the bending radius which causes an increase in fog of 0.05. This is illustrated in Fig. 4b. An analysis of variance was made to estimate the experimental error for averages of duplicate strips. It was found that a difference in radius of 0.3 mm is significant at a 95% confidence level.

The exposed strips are used to measure and characterize kink desensitization. Because of the difference in the natures of desensitization and fog formation, it would be impractical (as in the case of Emulsion A) to express kink desensitization in terms of the radius causing a critical response. It is convenient, however, to express the desensitization as depression of maximum density at a given bending radius. A bending radius of 2.3 mm has been chosen for this purpose. The dependence of the desensitization on the bending radius can be obtained readily from the same strip, but no information can be gained concerning a parallel shift of the H & D curve if this occurs in the particular emulsion.

It was observed that greater effects are obtained when single coated strips are bent with the emulsion side outermost. Apparently this is due to greater strain on the grains. The physical properties of the test material are sensitive to changes in the relative humidity with which the products are in equilibrium. It is therefore highly important to control this variable carefully in order to obtain meaningful results.

• Book Reviews and Abstracts

Photographic Sensitivity

Vol. 2. Tokyo Symposium. Editor-in-Chief, Shin Fujisawa. Maruzen Co. Ltd., Tokyo, 1958. 204 pp., illus., $4.50.

This volume contains English or German translations of the papers presented at the fourth symposium on photographic sensitivity held in Tokyo in October 1957, abridgments of some papers presented at the third symposium (Tokyo, June 1955), and a brief mention of some papers presented at the second symposium (Tokyo, May 1954). The papers of the first symposium, held at Lake Hakone in 1953, were published as Volume 1. These symposia were organized by the Research Group on Lattice Defects, under the auspices of the Physical Society of Japan and with the collaboration of the Photographic Society of Japan, for the purpose of "furthering efficient cooperation between research workers in both technical and academic fields of investigation."

It is inevitable that the papers presented in a symposium of this kind will vary in quality and that different readers will be primarily interested in different papers. A review can indicate little more than the broad scope of the symposium. Although most of the authors are Japanese, the United States, England, and the U.S.S.R. are represented. Review papers by F. C. Brown and F. Seitz on "Imperfections in the Silver Halides" and by J. W. Mitchell on "The Photolysis of Crystals of Silver Halides" are included. K. V. Chibisov reviewed various experiments on chemical sensitizing, and concluded that sensitization, latent image formation, and the initiation of development probably occur primarily at zones of physical disorder.

K. S. Bogomolov and I. F. Rasorenova found that the energy required to produce one silver atom by exposure to electrons was about 40 ev for two experimental emulsions, whereas only 5.6 ev were required in an exposure to light of 436 mμ. The required electron energy increased with decreasing grain size, whereas no dependence on grain size was noted in exposures to light. S. Fujisawa, E. Mizuki, and K. Kubotera concluded from studies of etching of submacroscopic silver bromide crystals by solvents that each crystal is divided into a number of more perfect sections separated by subboundaries, but the sections are larger than the usual photographic grains. K. Yamada, S. Oka, and T. Mukaibo found that silver, gold, and mercury, condensed on a silver bromide surface from vacuum, decreased the photoconductivity of the crystals. S. Totani and Y. Nishina studied the mechanism of latent image formation by ultrasonic waves, and concluded that plastic deformation is induced both at the surface and in the interior of the grains. E. Mizuki and S. Fujisawa found that the sensitivity of a silver iodobromide emulsion to high intensity light could be markedly decreased by a solvent treatment (e.g. with sulfite or thiocyanate solutions) which was substantially without effect on the sensitivity to low intensity light. They conclude that sensitivity specks on the grain surface are essential for high intensity sensitivity, but that sensitizing products in the gelatin medium surrounding the grains can act effectively to sensitize for low intensity exposures. From experiments on the temperature dependence of latent image formation, A. Miyauchi suggests that migration of silver ions through the bulk of the silver halide grains is important for long exposure times, whereas diffusion along internal surfaces and dislocations is important for short times. S. Makishima, T. Tomotsu, and S. Hayakawa showed the existence of several sources of low-temperature luminescence in silver chloride crystals, and conclude that only deep traps are involved in latent image formation. Other papers deal with the exciton in alkali halide crystals (T. Muto), the influence of chemical impurities on the optical properties of silver halides (K. Yamada, D. Heitkamp, and H. J. Oel), and the temperature dependence of photoconductivity in silver chloride crystals (N. Itoh and T. Suita).

The Editor-in-Chief and the Editorial Board are to be congratulated on the production of this volume within a relatively short time after the symposium was held in Tokyo. The quality of the English represents a definite improvement over Volume 1. — *T.H.J.*

The Detection and Measurement of Infrared Radiation

R. A. Smith, F. E. Jones, and R. P. Chasmar. Oxford University Press, 114 Fifth Ave., New York 11, N. Y., 1957. 458 pp.

The demands of the laboratory as well as those of the military services have resulted in such rapid changes in infrared apparatus materials and techniques that many workers in photography are not aware of the current state of the art in infrared. This volume covers the nonphotographic aspects of infrared comprehensively, and it should serve well as a reference text.

The laws and conditions pertaining to emission and absorption of radiation are treated extensively early in the book and many important formulae are derived. The many types of thermal detectors as well as photo detectors are described, analyzed, and evaluated in two substantial chapters. The limitations to the accuracy of measurements imposed by random fluctuations and fluctuations in amplifiers and instruments, covered in two more chapters, are appropriately followed by a thorough presentation of the ultimate sen-

sitivity of the detector under these conditions. The various sources of infrared radiation and their application, a large number of infrared optical materials and their properties, and a large variety of filters are also adequately covered. The equipments covered include infrared spectrometers and various amplifiers for use with infrared detectors.

A large number of charts and figures aid in presenting the material in this useful survey, and every chapter is replete with literature references. The extensive use of British devices and apparatus for example purposes does not detract from its over-all value, which will be high to all workers in infrared except possibly to the few who are very advanced. — *Edward K. Kaprelian*

The Reproduction of Colour

R. W. G. Hunt. Fountain Press, London, 1957 (Rayelle Publications, Philadelphia 44, Pa.). 208 pp., 11 color plates, 87 figures.

This broad presentation of the subject covers all aspects of making color reproductions of original scenes: photography, standards and calculations, masking, half-tone printing, color television, and light sources.

Physical color reproduction, the additive and subtractive principles, and various additive and subtractive color methods are well accounted for in the first five chapters and provide good reading in an area with which photographic scientists and engineers are more than ordinarily familiar. The matters of visual appreciations and the problems in color photography are well presented in two chapters. Four chapters cover in a clear and rather complete manner the main aspects of the color triangle, color standards and calculations, color correction by masking and three- and four-color half-tone printing. The preparation of these chapters has been such that the material should be readily assimilated by technical personnel desiring to learn the principles and methods involved. As an aid to those readers whose mathematics have fallen into disuse, an appendix explaining matrix algebra has been provided by the author.

A chapter on the transmission of color television signals, covering concisely, but adequately, bandwidth, dot interlacing, band saving, band sharing, phase sharing, two-signal color television, and gamma correction is, for the photographic class of reader, as lucid a 21-page presentation as is likely to be found anywhere. A chapter on light sources and one on assessment of the final result conclude this well-illustrated, well-written book. — *Edward K. Kaprelian*

The Effect of Triethanolamine on Photographic Emulsions

Several papers in the recent Russian literature have dealt with the hypersensitization of photographic emulsions by triethanolamine. This renewed interest in hypersensitization by an amine apparently stems from the observation by Demers that triethanolamine, used in aqueous solution as a prebath, can increase the sensitivity of nuclear track emulsions to ionizing particles.

Bogomolov, Ruditskaya, and Sirotinskaya report that the sensitivity of Type "R" nuclear emulsions to 15-million-electron-volt electrons was increased three-fold by treatment with a 3% aqueous solution of triethanolamine for 10 min, although the fog level was nearly doubled. The sensitivity to 250–600 million-electron-volt protons was increased about 50%. Zhdanov, Kartuzhanskii, Ryzhkova, and Shur likewise found the triethanolamine treatment effective and report substantial increases in the number of grains made developable per 100 μ in relativistic electron tracks. Breĭdo tried the effect of a prebath in 2% triethanolamine on the light sensitivity of 15 different photographic materials. He obtained a greater degree of hypersensitization when exposure was to low intensity light than when it was to high intensity, and the treatment decreased the low intensity reciprocity failure. The treatment did not alter the spectral sensitivity or the resolving power of the material. Very little hypersensitization was obtained with four plates used for astronomical photography, however.

Zhdanov and his co-workers have investigated the mechanism of hypersensitization by ethanolamine (*Doklady* reference, see below). They used two "light-type" emulsions and five nuclear emulsions, and made exposures to light, gamma radiation, protons, and alpha particles. They found that an optimum concentration of triethanolamine exists at 1–2%, a conclusion in agreement with the limited results of other workers. The speed of all emulsions tested was increased by the treatment, but the increase was greater the lower the original speed of the emulsion. In agreement with Breĭdo, they found that the effect on a high-speed emulsion, designed for use in aerial photography, was too small to be of much use. If the emulsions were first treated with 5% chromic acid solution to destroy surface sensitivity centers, hypersensitization by the triethanolamine was much less effective. Hence they conclude that the presence of sensitivity centers is important to the hypersensitization. They point out that the effect of the triethanolamine is similar to the hypersensitizing action of a short flash pre-exposure, and conclude that the triethanolamine treatment causes an increase in the size of the sensitivity centers and in their effectiveness as electron traps. The triethanolamine was not effective as a latensifying agent.

References cited: P. Demers, *Can. J. Research*, *25A:* 223–51 (1947). K. S. Bogomolov, I. A. Ruditskaya, and A. A. Sirotinskaya, *Zhur. Nauch. i Priklad. Fot. i Kinematograf* (*J. Sci. Appl. Phot. & Cinematog. USSR*), *3:* 52-53 (1958). A. P. Zhdanov, A. L. Kartuzhanskii, I. V. Ryzhkova, and L. I. Shur, *ibid.*, *3:* 53–54 (1958). I. I. Breĭdo, *ibid.*, *3:* 224–25 (1958). A. P. Zhdanov *et al.*, *Doklady Akad. Nauk SSSR*, *118:* 744–46 (1958). — *T.H.J.*

• Technicalia Photographica

FRANK SMITH

• Cameras and Accessories

Aerial Camera Using Polaroid Film

A hand-held aerial camera that uses Polaroid film has been developed by the Mast Development Co., Inc., 2212 E. 12th St., Davenport, Iowa. Known as Model 110, the camera was developed for aerial reconnaissance photography and has both civilian and military telephoto applications where instant photographs are needed.

This hand-held long-range camera uses 8-exposure Polaroid roll film in a standard Polaroid camera back and provides 60-sec in-camera development of exposures. Each 3 × 4-in. positive opaque photograph can be checked before leaving the location.

Additional features are the light weight (8 lb) and the cast-aluminum housing which extends beyond the lens and allows all-weather or open aircraft use.

Model 110 has a 10-in. focal length *f*/5.6 Raptar telephoto lens. Two Wratten Series 8 coated-glass filters, a K-2 (yellow) and a K-25A (red), are available as optional equipment. The camera is 5⅝ in. high, 9⅝ in. wide, and 11 in. long.

Fairchild Thinform 16mm Camera

An unusually compact and rugged 16mm motion-picture data camera, called the Thinform Model FDTF-001, has been introduced by Fairchild Data Devices Corp., 580 Midland Ave., Yonkers, N.Y. Designed specifically for flight test research, it is only 1¼ in. thick and is adapted to installation in thin airfoils or on the external surfaces of aircraft and missiles without pods. The overall outside dimensions are 1¼ in. thick, 8½ in. high, and 7-11/16 in. deep without connector. The weight without lens or film is 4.4 lb.

The camera has intermittent-type film transport and operates at speeds of 16, 24, 32, or 64 frames/sec. Frame rates are changed by substituting gear sets. The film capacity is 100 ft in the standard darkroom loading magazine which has been kept to a minimum size by its film displacement design. A 100-ft daylight loading magazine of slightly larger dimensions, and a 200-ft darkroom loading magazine are in process of development. All magazines are constructed to withstand severe impact shock so as to assure a maximum probability of recovering the film record undamaged after a test. Changing the film magazine is fast and simple since it is not necessary to thread the film.

The Thinform Camera has been tested to operate properly under the following environmental conditions: acceleration of 25 G on the three major axes; vibration of 20 to 55 cps at .060 d.a. and 56 to 500 cps at 10 G; 100,000 ft altitude; temperatures from −65° to +150°F.

Wollensak Developments in Photographic Instrumentation

Recent developments in photographic instrumentation by the Wollensak Optical Co., Rochester 21, N.Y., include a Stop-Start High Speed Fastax Camera and a rotatable Periscopic Lens for Fastair Camera, gun or "C" mount cameras.

The camera, called the WF 4S, is a 16mm Fastax with 400-ft film capacity using a daylight-loading spool. It is provided with a 2-in. 50mm *f*/2.0 Fastax Raptar Lens in focusing mount, integral viewfinder, and double timing light. Features of the camera include multiple-run start-stop operation as desired at all speeds, 350-9000 frames/sec without

Goose Control Unit or change of motors, interchangeable slit apertures permitting shutter speeds up to 0.00009 sec, remote control outlet, and convenient 115v ac-dc motors.

With stop-start provision, the camera can be rapidly stopped at any point, permitting multiple runs throughout a 400-ft roll and it is operable at any frame rate. Dynamic braking on drive-motor prism-shaft assembly and synchronized magnetic braking on feed-spindle and take-up motor are possible.

Size of the camera is 14 × 17 × 13 in. and the weight is approximately 85 lb in carrying case packed in carton for domestic shipment.

The other item, a new rotatable Periscopic Lens for Fastair Camera, gun or "C" mount cameras, is claimed to deliver sharp images at temperatures up to 100 F, e.g. where slip stream surface friction at high speed produces extreme heat.

Features of the Periscopic Lens are that it is an integral lens system, not a relay or attachment, that it has a focal length of 22mm, $f/3.5$ aperture with full 16mm coverage, and that it is T-stop calibrated. The lens possesses 360-deg rotation on the horizontal and vertical axes and the versatility of the mounting allows the camera to be placed inside the air frame. The lens extends outside (2 in. optional extension). The exposed optical element is solid quartz. The elements are air-spaced, not cemented. The lens housing is of stainless steel, and standard No. 5 drop-in filters are accommodated.

Beckman & Whitley High-Speed Cameras

Two new high-speed cameras for the photographic instrumentation field — the Dynafax High-Speed Motion-Analysis Camera and the Model 194 Continuous-Writing Streak Camera — have been announced by Beckman and Whitley, Inc., San Carlos, Calif.

The first of these, the Dynafax, provides high-speed motion-analysis photographs at an upper rate of 25,000 16mm frames/sec, and extends the range of previously recordable subject matter. A lightweight completely portable instrument, the Dynafax is arranged for simple, fast film processing, using standard 16mm film. Other features of the Dynafax camera include a stable framing rate during the operating cycle which is continually indicated on a built-in meter, absence of synchronizing requirements, exposure times easily adjustable between 1 and 5 μsec at the maximum rated framing speed of the camera, a total writing time of 9 msec at 25,000 frames/sec, and adaptability to the use of any 16mm ciné lens in a "C" mount. Requiring no external equipment beyond a common type of variable transformer, the Dynafax camera is 12 in. in diameter by 10 in. long overall and weighs 28 lb. It is arranged for operation on any tripod having a standard mount.

The second camera, the new Model 194 Continuous-Writing Streak Camera, is a research tool for the photo-instrumentation study of self-luminous transient events and produces a documentation which is a plot of space in one direction vs. time in a 90° direction.

Primary application will be in the study of explosions, shocktube manifestations, and flash-tube and spark discharge phenomena. Because of the continuous-writing feature, the requirement of synchronizing the camera and the event is eliminated, greatly simplifying use.

The camera mounts on its own base and control housing. Standard 35mm film, arranged for daylight loading and unloading, is used. The image is swept onto this film by a rotating triangular mirror driven by a high-speed turbine. Several types of these drives are available; the fastest, ranging from 200 to 5500 rpm, is driven by helium gas. This arrangement produces a maximum writing rate of approximately 8mm/μsec, a total writing time at top speed of 58 μsec, and a maximum time resolution of 2.5×10^{-8} using a 0.004-in. wide slit image and film having a resolution of 75 lines/mm.

The finished useful record is approximately 18.5 in. long. Its length is identified by three fiducial marks, automatically placed in the margin of the film. These locate the center of the record and the limit of useful data, which is 114° either direction.

The camera has the following control equipment: an events-per-unit time meter for accurate measurement of the mirror speed to provide a determination of writing rate; mirror speed adjustments; and controls for the capping shutter and the explosive-actuated blast shutter, used to prevent rewriting in the case of long-duration events.

Vought VDR-1630 Helmet Camera

A very small, compact, lightweight 16mm electrically-operated photographic recorder, designed especially for use on pilots' protective helmets, is a recent product of the Vought Co., P.O. Box 1350, Beverly Hills, Calif.

Called the VDR-1630, the camera satisfies many photographic data-recording problems where small space and light weight are essential.

The camera accommodates any ASA "C" mount lens and operates at 24 frames/sec at 24 v dc. Size of the camera is 2 × 2¼ × 5 in. and the weight is 18½ oz. Capacity is 30 ft of 16mm film.

Bell & Howell Motion-Picture Developments

A new, lower-priced, three-lens turret model 8mm electric eye camera and a new lower-priced 16mm sound-motion-picture projector are recent products of Bell & Howell, 7100 McCormick Rd, Chicago 45, Ill.

The first item, called the 390TA Perpetua Camera, will supplement the company's Model 393 three-lens turret electric eye camera. This camera has a 10mm *f*/2.3 normal lens, with 25mm telephoto and 6.5 wide-angle lenses in the Bell & Howell integrated safeguard rotating turret, automatically adjusting exposure for each lens whether indoors or out. Completely automatic in its operation, the 390TA requires no adjustment on the part of the user and has no provision for manual setting of exposure. The camera takes economical roll film and features a 10-ft film run plus a single frame release for special effects, as well as a continuous run to permit the photographer to get into the picture. Styled in a two-tone color combination of "fawn" and brown, in a die-cast aluminum housing, it features a picture-window viewfinder showing normal, wide-angle and telephoto fields of view instantly. A bright yellow, green and red color code is matched on each lens to the field of view outlined in the viewfinder.

The second item, Filmosound 384A 16mm motion-picture sound projector, is built to the quality specifications of the Filmosound line. It features a custom-made 5 × 7-in. oval speaker with sound baffling permanently built into the projector case so that it is always directed to the audience. A new high-fidelity 10-w amplifier system, and simplification of the projector by removal of clutch and reverse features permits a lower price.

The new unit includes square pattern shuttle with positive film advance stroke for steadier pictures on the screen and longer life, as well as all-gear drive for uniform synchronous operation.

Praktica Microscope Adapter

The Praktica Microscope Adapter, a new accessory for the Praktica FX-3 and FX-2 cameras as well as for other cameras with a similar screw mount for the lens, has been announced by Standard Camera Corp., 319 Fifth Ave., New York 16. With this accessory, photomicrographs may be made on 35mm black-and-white or color film.

The Praktica Microscope Adapter consists of a hinged adapter which is fastened to the draw-tube of the microscope, an extension tube 50mm in length, and an adapter for the camera. The hinged adapter enables the photographer to swing his camera away from the draw-tube for observation and focusing. Pictures can be made with the ocular removed from the draw-tube or with the ocular in its usual place, if additional magnification is desired.

A Spectrograph Attachment for High-Speed Cameras

D. P. C. Thackeray, *J. Sci. Instr.*, *35*: 248–252 (1958).

An attachment is described which will convert any camera into a spectrograph. Used with two typical high-speed cameras, time-resolved spectrography of small sources is possible with a wavelength resolution of 3 A to 5780 A and resolution times down to less than 10^{-7} sec. With a third camera, spectra of phenomena having a spatial dimension may be recorded at rates up to 1.6×10^{8} frames/sec. Illus., 11 ref.

Traid High-Speed 16mm Airborne Camera

A compact 16mm airborne instrumentation camera, developed by Traid Corp., Encino, Calif., shoots 200 frames/sec, holds 200 ft of film on daylight loading spools, and weighs only 6.75 lb loaded.

The new camera, called the Traid 560 Fotomatic, meets Mil Spec No. 5272A and withstands acceleration to 25 G. Stacked-spool design makes possible its compactness: 8 in. long, 53/16 in. wide and 6¼ in. high. Continuous or intermittent operation is provided by the camera's 28-v dc governor-controlled motor. Shutter opening of 72° provides exposure speed of 0.001 sec at 200 frames/sec. The Traid 560 is available with standard "C" lens mount or GSAP mount. Accessories include boresights, tracking finder, and various 16mm lenses including the Fotoperiscope lens assembly for "around-the-corner" shooting. Among the optional features are a timing system, output pulse installation, positive viewfinder with three-objective turret, and shutters from 7° to 204°.

Currently in use on the Q-2A Ryan Firebee jet drone, the Traid 560 has proved reliable at high speeds and at the low temperatures of jet altitudes.

• Illumination and its Measurement

Simplified Weston Direct Reading Exposure Meter

A new simplified and compact exposure meter which, it is claimed, removes all complexities that ordinarily result in confusion or loss of time in shooting, has been introduced by Weston Instruments, Div. of Daystrom, Inc.

In designing the new meter, known as the DR, the objective was a meter simple enough for even a beginner to operate accurately. Film speed and shutter speed are preset when the camera is loaded and the DR is then ready to use.

Both the instrument movement and the photocell in the DR are made by Weston. The movement has a spring-backed jewel bearing to enable it to withstand shock and vibration without impairing accuracy. Extremely compact, and finished in green, the DR can be used with any camera — still, motion-picture, or EVS.

A Method of Flash Synchronization for High-Speed Cinematography

J. D. Lewis and G. T. Peck, *J. Sci. Instr.*, *35:* 338–340 (1958).

Described is the method used to synchronize a high-power stroboscope for use as the light source for high-speed cinematography. The essential requirements were that modifications of the camera should be kept to a minimum and that synchronization should be effective over a speed range from 200 to 8000 frames/sec. Synchronization is accomplished by the use of an electromagnetic reluctance pickup placed adjacent to the teeth on the film-driving sprocket. Illus., 3 ref.

General Electric PR-3 Golden Crown Exposure Meter

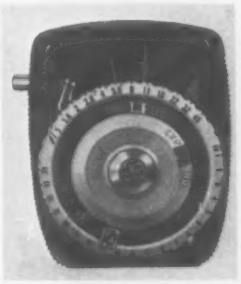

A new highly sensitive, photoelectric exposure meter has been announced by The General Electric Co., 40 Federal St., West Lynn, Mass. The meter the Golden Crown (Type PR-3) — is direct-reading and possesses several new features. One of these is the new Dynacell light multiplier attachment which provides four times greater reflected light sensitivity than any previous GE meter. The Dynacell may be easily attached, removed, or left on the meter.

Other features include: film exposure range of 0.1 to 20,000 ASA; a new red fluorescent pointer for quicker readability; and bright red frames-per-second window for easily read motion-picture settings.

Use of Electronic Flash in Photomicrography

David A. Erasmus, (Letters to the Editor), *Nature*, *181:* 1290 (May 3, 1958).

Describes a method wherein an electronic flash is incorporated in an optical bench and an attempt made to concentrate the flash onto the microscope mirror so that a fairly critical illumination is obtained. Illus., 2 ref.

A Simple Photomultiplier Photometer

R. Barer and R. G. Underwood, *J. Micro-optical Soc.*, Part 4, Series III, *76:* 149–155 (1956 — published April 1958).

The great sensitivity of photomultipliers offers many advantages over photocell-amplifier systems for the measurement or comparison of low levels of illumination. A highly stabilized power supply is generally considered essential. However, tests have shown that for many purposes such supplies are not necessary.

A simple and compact instrument based on a non-stabilized power supply has been developed. An important feature is the incorporation of a device for ensuring that the same total voltage is applied to the photomultiplier every time a reading is taken. The instrument can thus be regarded as manually stabilized. It has found widespread applications as

an exposure meter in phase-contrast, interference, fluorescence, and electron microscopy, and can be used as the basis for many types of instruments in which the measurement of very low light intensities is required. Illus., 3 ref.

Army Starlight Night Vision Device

A new night-vision device which enables troops to see military objectives at night with the aid of light obtained from the stars has been announced by the Department of the Army. Developed by the U.S. Army Engineer Research and Development Laboratories, Fort Belvoir, Va., and Radio Corporation of America, Harrison, N.J., the new device is known as the "Cascaded Photosensitive Image Intensifier."

Differing from other night-vision devices which utilize infrared, radar, and other mediums, the new development gathers the reflected starlight or diffused light from skyglow falling upon the objective. It then intensifies or amplifies the diffused light sufficiently to present a distinguishable image. The device is free from the complexities associated with low-level light-intensifier television systems and requires no source of artificial light or radiation.

The intensity of light furnished by the stars is so low as to be of little or no value to the unaided eye in seeing military objectives at night. With this new development, however, objects which would otherwise be obscured by darkness may be seen at tremendously increased ranges.

Heart of the instrument is a cascaded image tube, actually two tubes working in series and operating through an optical system which focuses the light reflected from objects in the field. The first tube acts as a preamplifier for the second which in turn further amplifies or intensifies the light and presents the image on the viewing surface. The tube is powered by current at approximately 25,000 v, furnished by a compact 6-v battery through a system of transformers and transistors.

• Optics

Photographs with Prismatic Binoculars

E. Weber, *Camera* (Lucerne), *No. 5:* 224–227 (May 1958).

A brief discussion covering the use of prismatic binoculars for increasing the focal length of a lens. The author concludes that prismatic field glasses provide the possibility of photographing, in large size, objects which cannot be closely approached. Illus.

Design of Photographic Objectives of the Triplet Family

I. The Design of the Triple Type III Objective, F. D. Cruickshank, *Australian J. Phys., 11:* 41–54 (March 1958).

A general study has been made of the initial design of the triplet family of photographic objectives. A classification is suggested. The point is made that it is convenient to regard the first two members of a triplet as constituting a compound corrector system to the rear positive member. Illus., 4 ref.

Bonding Optical Components to Metal Mounts

K. H. Spring, *Brit. J. Appl. Phys.*, 9: 242–246 (1958).

Various methods of bonding optical components to metal mounts, using synthetic resin adhesives, are described. In some cases a rubber interlayer is necessary to maintain resilience and prevent strain in the glass. A sandwich-type silicone rubber interlayer may be used to maintain resilience at temperature extremes. The tensile strength and shock resistance of the various types of bond are discussed, and a laboratory shock tester suitable for small specimens is described. Illus.

• Graphic Arts

Du Pont Photopolymer Process

The first public demonstration of letterpress platemaking by Du Pont's experimental photopolymer (light-sensitive plastic) was given on Sept. 27, 1958, at a Letterpress Forum held in New York City.

To make a photopolymer plate, a high-contrast negative containing text and illustrative matter is placed in contact with a metal-backed, photosensitive plastic plate. The plastic plate then is exposed to ultraviolet light for several minutes. Next, unexposed and hence unaffected plastic is "washed out" by a simple alkaline solution in about 6 min, leaving a high-relief image on the washed-out plate.

Life of unexposed photopolymer plates is said to be about one year. The entire photopolymer process may be conducted under normal tungsten illumination, but exposure to direct daylight and to high ultraviolet-content indoor light sources should be avoided.

Spokesmen for Du Pont said the experimental plates have performed successfully in nine months of steady field-testing, but that neither commercial availability nor commercial price is yet known.

• Photo Products and Processing

"Piggy-Back" 35mm Processor

What is said to be the world's fastest 35mm film processor is described by Joe Henry in the August 1958 issue of *American Cinematographer*. This "piggy-back" Thixotrol (monobath) processor, a development of the Fairchild Camera and Instrument Corp., Syossett, L. I., N.Y., for the U.S. Air Force, is designed to attach directly to a motion-picture camera and to process the film at camera speed. By using reversal film, the film can be projected immediately. The Thixotrol processor can process 500 ft of film per minute, or it can be set to process at a slower rate, if desired.

Heart of the processor is the viscous Thixotrol chemical which is spread onto the film in a thin even layer through slight pressure. One of the advantages of the chemical is that being a thick viscous substance of the consistency of axle grease, it will not leak or evaporate at high altitudes.

A System for Oscilloscope Camera-Positioning

Paul L. Kerley, *Electronic Industries*, *17:* 70–71 (Aug. 1958).

A system for taking multiple-sweep exposures on each print is described. Complete information is given for the construction and operation of such a system. Illus.

A Color "Electrofax" Process

J. S. Rydz and S. W. Johnson, *RCA Rev.*, *19:* 465–486 (1958).

Recent developments with Electrofax toners have resulted in color Electrofax prints. These prints, while similar in appearance to photographic results, do not follow the subtractive color-mixture laws which describe dye images.

The present paper discusses the basic principles of pigment mixtures and the application of the Kubelka analysis to the color Electrofax process. A method of separating colors for producing line work is also discussed. The method differs from the conventional techniques of using tricolor filters in that the separation of colors is achieved by controlling the amount of exposure on a scene. The mixing of colors which occurs due to the fusing operation in the Electrofax process provides the potential means for a color print system based on particle mixing rather than overlaying dyes as in a halftone printing ink process. Illus., 6 ref.

Bruning Diazotype Multicolor Kit

The Charles Bruning Co., Inc., Mount Prospect, Ill., has announced a new, novel, easy-to-use kit containing materials for making multicolor diazotype films and glossy prints from ordinary black-and-white translucent originals. The kit, called Multicolor Kit No. 100, makes possible the fast, simple production of colored motion-picture and slide-film titles, "static" and "dynamic" projection films, charts, diagrams, and overlays.

Clear films, glossy white or aluminum prints, each containing one, two, three or numerous colors on a single sheet are made by exposing a translucent original and a sheet of Bruning Multicolor film or paper to any ultraviolet light source. The exposure produces a latent image on the print which is an exact duplicate of the original. The image can then be transformed into any number of colors by the application, by hand, of various Bruning Multicolor developers. No darkroom is required. The kit includes a selection of films and papers, fine developers in pressurized dispenser cans, cotton swabs, and a bleach solution.

Cronar-Base Sheet Films

The Du Pont Photo Products Department has announced conversion of a major part of their portrait, press, and industrial films from acetate to fast-drying, extremely durable Cronar polyester photographic film base.

• Printers and Enlargers

Bruning Copytron Electrostatic Enlarger-Printer

A compact reproduction machine which makes enlargements of microfilmed drawings and records at a cost of only a few cents per print, has been developed by the Charles Bruning Co., Inc., 1800 W. Central Rd., Mount Prospect, Ill.

The Bruning Copytron Model 1000 Enlarger-Printer works on an electrostatic principle to produce permanent black-on-white enlargements of drawings and records which have been reduced to 35mm microfilm size. It enlarges the microfilm 14 to 16 times and prints the enlargements on standard size sheets ranging from $8^1/_2$ by 11 in. to 18 by 24 in. The

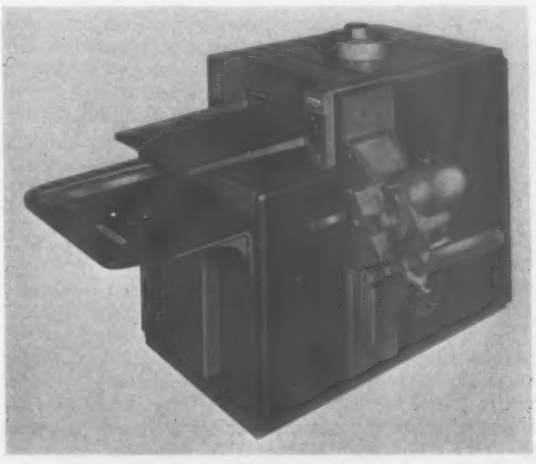

enlarging and printing are done continuously, and finished prints are delivered at the rate of about four per minute.

The Copytron Model 1000 utilizes a low-cost paper capable of holding an electrostatic charge. The machine is self-contained and consists of two main sections — an enlarger unit which protects the image onto the paper, and a reproduction section. In a continuous, automatic operation, the paper is charged, exposed, and then dry-developed with a charged powder which forms a positive, black-line enlargement on the paper. In a final step, the machine fuses the image on the paper and makes it as permanent as an impression of printer's ink.

The machine will accommodate reel, strip, or card-mounted microfilm, and incorporates a magnifying scanner which permits the operator to view the microfilm image before the print is made. The machine, which operates on 115-v ac, stands 43 in. high and occupies 53 by 32 in. of floor space.

Microfilm Reader-Enlarger-Processor

On-the-spot reproduction of microfilmed engineering drawings for reference purposes can be made at low cost on a new microfilm reader-enlarger-processor called the REP II, developed by Remington Rand Division, Sperry Rand Corp., 315 4th Ave., New York, N.Y.

Basically, the REP II is a self-contained, semiautomatic unit consisting of a projection system with an enlarging easel and a single sheet processor. "D" size frames are enlarged from tabulating aperture cards in a ratio of 13.75 to 1. The REP II provides for opaque visual reference to filmed drawings, enlarging them to a 17 × 22-in. size on the reading table. If one or more prints of the drawing are desired, the viewing table is swung out of the way. A conveyor belt system beneath it brings a sheet of sensitized photographic copy paper into position under glass beneath the enlarging projector. REP II can use either standard-weight photographic enlarging paper or a translucent paper for ultimate further reproduction on spirit, diazo, or blue print machines.

The processing section contains tanks for developer and stabilizer, and motor-driven chain-geared rollers for moving paper through processing solutions. The complete print is delivered automatically, damp-dry, 50 sec after exposure.

Time-O-Lite Monitor Line Voltage Controller

Industrial Timer Corp., 1407 McCarter Highway, Newark, N.J., has announced availability of the new Monitor Line Voltage Controller, which provides visual and manual control of voltage to an enlarger or printer.

Since maintenance of Kelvin temperature is of the utmost importance in the new color techniques, the Monitor is designed to perform this function accurately. The Monitor can be used in conjunction with a timer, thereby providing accurate timing as well as precise voltage control. The Monitor regulates voltages from 6 v to 135 v and will carry loads of up to 500 w. It normally operates on 115-v 60-cycle ac.

Copease Improved Book Photocopy Machine

A new, improved book photocopy machine combining an exposer and printer in a single unit has been introduced by the Copease Corp., 425 Park Ave., New York 22, N.Y.

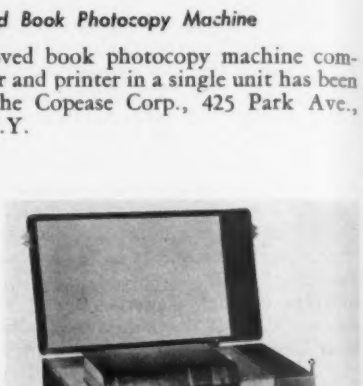

Called the Copease Duplex Book Copier, Model B, it makes perfect, dry, positive black-on-white copies in seconds under any lighting conditions of any original written or printed page, either single sheets or pages of books, without loss of margin.

Exclusive feature of the machine is its sponge-rubber head which adjusts to the thickness of the book to produce uniform contact and even pressure on copy surface, assuring the best possible quality. The Model B has a copying surface 14 × 17 in. and is especially suitable for libraries and research organizations. A smaller copier, size 8½ × 14 in., is designed for copy work in the average office.

• Techniques and Applications

High Resolution Cinematography of the Solar Photosphere

R. E. Loughhead and V. R. Burgess, *Australian J. Phys., 11:* 35–40 (March 1958).

A description is given of a new photoheliograph designed for time-lapse cinematography on 35mm film of any selected portion of a 20-cm solar image. The interval between successive photographs can be varied from 5 to 120 sec. Air-suction devices have been incorporated to suppress bad seeing originating within the telescope. The performance of the telescope is discussed briefly and the advantages of the cinematographic technique indicated. A discussion of the effects of atmospheric seeing emphasizes the great caution needed in the interpretation of solar photographs. Illus., 6 ref.

New Optical Methods Spot Hidden Corrosion

J. M. Holeman, *Chem. Eng., 65:* 170, 172, and 174 (1958).

Describes an improved borescope that takes panoramic photographs of corrosion on the inside of pipes. This is a new technique that takes flattened-out pictures of cylindrical parts and plastic impressions to permit the study of corrosion in inaccessible areas.

The panoramic borescope which is of particular interest incorporates an extreme wide-angle lens and shows in a single field of view a strip all the way around the pipe interior an inch or more in length. To this instrument was added a 16mm motion-picture camera and a drive mechanism to feed the camera into the pipe at a slow constant speed. When the film is processed and projected, the effect is that of travelling through a large well-lighted tunnel. Illus., 15 ref.

Optical Tracking of Artificial Earth Satellites

Fred L. Whipple, *Science, 128:* 124–129 (18 July 1958).

The Moonwatch program and the precision photographic program supply much of the raw orbit data. Illus., 6 ref.

Photographic Observations of Artificial Earth Satellites

M. J. Smyth, *Spaceflight, 1:* 247–251 (1958).

An informative description of the means and methods with which amateur astronomers may obtain useful photographic data on artificial earth satellites by using ordinary camera equipment and films. The author used a 35mm Leica camera equipped with a 5-cm *f*/2 Sumimicron lens. Kodak Tri-X Film was used and excellent results were obtained. Illus.

Surveillance Photography

Anthony B. Orefice and Abraham Schwartz, *Signal, 12* (No. 11): 32–33 (July 1958).

A night aerial photographic system for use in pilotless aircraft is described briefly. The system was developed for the U.S. Army by the U.S. Army Signal Research and Development Laboratory, Fort Monmouth, N.J., and consists essentially of a lightweight aerial camera, the KA-28, and integral illumination provided by photoflash cartridges. The system is mounted in a radio-controlled drone RP-71, with a flight range of 200 miles. Night photographs can be taken at altitudes of 750–3000 ft at speeds of 200 mph, providing photographic coverage for an area 5 miles long and $^1/_2$ mile wide. Camera KA-28 weighs 15 lb and takes fourteen $4^1/_2 \times 4^1/_2$-in. photos in 30 sec. A solenoid capping-type shutter is used. Illus.

A Photographic Method of Brightness Recording

E. & C. Marsh, *Illuminating Eng., 53:* 355–357 (1958).

Briefly described is a technique for recording brightness contours which show all areas of that brightness present in the photograph. These contours of equal brightness are produced by increasing the contrast of the negative until there is a sharp boundary without gradation between black and white areas of the photograph. The contours are found at this boundary. Illus.

Recent Developments in Electron Microscopy

V. E. Cosslett, *Brit. J. Appl. Phys., 9:* 253–256, 273-279 (1958).

A highly selective review covering some quite new electron-microscope instruments, of which the most important appear to be the interference and the scanning microscopes. Also covered are problems in biology, direct imaging of molecular lattices, etc. Illus., 40 ref.

• Miscellaneous

Facsimile Recording Using Magnetic Tape

J. Wade Dorsett (From a paper presented at the AFCEA 12th Annual Convention, Washington, D.C., June 4, 1958).

The general process of transmitting graphical data, such as maps, photographs, etc., by means of facsimile is outlined and a system for recording and reproducing this material on magnetic tape is described. The discussion is centered on the Ampex "Faxtape" system. Beginning with the generation of the electrical signal in the facsimile transmitter, the signal path is traced through the various component parts of the Faxtape system and a functional description of the individual units is given. There is a detailed study of the parameters affecting picture quality, such as jitter and skew, and results of operational tests performed on the system are described. Applications of the system and possible modifications for specialized usage are discussed.

A Nuclear Plate Camera for Angular Distribution Measurements with Gaseous or Solid Targets over a Wide Range of Angles

W. M. Jones and D. G. Waters, *J. Sci. Instr., 35:* 286–288 (1958).

A nuclear plate camera for the investigation of the angular distributions of charged particles from either solid or gaseous targets is described. The instrument has been checked by comparing the angular distributions of deuterons elastically scattered from gold and xenon targets with the Rutherford scattering law down to 8° in the forward direction. Illus., 5 ref.

Victor 16mm Film Viewer

A new 16mm motion-picture film viewer, designated the Victor Viewer Model VE 16, is specifically designed for use by the professional photographer for inspecting and editing films, according to an announcement from the Victor Animatograph Corp., Div. of Kalart, Plainville, Conn

The viewer has focusing and framing adjustments, built-in frame marker, and automatic projection lamp switch which is controlled by the film gate. The film is shown on hooded ground-glass screen, $3^1/_4 \times 4^1/_4$ in. Illumination is furnished by a 75-w lamp, and the picture is bright enough to permit comfortable viewing in normally lighted rooms. Filmed action can be timed to fractions of a second. The capacity is 99,999 frames, i.e. 2,500 ft, without resetting.

Artifacts in Xerographic Images on Vitreous Selenium Films

H. R. Limb and K. A. Metcalfe, *Australian J. Appl. Sci., 9:* No. 2, June 1958.

Artifacts in xerographic images are described. Microexamination of xerographic images and the underlying films of vitreous selenium shows some of the artifacts associated with visible defects introduced into the selenium layer in the preparation of the xerographic plates. These are in the minority, however, and generally the artifacts examined are not associated with visible structural features of the selenium film. The size of the developed artifacts depends to some extent on the level of electrostatic charge on the selenium film. Illus., 9 ref.

Optical T-Bench Method of Measuring Longitudinal Spherical Aberration

A specially constructed optical T-bench equipped with a nodal slide and an angle-measuring telescope is used at the National Bureau of Standards, Washington, D.C., for measuring longitudinal spherical and chromatic aberration by visual means. A brief description of the apparatus used and the results of measurements on a few typical lenses and an analysis of the sources of error are given in *NBS Research Paper 2880* by Francis E. Washer. A full reprint of this paper appears in *Journal of Research*, NBS, for July 1958.

Fairchild Data Reader

The Fairchild Data Reader, a development of the Fairchild Data Devices Corp., 580 Midland Ave., Yonkers, N.Y., offers a fast, accurate, and convenient means of reducing photographic data to digital form for electrical transcription. It can be used to measure photographic transparencies on plates, sheet film, or roll film. X and y ordinates are measured to a least count of 0.001 in., and angles of 0.1°.

Analog-to-digital transducers of Fairchild design present the measurements for visual display and also for electrical transcription by standard transcribing and recording equipment. Numerical data may be inserted into the transcription system through punch keyboards and rotary switch panels. Quick-change keyboard programming plugs and an accessory plugboard programmer assist in organizing the data output.

The large screen, with its 2.5× projected image, enables the operator to position a target reference point within the small screen area, and to read from the transparency any pertinent numerical or coded data. The small screen shows a 30× projection of a 0.15 by 0.15-in. area of the transparency. This screen carries the reference cross-lines for measuring ordinate distances, and also the rotatable goniometer reference line. A specially designed analog-to-digital converter in the goniometer system gives display reading and electrical read-out to a maximum quantity of 359.9°. Further rotation returns the reading to 0°.

Over-all accuracy of measurements taken by the Fairchild Data Reader is 0.005-in. Distances along x and y axes are measured, through analog-to-digital transducers, by moving the data transparency on precision built carriages by means of differential wire drives. Since all measurements are taken at the same point in the projection system, optical errors are largely eliminated.

Norelco Instrument for X-Ray Microscopy

A new Norelco Projection Microradiograph, designed for x-ray microscope techniques and other applications, is available from the Instruments Div., Philips Electronics, Inc., 750 S. Fulton Ave., Mt. Vernon, N.Y.

The unit employs an x-ray source approximately 1 μ in size to produce enlarged images of specimens placed close to the radiating surface. Contrast is

controlled to some extent by varying the accelerating potential of the electron beam and by changing target materials. Sharp, clear images are observed on a viewing screen and are recorded with a camera that accommodates five exposures on a 2 × 10-in. plate. Exposure time is approximately 1 min at 10–12 kv. Resolution is 1.0 μ or better at 2–20 kv.

Direct magnifications up to 70× are possible on the photographic plate and up to 250× on the viewing screen–binocular combination. Total useful photographic enlargement is 1500×. Field of view at 2× magnification is approximately 15 mm and at maximum magnification is about 0.5 mm.

The x-ray tube has six different targets which can be changed during operation by means of exterior controls. High voltage on the x-ray tube covers a range of 2–50 kv and is continuously variable. Line voltage is regulated to ± 0.05%.

A New Composite Image Amplifier/Converter

According to a technical note in the *Engineers' Digest* (London) for July 1958, there has been developed in Great Britain an image amplifier/converter of the screen type which produces on one side of the screen an amplified image of the image received on the other side if the radiation is visible. If the received radiation is invisible, the screen acts as a converter.

The screen consists of two layers of material dispersed in glass. One of the layers is a photoconductive material while the other is a photoluminescent material. Interposed between these layers is a layer of insulating material having a high specific inductive capacity.

The editor of *Engineers' Digest* informed the writer that the technical note is based on British Patent No. 795,877, assigned to The British Thomson-Houston Co., Ltd., Crown House, Aldwych, London, W.C. 2, England, on June 4, 1958.

Electron-Permeable Window for Cathode-Ray Tubes

One of the needs for better systems of electron microscopy and electronic photography is an electron-permeable window for conveying the electrons outside the cathode-ray tube for recording. Although such windows have been in existence for some time, as exemplified in the Lenard tube, they have not been generally satisfactory.

Jerrold Seehof, Stuart Smithberg, and Melvin Armstrong, writing in the September 1958 issue of *The Review of Scientific Instruments*, describe an ultra-thin window of improved properties, permeable to low-energy electrons, which has been developed for use with cathode-ray tubes and associated devices. This window, some 70 μin. thick, has the ability to withstand a pressure differential greater than one atmosphere and, at the same time, allows a 15-kv. electron beam to penetrate it. The window structures are composed of a $^1/_4$-in. square matrix (80-mesh nickel screen) of supported bentonite clay film. The authors state that it is expected that larger area configurations can be developed. The films are claimed to be relatively gastight and are insensitive to temperatures of at least 400°C.

The Lyot Ha Heliograph at the Cape of Good Hope

M. A. Ellison, *Nature* (London), *182:* 624–626 (1958).

The Lyot Ha Heliograph, installed at the Royal Observatory, Cape of Good Hope, consists of three separate optical trains, one of which is the monochromatic telescope consisting of an objective of 14 cm aperture working at *f*/10. A second optical train is that of the electronic guider and exposure meter, and a third optical system contains a clock and calendar and an echelon of 8 circular spots focused below the clock in order to provide a photometric calibration.

The camera is placed in the breech of the telescope and forms there a solar image 15 mm in diameter. Exposures are made on standard 35mm film using Kodak Micro-File Film. Normal exposure time is 2 sec and the duration between exposures may be preselected for intervals of 60, 30, or 15 sec. The images on Micro-File film can be enlarged to a diameter of 6 in. before the film grain becomes noticeable. About 25 ft of film per day is taken and it is developed at the Cape. Illus., 3 ref.

Photographic Science and Engineering

Volume 2—June, August, October, December 1958

TITLE INDEX

Analysis of the Variability Among Density-Log Exposure Curves of Black-and-White Negative Films by the Method of Principal Components
J. L. Simonds No. 4, p. 205

Analytical Recording Densitometer
W. E. White and C. A. Morrison No. 3, p. 164

Apparatus and a Laboratory for Processing Thick Nuclear Track Emulsions
John F. Garfield No. 2, p. 85

Book Reviews
Microphotography, by G. W. W. Stevens, reviewed by Frank Smith No. 3, p. 177

Concepts of Classical Optics, by John Strong, reviewed by E. K. Kaprelian No. 3, p. 177

Photographic Sensitivity, Tokyo Symposium, reviewed by T. H. James No. 4, p. 234

Detection and Measurement of Infrared Radiation, by Smith, Jones, and Chasmar, reviewed by E. K. Kaprelian No. 4, p. 234

Reproduction of Colour, by R. W. G. Hunt, reviewed by E. K. Kaprelian No. 4, p. 235

Clerc, Louis-Philippe (a citation)
Walter Clark No. 4, p. 185

Color Response of Current Amateur Reversal Color Films to Three Electronic Flash Units
R. E. Grimm No. 1, p. 40

Combined Development and Fixation of Photographic Images with Monobaths
Marilyn Levy No. 3, p. 136

Continuous Rapid-Processing System for Side-Looking Radar Mapping
Edgar D. Seymour No. 2, p. 91

Degradation of Phenidone in Developer Solutions During Storage
G. C. Alletag No. 4, p. 213

Evaluation of the Crabtree-Ross Procedure for Residual Hypo in Processed Film
E. P. Przybylowicz, C. W. Zuehlke, and A. E. Ballard No. 3, p. 148

Evaluation of Optical Images
George C. Higgins and Fred H. Perrin No. 2, p. 66

Influence of Observer Adaptation on the Acceptance of Color Prints
C. J. Bartleson No. 1, p. 32

Internal Gelatin in Photographic Silver Halide Grains
A. E. Ballard, C. W. Zuehlke, and R. S. Miller No. 4, p. 186
Note, P. Davis No. 4, p. 190

Japanese Photographic Objectives for Use with 35mm Cameras
Kogoro Yamada No. 1, p. 6

Measurement of the Ratio of Lateral to Vertical Dye Diffusion Rates in Swollen Gelatin Coatings
R. B. Pontius and J. A. Wenrich No. 3, p. 131

Minimum Energy Detectable by Photographic Materials
R. Clark Jones
Part II. Results for Four Current Kodak Films No. 4, p. 191
Part III. Energy Incident on a Microscopic Area of the Film No. 4, p. 198

Moisture in Photographic Film and Its Measurement
E. K. Colton and E. J. Wiegand No. 3, p. 170

Neutral Image Tones with Kodak High Resolution Plates
J. H. Altman and R. L. Lamberts No. 3, p. 160

Notes from the Editor
Peter Krause No. 2, p. 119

Patent Postscripts
Robert H. Zappert No. 1, p. 55; No. 2, p. 120

Photographic Emulsions for Missile Photography
Hutson K. Howell No. 2, p. 95

Photographic Exposure Guides and Meters
E. P. Wightman
Part I — Introduction No. 1, p. 14
Part II — Exposure Tables, Charts, and Calculators No. 1, p. 19

Photographic Techniques in Radar Meteorology
Myron G. H. Ligda and James D. Sullivan No. 1, p. 1

Production of Precision Resolving Power Test Reticles
P. Hariharan No. 2, p. 77

Projection of Photographic Data Recording Two-Tenths Second After Exposure
CARL ORLANDO No. 3, p. 142
Quantitative Estimation of Photographic Kink Susceptibility
BEAT MEERKÄMPER No. 4, p. 231
Quantum Efficiency of Photographic Negatives
R. CLARK JONES No. 2, p. 57
Relation Between Accelerating and Retarding Tendencies of Some Active Substances in Physical Ripening of Silver Chloride Suspensions
YASUSHI OH-YAMA AND KIYOSHI FUTAKI No. 3, p. 128
Revision of the Relation Between American Standard Exposure Index and DIN Speed Resulting from a Recent Revision of the German DIN 4512 Standard
J. L. SIMONDS No. 3, p. 162
Sensitization of Mercurous Oxalate by Dyes
P. A. VAN DER MEULEN AND ROBERT H. BRILL No. 3, p. 121
Sensitometric Processing Machine Using Small Film Strips and Small Developer Volume
R. W. HENN AND K. R. HUGHES No. 2, p. 81
Some Simplified Shutter, Flash Synchronization, and Motion-Picture Camera Tests
SAMUEL L. LOVE No. 4, p. 219
System Analysis and Performance of a Feedback Scanning Printer
L. L. BLACKMER AND J. C. MARCHANT No. 4, p. 225
Technicalia Photographica
FRANK SMITH No. 1, p. 43; No. 2, p. 105; No. 3, p. 178; No. 4, p. 236
Use of Electronic Image Intensification in Cinéfluorography
JOHN H. TOLAN AND JOSEPH L. DE CLERK No. 3, p. 154
Use of Principal-Component Description of *D*-log *E* Curves in a Study of the ASA-DIN Speed Relationships
J. L. SIMONDS No. 4, p. 210

AUTHOR INDEX

ALLETAG, G. C.
The Degradation of Phenidone in Developer Solutions During Storage No. 4, p. 213
ALTMAN, J. H., AND LAMBERTS, R. L.
Neutral Image Tones with Kodak High Resolution Plates No. 3, p. 160
BALLARD, A. E., PRZYBYLOWICZ, E. P., AND ZUEHLKE, C. W.
An Evaluation of the Crabtree-Ross Procedure for Residual Hypo in Processed Film No. 3, p. 148
———, ZUEHLKE, C. W., AND MILLER, R. S.
Internal Gelatin in Photographic Silver Halide Grains No. 4, p. 186
BARTLESON, C. J.
Influence of Observer Adaptation on the Acceptance of Color Prints No. 1, p. 32
BLACKMER, L. L., AND MARCHANT, J. C.
System Analysis and Performance of a Feedback Scanning Printer No. 4, p. 225
BRILL, ROBERT H., AND VAN DER MEULEN, P. A.
Sensitization of Mercurous Oxalate by Dyes No. 3, p. 121
CLARK, WALTER
Louis-Philippe Clerc (a citation) No. 4, p. 185
COLTON, E. K., AND WIEGAND, E. J.
Moisture in Photographic Film and Its Measurement No. 3, p. 170
DAVIS, P.
Note on *Internal Gelatin in Photographic Silver Halide Grains* No. 4, p. 190
DE CLERK, JOSEPH L., AND TOLAN, JOHN H.
The Use of Electronic Image Intensification in Cinéfluorography No. 3, p. 154
FUTAKI, KIYOSHI, AND OH-YAMA, YASUSHI
Physical Ripening of Silver Chloride Suspensions No. 3, p. 128
GARFIELD, JOHN F.
Apparatus and a Laboratory for Processing Thick Nuclear Track Emulsions No. 2, p. 85
GRIMM, R. E.
Color Response of Current Amateur Reversal Color Films to Three Electronic Flash Units No. 1, p. 40
HARIHARAN, P.
The Production of Precision Resolving Power Test Reticles No. 2, p. 77
HENN, R. W., AND HUGHES, K. R.
A Sensitometric Processing Machine Using Small Film Strips and Small Developer Volume No. 2, p. 81
HIGGINS, GEORGE C., AND PERRIN, FRED H.
The Evaluation of Optical Images No. 2, p. 66
HOWELL, HUTSON K.
Photographic Emulsions for Missile Photography No. 2, p. 95
HUGHES, K. R., AND HENN, R. W.
A Sensitometric Processing Machine Using Small Film Strips and Small Developer Volume No. 2, p. 81
JAMES, T. H.
Review of *Photographic Sensitivity*, Tokyo Symposium No. 4, p. 234
JONES, R. CLARK
On the Quantum Efficiency of Photographic Negatives No. 2, p. 57
———, On the Minimum Energy Detectable by Photographic Materials

Part II. Results for Four Current Kodak Films No. 4, p. 191
Part III. Energy Incident on a Microscopic Area of the Film No. 4, p. 198

KAPRELIAN, E. K.
Review of *Concepts of Classical Optics*, by John Strong No. 3, p. 177
———, Review of *Detection and Measurement of Infrared Radiation*, by Smith, Jones, and Chasmar No. 4, p. 234
———, Review of *Reproduction of Colour*, by R. W. G. Hunt No. 4, p. 235

KRAUSE, PETER
Notes from the Editor No. 2, p. 119

LAMBERTS, R. L., AND ALTMAN, J. H.
Neutral Image Tones with Kodak High Resolution Plates No. 3, p. 160

LEVY, MARILYN
Combined Development and Fixation of Photographic Images with Monobaths No. 3, p. 136

LIGDA, MYRON G. H., AND SULLIVAN, JAMES D.
Photographic Techniques in Radar Meteorology No. 1, p. 1

LOVE, SAMUEL L.
Some Simplified Shutter, Flash Synchronization, and Motion-Picture Camera Tests No. 4, p. 219

MARCHANT, J. C., AND BLACKMER, L. L.
System Analysis and Performance of a Feedback Scanning Printer No. 4, p. 225

MEERKÄMPER, BEAT
Quantitative Estimation of Photographic Kink Susceptibility No. 4, p. 231

MILLER, R. S., ZUEHLKE, C. W., AND BALLARD, A. E.
Internal Gelatin in Photographic Silver Halide Grains No. 4, p. 186

MORRISON, C. A., AND WHITE, W. E.
An Analytical Recording Densitometer No. 3, p. 164

OH-YAMA, YASUSHI, AND FUTAKI, KIYOSHI
Physical Ripening of Silver Chloride Suspensions No. 3, p. 128

ORLANDO, CARL
Projection of Photographic Data Recording Two-Tenths Second After Exposure No. 3, p. 142

PERRIN, FRED H., AND HIGGINS, GEORGE C.
The Evaluation of Optical Images No. 2, p. 66

PONTIUS, R. B., AND WENRICH, J. A.
Measurement of the Ratio of Lateral to Vertical Dye Diffusion Rates in Swollen Gelatin Coatings No. 3, p. 131

PRZYBYLOWICZ, E. P., ZUEHLKE, C. W., AND BALLARD, A. E.
An Evaluation of the Crabtree-Ross Procedure for Residual Hypo in Processed Film No. 3, p. 148

SEYMOUR, EDGAR D.
A Continuous Rapid-Processing System for Side-Looking Radar Mapping No. 2, p. 91

SIMONDS, J. L.
A Revision of the Relation Between American Standard Exposure Index and DIN Speed Resulting from a Recent Revision of the German DIN 4512 Standard No. 3, p. 162
———, Ana'ysis of the Variability Among Density-Log Exposure Curves of the Black-and-White Negative Films by the Method of Principal Components No. 4, p. 205
———, The Use of Principal-Component Description of *D*-log *E* Curves in a Study of the ASA-DIN Speed Relationships No. 4, p. 210

SMITH, FRANK
Technicalia Photographica No. 1, p. 43; No. 2, p. 105; No. 3, p. 178; No. 4, p. 236.
———, Review of *Microphotography*, by G. W. W. Stevens No. 3, p. 177

SULLIVAN, JAMES D., AND LIGDA, MYRON G. H.
Photographic Techniques in Radar Meteorology No. 1, p. 1

TOLAN, JOHN H., AND DE CLERK, JOSEPH L.
The Use of Electronic Image Intensification in Cinéfluorography No. 3, p. 154

VAN DER MEULEN, P. A., AND BRILL, ROBERT H.
Sensitization of Mercurous Oxalate by Dyes No. 3, p. 121

WENRICH, J. A., AND PONTIUS, R. B.
Measurement of the Ratio of Lateral to Vertical Dye Diffusion Rates in Swollen Gelatin Coatings No. 3, p. 131

WHITE, W. E., AND MORRISON, C. A.
An Analytical Recording Densitometer No. 3, p. 164

WIEGAND, E. J., AND COLTON, E. K.
Moisture in Photographic Film and Its Measurement No. 3, p. 170

WIGHTMAN, E. P.
Photographic Exposure Guides and Meters
Part I — Introduction No. 1, p. 14
Part II — Exposure Tables, Charts, and Calculators No. 1, p. 19

YAMADA, KOGORO
Japanese Photographic Objectives for Use with 35mm Cameras No. 1, p. 6

ZAPPERT, ROBERT H.
Patent Postscripts No. 1, p. 55; No. 2, p. 120

ZUEHLKE, C. W., PRZYBYLOWICZ, E. P., AND BALLARD, A. E.
An Evaluation of the Crabtree-Ross Procedure for Residual Hypo in Processed Film No. 3, p. 148

———, BALLARD, A. E., AND MILLER, R. S.
Internal Gelatin in Photographic Silver Halide Grains No. 4, p. 186

Ta

Execu
Enginee
Edit
Finan

Bing

Ba

Mon

Ne

Ro

South

The Society of Photographic Scientists and Engineers

Box 1609 • Main Post Office • Washington, D.C.

OFFICERS

President	GEORGE T. EATON, Bldg. 59, Kodak Park, Rochester 4, New York
Executive Vice President	STEVEN LEVINOS, Ansco, Binghamton, New York
Engineering Vice President	JOHN A. MAURER, 116–118 West 29th Street, New York 1, New York
Editorial Vice President	PETER KRAUSE, 29–11 Bell Boulevard, Bayside, New York
Financial Vice President	HERBERT MEYER, 325 Sequoia Drive, Pasadena 2, California
Secretary-Treasurer	NORTON GOODWIN, 826 Connecticut Avenue NW, Washington 6, D.C.
Managing Secretary	EDWARD S. COBB, Box 1609, Main Post Office, Washington, D.C.

CHAPTERS *and* CHAPTER OFFICERS

Binghamton, New York	*President*	IRA B. CURRENT, 26 Woodland Avenue, Binghamton, N. Y.
	Secretary	E. SCUDDER MACKEY, Stone Road, RD No. 2, Binghamton, N. Y.
Boston, Massachusetts	*President*	NICHOLAS CEDRONE, 73 Pond Street, Waltham, Mass.
	Secretary	ARTHUR J. ROSENBAUM, 44 Gleason Street, Framingham, Mass.
Cleveland, Ohio	*President*	R. E. BIRR, c/o General Electric Lamp Division, Nela Park No. 281, Cleveland 12, Ohio
	Secretary	CLINTON K. HAMLINK, 2230 South Overlook Road, Cleveland 6, Ohio
Ithaca, New York	*President*	COLONEL WILLIAM ALLEN, 216 Forest Home Drive, Ithaca, New York
	Secretary	DAVID O. FLETCHER, 1314 East State Street, Ithaca, New York
Monmouth, New Jersey	*President*	JOSEPH MANGIARACINA, 30 Brook Avenue, Little Silver, New Jersey
	Secretary	MISS MARILYN LEVY, 100 McLaren Street, Red Bank, New Jersey
New York, New York	*President*	FRANK G. BACK, 55 Sea Cliff Avenue, Glen Cove, New York
	Secretary	LT. HAYDEN B. PEAKE, Army Pictorial Center, 35-11 35th Avenue, Long Island City 1, New York
Rochester, New York	*President*	DONALD B. GRIM, Building 29, Eastman Kodak Company, Rochester 4, New York
	Secretary	ROBERT W. MAHER, Eastman Kodak Company, 343 State Street, Rochester 4, New York
Southern California	*President*	HERBERT MEYER, 325 Sequoia Drive, Pasadena 2, California
	Secretary	GEORGE W. BOEMLER, 22632 Collins Street, Woodland Hills, California
Southern Lake Michigan	*President*	HENRY COOPMAN, 9118 Greenwood Avenue, Ballard Acres, Des Plaines, Illinois
	Secretary	ROBERT J. MAZOR, 1438 West 123rd Street, Chicago 43, Illinois
Washington, D.C.	*President*	DWIN R. CRAIG, 815 Fisher Street, Falls Church, Virginia
	Secretary	LEE M. RECORDS, 1335 Tewksbury Place NW, Washington, D.C.

Sustaining Members / Society of Photographic Scientists and Engineers

Abrams Instrument Corporation

Aero Service Corporation

Ansco

Atkinson Laboratory, Incorporated

Bar-Ray Products, Incorporated

Bell & Howell Company

Burke & James, Incorporated

Charles Beseler Company

Chemco Photoproducts Company, Incorporated

Chicago Aerial Industries, Incorporated

Consolidated Film Industries

E. I. du Pont de Nemours & Company

Eastman Kodak Company

Ednalite Optical Company, Incorporated

Elgeet Optical Company, Incorporated

Fairchild Camera & Instrument Corporation

Farrand Optical Company, Incorporated

The F-R Corporation

General Electric Company

General Film Laboratories Corporation

Graflex, Incorporated

Grant Photo Products

W. & L. E. Gurley Company

Haloid Xerox Incorporated

Hardale Associates

Hi-Speed Equipment, Incorporated

Houston-Fearless Corporation

Charles A. Hulcher Company

Philip A. Hunt Company

Hycon Manufacturing Company

Kalart, Incorporated

Kollmorgen Optical Corporation

LogEtronics, Incorporated

L. W. Photo Products Company

J. A. Maurer, Incorporated

The Morse Instrument Company

National Research and Chemical Company

North American Aviation, Incorporated

Pako Corporation

Photogrammetry, Incorporated

Polaroid Corporation

Simmon Brothers, Incorporated

Technicolor New York Corporation

Viewlex, Incorporated

Wollensak Optical Company

Zoomar, Incorporated